HARMONIC DETECTION AND MITIGATION IN POWER SYSTEMS USING WAVELET PACKET TRANSFORM

BY

MUHAMMAD IJAZ

A Thesis Presented to the
DEANSHIP OF GRADUATE STUDIES

KING FAHD UNIVERSITY OF PETROLEUM & MINERALS

DHAHRAN, SAUDI ARABIA

In Partial Fulfillment of the
Requirements for the Degree of

MASTER OF SCIENCE

In

ELECTRICAL ENGINEERING

May 2015

KING FAHD UNIVERSITY OF PETROLEUM & MINERALS

DHAHRAN- 31261, SAUDI ARABIA

DEANSHIP OF GRADUATE STUDIES

This thesis, written by **MUHAMMAD IJAZ** under the direction his thesis advisor and approved by his thesis committee, has been presented and accepted by the Dean of Graduate Studies, in partial fulfillment of the requirements for the degree of **MASTER OF SCIENCE IN ELECTRICAL ENGINEERING.**

Dr. Mohammad Ali Abido
(Advisor)

Dr. Ali Ahmad Al-Shaikhi
Department Chairman

Dr. Mohamed A. Deriche
(Member)

Dr. Salam A. Zummo
Dean of Graduate Studies

Dr. Ibrahim Omar Habiballah
(Member)

9/6/15
Date

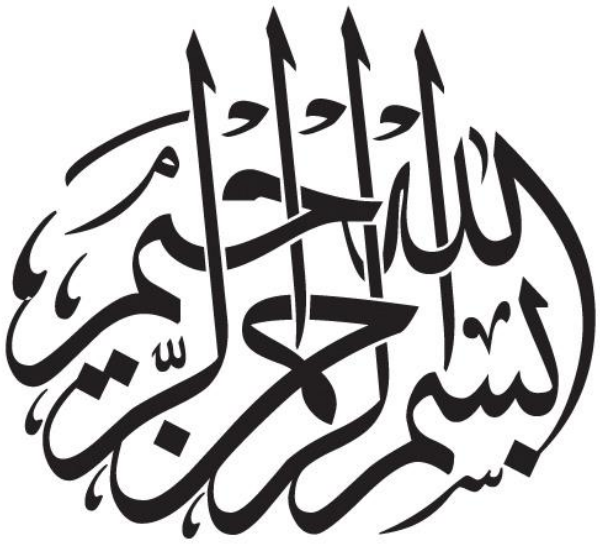

This Thesis is dedicated to

My Beloved Parents

My Brothers and Sisters

And

My Teachers

Every Bit of me is a little bit of you

ACKNOWLEDGMENTS

In the name of Allah, the most Merciful, the most Gracious

"All praise is to Allah, the Lord Of The Creation (1). The Most Gracious, the Most Merciful (2). Owner of the Day of Recompense (3). You alone we worship and from You alone we seek help (and may we always) (4). Guide us on the Straight Path (5). The path of those whom You have favored (6). Not the path of those who earned Your anger - nor of those who are astray (7)." Ameen

Surah Al-Fatihah

All praise is due to ALLAH and peace be upon the Prophet Muhammad ﷺ and his family, his companions (may ALLAH be pleased with them) and his followers.

With immense respect, I would like to extend my deepest gratitude to my family because without their prayers, love, positive reception and affection I would not have been able to achieve my desired goal in life. I will always be thankful to them for their continuous moral and emotional support and ever-needed prayers.

It has been my honor to be able to work with Dr. Muhammad A. Abido. I would like to admire his supervision, suggestions and guidance right from the beginning till the end of this research. His constant motivation helps me to produce quality work. I would like to thank my committee members: Dr. Mohamed A. Deriche and Dr. Ibrahim Omar Habiballah for their useful response, advice and the time they spent reviewing this thesis.

I am very obliged to King Fahd University of Petroleum & Minerals for providing me an opportunity to pursue my graduate degree. I would also like to appreciate all the support that I received from the Electrical Engineering Department in carrying out this research.

I would like to thank all my friends Shahid, Usman, Naseer, Waqar, Adil, Tanvir, Musadiq, Bilal, Faraz, Shehryar and all the seniors at KFUPM for providing the moral support, pleasant atmosphere and never forgettable moments.

TABLE OF CONTENTS

LIST OF TABLES

LIST OF FIGURES

LIST OF ABBREVIATIONS

APF	:	Active Power Filters
ANN	:	Artificial Neural Network
CT	:	Clark Transformation
CF	:	Crest Factor
CWT	:	Continuous Wavelet Transforms
DE	:	Differential Evolution
DF	:	Distortion Factor
DFT	:	Discrete Fourier Transform
FIR	:	Finite Impulse Response
FS	:	Fourier Series
FT	:	Fourier Transform
IEC	:	International Electrotechnical Commission
IEEE	:	Institute of Electrical and Electronics Engineers
IIR	:	Infinite Impulse Response
NI	:	National Instrument
PCC	:	Point of Common Coupling

PLL	:	Phase Lock Loop
PQ	:	Power Quality
RMS	:	Root Mean Square
RTDS	:	Real Time Digital Simulator
SAPF	:	Shunt Active Power Filter
STFT	:	Short Time Fourier Transform
THD	:	Total Harmonic Distortion
TDD	:	Total Demand Distortion
VI	:	Virtual Instruments
WPT	:	Wavelet Packet Transform
WT	:	Wavelet Transform

LIST OF SYMBOLS

$\boldsymbol{a}$	:	Wavelet Scaling Factor
$\boldsymbol{a_o}$	:	First Level Wavelet Approximation Coefficients
$\boldsymbol{b}$	:	Wavelet Shifting Factor
$\boldsymbol{C_k}$	:	DFT Spectral Component Corresponds to k^{th} DFT Bin
$\boldsymbol{C_{dc}}$	:	Capacitance of the dc Side Capacitor
$\boldsymbol{d_j}$	:	Wavelet Detail Coefficients Corresponds to Level j
$\boldsymbol{d-q}$	:	Synchronous Reference Frame Control
$\boldsymbol{f_o}$	:	Fundamental Frequency
$\boldsymbol{f_s}$	:	Sampling Frequency
$\boldsymbol{F_v}$	:	Wavelet Feature Vector
$\boldsymbol{G_n}$	:	Harmonic Group Number n
$\boldsymbol{h}$	:	Harmonic Group Number
$\boldsymbol{H}$	:	Maximum Harmonic Order
$\boldsymbol{I_{rms}}$	:	Root Mean Square Value of Current
$\boldsymbol{I_{fabc}}$	:	Three-Phase Active Power Filter Current
$\boldsymbol{I_{Labc}}$	:	Three-Phase Load Current

$\boldsymbol{p-q}$	:	Instantaneous Active and Reactive Power Control
$\boldsymbol{V_{rms}}$	:	Root Mean Square Value of Voltage
$\boldsymbol{V_{dc}}$	:	dc Link Voltage
$\boldsymbol{\Phi(t)}$	:	Wavelet Scaling Function
$\boldsymbol{\Psi(t)}$	:	Mother Wavelet

ABSTRACT

Full Name : Muhammad Ijaz

Thesis Title : Harmonic Detection and Mitigation in Power Systems using Wavelet Packet Transform

Major Field : Electrical Engineering

Date of Degree : May 2015

Power Quality (PQ) is nowadays an important issue that involves electrical energy producers, consumers and electrical equipment manufacturers. The broad usage of electronic equipment, such as computers, power electronic devices and drives, controllers and lighting led to a complete different nature of loads as compared to the conventional ones. The extensive usage of power electronic devices leads the power quality problem to be more severe. PQ problems are becoming a great threat to the safety and security of power systems.

In this thesis, two novel techniques based on wavelet packet transform (WPT) and infinite impulse response (IIR) filter bank are proposed to measure the harmonic and interharmonic distortion in power systems. Furthermore, a new technique based on wavelet transform (WT) and optimized artificial neural network (ANN) is proposed for PQ disturbance classification. Finally, two control strategies are designed and implemented for shunt active power filter (SAPF) to mitigate the harmonics in distribution networks.

The proposed harmonic monitoring, detection and control strategies are implemented in a laboratory scale prototype using LabVIEW software, data acquisition cards, digital processors, real time inverter and programmable source and loads. The necessary experimental setup is established to validate the results of proposed methods. The results show the effectiveness of the proposed approach to detect and mitigate the harmonics and interharmonics in power systems. The comparisons of the experimental results demonstrate a good agreement with the simulation results. It can be concluded that, the developed prototype is capable to successfully detect, measure and mitigate the harmonic contents to ensure the successful operation of the power systems.

ملخص الرسالة

الاسم الكامل: محمد إعجاز

عنوان الرسالة: كشف التوافقيات والتخفيف من آثارها في أنظمة الطاقة باستخدام تحويل حزم المويجات

التخصص: هندسة كهربائية

تاريخ الدرجة العلمية: مايو , 2015

جودة الطاقة هي في الوقت الحاضر قضية مهمة تنطوي على منتجي الطاقة الكهربائية والمستهلكين والشركات المصنعة للمعدات الكهربائية. الاستخدام الكبير للأدوات الإلكترونية، مثل أجهزة الكمبيوتر، أجهزة الالكترونيات والمحركات، ووحدات التحكم والإضاءة أدى إلى طبيعة مختلفة كاملة من الأحمال بالمقارنة مع الأحمال التقليدية. الاستخدام الواسع للأجهزة الإلكترونية يؤدي الى مشكلة جودة الطاقة والتي أصبحت تشكل تهديدا كبيرا لسلامة وأمن أنظمة الطاقة.

في هذه الأطروحة، اثنتان من التقنيات الجديدة على أساس تحويل حزمة المويجات (WPT) والبنك المرشح للاستجابة النبضية اللانهائية (IIR) لقياس التشوه التوافقي والتوافقي المتداخل في أنظمة الطاقة. وعلاوة على ذلك، تم اقتراح تقنية جديدة تعتمد على تحويل المويجات (WT) والشبكة العصبية الاصطناعية (ANN) لتصنيف الاضطرابات وتنفيذهما في جودة الطاقة PQ. وأخيرا، فقد تم تصميم طريقتين وتنفيذهما لمرشح تحويلة الطاقة النشطة (SAPF) للتخفيف من التوافقيات في شبكات التوزيع.

الطرق المقترحة في مراقبة الموجات التوافقية وكشفها واستراتيجيات التحكم بها تم بناؤها في نطاق المختبر باستخدام برنامج (LabVIEW)، وبطاقات الحصول على البيانات، والمعالجات الرقمية، العاكس الوقت الحقيقي، ومصدر مبرمج وأحمال. تم تجهيز الإعدادات التجريبية الضروريه للتحقق من صحة نتائج الأساليب المقترحة.

النتائج أظهرت مدى فعالية الأساليب المقترحة للكشف بنجاح والتخفيف من محتويات التوافقية لضمان عملية ناجحة لنظام الطاقة. وبمقارنة النتائج العملية بالنتائج النظرية نلاحظ أن هناك توافق كبير بينهما لذلك يمكننا القول بأن النموذج المطور قادر بما فيه الكفاية للكشف بنجاح والتخفيف من محتويات التوافقية لضمان عملية ناجحة لنظام الطاقة.

درجة الماجستير في العلوم
جامعة الملك فهد للبترول والمعادن
الظهران المملكة العربية السعودية
مايو 2015

CHAPTER 1

INTRODUCTION

1.1 Background

The increasing use of non-linear loads threatens the reliability and stability of the power systems. The non-linear devices draw non-linear current from the power system, this non-linear current circulates throughout the distribution system and distorts the voltage waveform, which ultimately affects the whole power system. The potential effects of harmonic distortions are not only included the long term effects on power systems like neutral overload in three phase system, overheating conductors and transformer, overvoltage and metering problems due to higher frequency components but also include the short term effect due to harmonic burst which ultimately results in the malfunctioning of the equipment due to their high sensitivity to power quality [1]–[3].

Harmonics are the sinusoids having frequencies that are integer multiple of fundamental power system frequency. To reduce the potential threats to the power system from harmonics, Institute of Electrical and Electronics Engineers (IEEE) and International Electrotechnical Commission (IEC) define standard limits below which the harmonic content should be maintained for successful operation of the system. Therefore, proper harmonic detection, measurement and mitigation strategy are a need of time [4], [5].

Along with technological advancement, there are many companies working on PQ problems around the globe. The most affected areas by PQ problems are the continuous process industry and the information technology services. When a disturbance occurs, huge financial losses may happen, with the consequent loss of productivity and competitiveness.

Given this brief background, this thesis proposes new and efficient techniques using wavelet transform and infinite impulse response filter bank to accurately detect, classify, measure and mitigate the harmonic and interharmonic distortions. The proposed approaches are implemented for real monitoring via LabVIEW software, advanced digital signal processors, and data acquisition modules. Furthermore, a control strategy for harmonic mitigation is developed using shunt active power filter. The proposed control strategy is simulated and tested using hardware in loop real time digital simulator (RTDS) and dSPACE controller. A laboratory scale prototype is also developed for the harmonics elimination using a programmable source, loads and an inverter.

1.2 Thesis Motivation

The motivation of this thesis work is inspired by some of the non-resolved issues in the related work on the problems of accurate detection, measurement and mitigation of harmonics in power systems. Previously, Discrete Fourier Transform (DFT) was proposed as signal processing technique in IEC-61000-4-7 for the measurement of harmonic distortion in electric systems. However, the standard itself states that "*the use of the Fourier analysis does not preclude the application of other analysis principles*" [6].

From the literature, it has been observed that there are several signal processing techniques, which can be used for harmonics and interharmonics measurement. However, most of them

are not suitable for real time applications. Also, there is a drive to apply the latest technology for data acquisition and advanced signal processing tools (Wavelet transforms) using high level programing language (LabVIEW) to build complete monitoring system.

To conclude, all the problems mentioned show that the research in this area is very challenging but promising. A system which is able to automatically detect, measure and mitigate the PQ disturbances is desired. Therefore, a proper harmonic detection, measurement and mitigation strategy is inevitable to cope with the era of complex power systems.

1.3 Thesis Objectives

This aim of this research is to develop and implement an advance digital signal processing technique to detect and measure the harmonics and interharmonics distortion in the voltage and current signals. Additionally, it aims to design and implement a state of the art control strategy to mitigate the harmonics and ensure the reliability of the power systems. The main objectives of this study can be stated as:

1. Development of digital signal processing techniques for the measurement of harmonics distortion in power systems.
2. Implementation of the developed technique for the measurement of harmonic groups according to the specifications of IEC standard 61000-4-7 in real time.
3. Detection and measurement of interharmonic and subharmonic group distortions using wavelet packet transform.
4. Implementation of harmonics mitigation strategy based on Active Power Filters.

5. Development of a laboratory scale prototype for the detection, measurement and mitigation of harmonics in power systems.

1.4 Thesis Methodology

The work that will be done to achieve the thesis objectives can be divided into the following tasks which is fully achieved.

Task 1: Technology assessment and literature Survey

- Assessing technological advances in monitoring and mitigation of harmonics in electrical system.
- Surveying application of signal processing on the harmonic analysis in energy systems.

Task 2: Developing and testing the monitoring and mitigation system.

- Developing the monitoring system.
- Developing the computer program of digital signal processing controller.
- Developing a linking protocol between digital signal processing controller and typical power system model.

Task 3: Testing the proposed codes.

- Testing the proposed algorithms for detection and mitigation of harmonics.

Task 4: Building the laboratory prototype

- Building a prototype for monitoring and detection system.
- Building a prototype of proposed control strategies.

Task 5: Implementation of detection and mitigation strategy on the laboratory prototype

- Implementation of the proposed detection and mitigation using the necessary hardware devices.

Task 6: Testing and evaluation of laboratory prototype performance

- Experimental investigation of the monitoring and detection prototype.
- Experimental investigation of the control strategy prototype.

Task 7: Results and discussion

- Comparing the simulation results with the experimental results.
- Comparing the obtained results with the published literature.
- Highlighting the main findings and recommendations.

1.5 Thesis Contribution

The main contribution of this work is proposing new efficient techniques for real time detection and measurement of harmonic and interharmonic distortion in voltage and current signals. Furthermore, it is aimed at build a harmonic mitigation system of PQ problems using the proposed methods in a laboratory scale prototype.

The specific thesis contributions can be stated as:

- Two new methods based on wavelet packet transform and infinite impulse response filter bank have been proposed for real time detection and measurement of harmonics and interharmonics.

- A prototype for real time monitoring and measurement of harmonics and interharmonics along with other power quality parameters has been built in the laboratory using the developed methods.
- A novel power quality disturbance classifier is designed based on wavelet transform and optimized artificial neural networks.
- Two control strategies for shunt active power filter are designed and implemented to mitigate the harmonics in distribution systems.
- A laboratory scale prototype has been developed for real time monitoring, measurement and mitigation of harmonics and interharmonics in distribution system.

1.6 Thesis Breakdown

Having presented the rationale for the research problem and laid down the foundation of the problem area in the first chapter, the second chapter will briefly explain the fundamental concepts, power quality standards and background technologies used for the measurement and mitigation of harmonics and interharmonics. Chapter 3 and Chapter 4 presents the harmonics and interharmonics measurement using using proposed techniques wavelet packet transform and infinite impulse response filter bank respectively. Chapter 5 presents the experimental implementation of the proposed harmonic measurement techniques. A novel and efficient power quality classifier based on wavelet transform and optimized neural networks is presented in Chapter 6. A harmonic mitigation strategy based on shunt active power filter is presented in chapter 7. Chapter 8 presents the experimental

implementation of shunt active power filter and its control algorithms. Finally, chapter 9 concludes the findings and suggests the future work.

CHAPTER 2

LITERATURE REVIEW

This chapter introduces the harmonic measurement standards. It also presents a comprehensive literature review of power quality, application of digital signal processing techniques for the measurement of harmonics and interharmonics in voltage and current signals. In addition, this chapter discusses the literature review of harmonic mitigation strategies using shunt active power filter.

2.1 Overview

Recent development in power electronics has severely threaten the reliability and stability of power system due to the excessive injections of harmonics in power system. These non-linear loads draw harmonic current from the electrical source, which are consequently transferred into distorted voltage supply on the mains of the electrical power systems. The distorted voltage and current signals have numerous harmful effects such as overheating of transformers, excessive neutral current, malfunctioning of sensitive electronic equipment, false tripping of circuit breakers, low system efficiency, skin effect and interference in the nearby communication systems. Harmonics cause skin effect, as they do not fully penetrate the conductor rather they travel on the outer edge of the conductor. This phenomenon decreases the effective cross sectional area of the conductor and ultimately increases the resistive losses, which in turn heats up the conductors and anything connected to them. Therefore, a fast, robust and adequate harmonic measurement and mitigation techniques are the need of time.

2.2 Sources and Effects of Harmonics and Interharmonics

Sources of harmonics are mainly the modern electronic equipment such as:

- Non-linear loads like variable frequency drives, switching mode power supplies and inverters.
- Frequency conversion (Variable speed drives)
- Household appliances (personal computers, televisions, micro-wave furnaces and LED lightening)
- Industrial equipment like arc furnaces and arc welding equipment are also significant producers of harmonics.
- Power transformers working in the saturation region are also considered as harmonics source.

When a voltage or current waveform is distorted due to harmonic pollution, it causes abnormal operating conditions in a power system such as:

- Overheating problem in induction and synchronous motors and generators [7].
- Weakening the cable due to excessive heating, it can break insulation and windings.
- Malfunctioning of electronic equipment due to the desynchronization in timing.
- Electromagnetic interference can be caused in motor winding due to current harmonics while voltage harmonics can create interference with nearby communication equipment.
- Heating losses in circuit breakers and switch-gear can increase due to the flow of current harmonics.

- Interharmonics produce a light flicker in incandescent and fluorescent lamps [8], [9]
- Tripping of circuit breakers and relays due to the flow of current harmonics.
- Low system efficiency.

2.3 Harmonics, Interharmonics and Subharmonics: An Overview

The electric utilities are designed to supply energy to their facilities and connected customers through the distribution lines of 110/220 V rms and 50/60 Hz frequency. The characteristics of supply voltage are set in standard [6]. However, some higher frequency components in the supply voltage degrade the quality of energy supplied. These higher frequency components can be categorized as [7]:

- DC Component: $f = h \times f_o$ Where $h = 0$
- Harmonics: $f = h \times f_o$ Where $h > 0$ and h is an integer
- Interharmonics: $f = h \times f_o$ Where $h > 0$ and h is not an integer
- Subharmonics $0 \text{ Hz} < f < f_o$ Where $f = h \times f_o$ and $0 < h < 1$

2.3.1 Harmonics

Harmonic disturbances have been extensively studied since the beginning of the distribution system. Recent developments in signal processing techniques have gained a larger interest of researchers for the harmonic measurement and mitigation.

Harmonics are the sinusoidal waveform having frequency integer multiple of fundamental frequency. The non-linear loads connecting to the network produce the harmonics components. The non-linear devices draw non-linear currents from the power system, this

non-linear currents circulate throughout the distribution system and distort the voltage waveforms, which ultimately affect the whole power system. In general, the major sources of harmonics in industrial systems include the rectifiers, arc furnaces, welding units, and nonlinear loads. Harmonic sources in domestic systems include the florescent lightning, discharge lamps, switch mode power supplies, computers, motors, air conditioners and retreaters [10], [11].

Under periodic steady state conditions, Fourier Series (FS) can be used to express the harmonically distorted waveforms as

$$f(t) = C_o + \sum_{h=1}^{\infty} C_h \cos(h\omega t + \theta_h) \tag{2.1}$$

$$C_o = \frac{1}{T}\int_0^T f(t)dt \tag{2.2}$$

$$C_h = \sqrt{A_h^2 + B_h^2}, \qquad \theta_h = \tan^{-1}(-\frac{B_h}{A_h}) \tag{2.3}$$

$$A_h = \frac{2}{T}\int_0^T f(t)\cos(h\omega t)dt, \qquad B_h = \frac{2}{T}\int_0^T f(t)\sin(h\omega t)dt, \qquad T = \frac{2\pi}{\omega} \tag{2.4}$$

where C_o is the direct component of FS while C_h are FS coefficients for sinusoidal components of the distorted waveform *f(t)*. The harmonic number is represented by *h*, where ω and θ are the angular frequency and phase angle for the h^{th} harmonic component respectively. Figure 2.1 shows a typical voltage waveform consisting of fundamental and 3rd harmonic component.

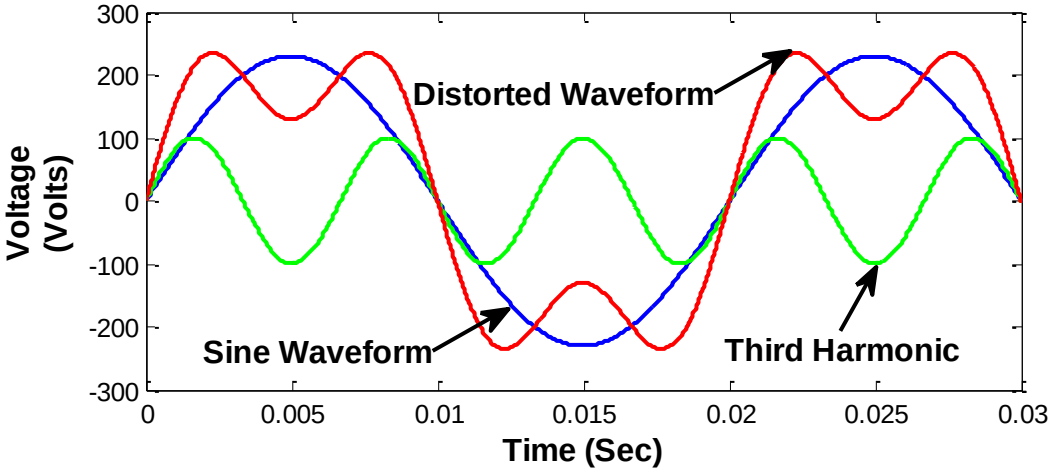

Figure 2.1 Effect of Third Harmonic Distortion in Supply Voltage

Harmonics distortion can be evaluated in the following ways.

- ***Total Harmonic Distortion (THD)*** is used to measure the harmonic distortion in power systems. It is defined as the ratio of the sum of power of all harmonic components to the power of the fundamental component as:

$$THD(V) = \frac{\sqrt{\sum_{h=2}^{H} V_h^2}}{V_1}, \qquad THD(I) = \frac{\sqrt{\sum_{h=2}^{H} I_h^2}}{I_1} \tag{2.5}$$

where

V_1 and I_1: RMS value of voltage and current fundamental component

V_h and I_h: RMS value of voltage and current harmonic components

H: Maximum harmonic order considered for calculation

h: Harmonic order

- ***Total Demand Distortion (TDD)*** is defined as the ration between the harmonic current distortion to the maximum demand load current lasting for 15 to 30 mins.

$$TDD(I) = \frac{\sqrt{\sum_{h=2}^{H} I_h^2}}{I_{M_L}} \tag{2.6}$$

where I_{ML} represents the maximum demand load current.

- ***Distortion Factor (DF)*** is used to measure the distortion in the received signal. DF can be defined as the ration between the rms of the fundamental component to the total rms of the received signal as:

$$DF(V) = \frac{V_1}{V_{rms}}, \qquad DF(\mathrm{I}) = \frac{I_1}{I_{rms}} \tag{2.7}$$

V_1 and I_1: rms value of voltage and current fundamental components

V_{rms} and I_{rms}: Total rms value of the voltage and current signals

The ration is equal to unity for a pure sinusoidal current and voltage waveforms and reduced as the harmonic distortion increases in the waveforms.

- ***Crest Factor (CF)*** gives a quick idea how much the available distortion is affecting the sinusoidal current waveform. CF is the ratio of the peak value of a waveform to its rms value as:

$$CF(V) = \frac{V_{peak}}{V_{rms}}, \qquad CF(I) = \frac{I_{peak}}{I_{rms}} \tag{2.8}$$

V_{peak} and I_{peak}: Peak values of voltage and current waveforms

Vrms and I_{rms}: Total rms values of the voltage and current signals

The value of CF for purely sinusoidal waveforms is 1.414 and increases as the distortion in the voltage or current waveform increases.

2.3.2 Interharmonics

IEC-61000-2-1 [12] defines interharmonic as follows:

"Between the harmonics of the power frequency voltage and current, further frequencies can be observed which are not an integer of the fundamental. They can appear as discrete frequencies or as a wide-band spectrum."

The measurement of interharmonics is not a trivial task. An interharmonics waveform may not be necessarily regular. Interharmonics are mainly produced by cycloconverters in rolling-mill and linear motor drives. Other sources of interharmonics include arc furnace, arc welding and all loads that are not pulsating with fundamental frequency [13]. Figure 2.2 shows the 10 periods of the 50 Hz waveform consisting of harmonics and interharmonics components listed in Table 2.1. Figure 2.2 clearly shows that the resulting waveform is an aperiodic waveform and even asymmetric depending upon the observation window.

The sampling window plays a vital role in the measurement of interharmonics. If the signal is measured using an acquisition window whose duration is an integer multiple of fundamental frequency, significant errors might occur in the observations. The sampling window length should be increased so that it becomes synchronous with signal to be analyzed. This can be achieved if the duration of the window would offer a frequency resolution equals to the least common multiple of different frequency components in the signal. On the other hand, by increasing the duration of the sampling window, the non stationary interharmonics might not be observed correctly and results in larger errors in the observations [14], [15].

The potential and harmful effects of interharmonics in power systems include the low frequency oscillations, flicker in lightening system, overloading of shunt filters, saturation of current transformers, interference with the telecommunication and other protection and control equipment [16], [17].

Table 2.1 Harmonic and Interharmonic Contents

Frequencies (Hz)	**Amplitudes (pu)**
50	1
117	0.1
128	0.2
570	0.25
730	0.2
250	0.4

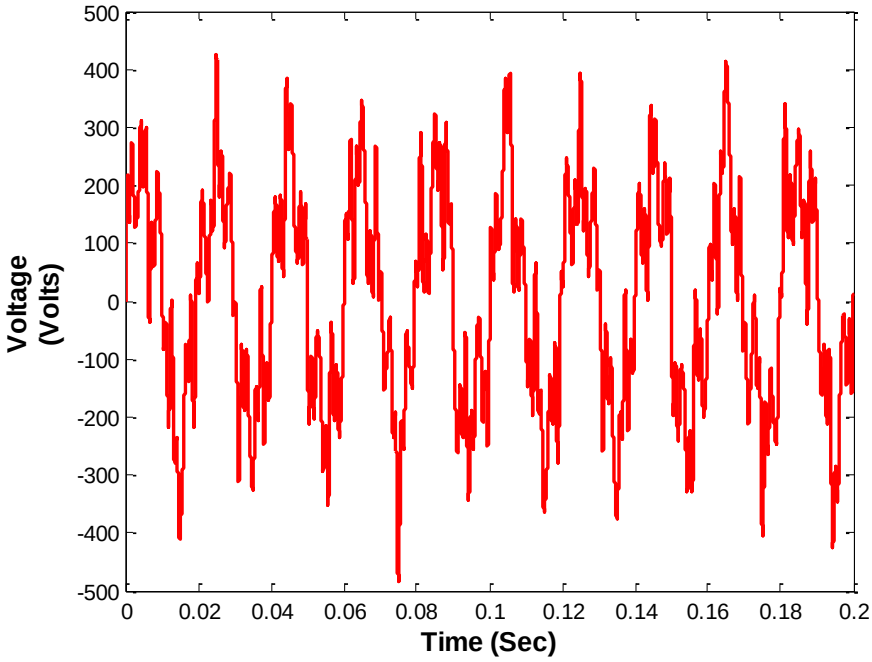

Figure 2.2 Distorted Voltage Supply with Harmonics and Interharmonics Distortion

2.3.3 Subharmonics

Subharmonics are the non integer sinusoidal frequency components whose frequencies are less than the fundamental frequency. Subharmonics in voltage and current signals have no official definition in the measurement standards. It can be treated as a special case of interharmonics for frequency components less than the fundamental frequency of power system. It can be defined mathematically as:

$$0 < f < f_o \tag{2.9}$$

The presence of subharmonics in power systems has a large impact on the performance of power system. The major sources of subharmonics are cycloconverters, wind generators and power converters. The potential effects of subharmonics includes malfunction of control equipment, useful life reduction of induction motor, thyristor wrong shot and life aging by thermal effect [18]–[21].

2.4 Harmonics and Interharmonics Measurement Standards

The international organizations working on PQ issues including IEEE and IEC set standards IEEE-519 and IEC-61000-4-7 to define the measurement standards and permissible range for harmonics pollution and voltage distortion [4], [5]. The standards set recommended limits on both current and voltage distortion.

2.4.1 IEC Standard 61000-4-7

Harmonics are the sinusoids having frequencies integer multiples of fundamental frequency while interharmonics are the non-integer multiples of fundamental frequency. For the better representation of harmonic distortion and reduction in expected spectral

leakage for the measurement of harmonics, IEC defines in 6000-4-7 [5] the harmonic groups and interharmonic groups as the measurement standards for harmonics instead of single frequency component. The IEC 61000-4-7 standard establishes the definition of different groups based on the grouping of DFT spectral lines as shown in Figure 2.3. Each of these groupings of spectral lines corresponds to the calculation of effective rms value of a particular cluster of spectral lines. The standard defines the following groups:

- ***Harmonic groups*** are defined as the sum of the spectral components adjacent to the harmonic frequency in IEC sampling window. The nth harmonic group $G_{g,n}$ can be represented using DFT spectral lines as:

$$G_{g,n}^2 = \frac{C_{k-5}^2}{2} + \sum_{i=-4}^{4} C_{k+i}^2 + \frac{C_{k+5}^2}{2} \tag{2.10}$$

  where C_{k+i} represents the DFT spectral component corresponds to $k+i$ location.

- ***Interharmonic groups*** consist of the spectral lines between two successive harmonic frequencies in the IEC window such as:

$$G_{g,n}^2 = \sum_{i=1}^{9} C_{k+i}^2 \tag{2.11}$$

- ***Harmonic Subgroup*** includes the harmonic frequency and the two immediate adjacent spectral components. The mathematical definition of nth order harmonic subgroups can be written as:

$$G_{g,n}^2 = \sum_{i=-1}^{1} C_{k+i}^2 \tag{2.12}$$

- ***Interharmonic Subgroup*** includes all the spectral components between two consecutive harmonic frequencies excluding the interharmonics adjacent to the harmonic frequencies.

$$G_{g,n}^2 = \sum_{i=2}^{8} C_{k+i}^2 \tag{2.13}$$

where $G_{g,n}$ represents the nth order interharmonic subgroup.

IEC sampling window defines the measurement interval for harmonic and interharmonic distortion which is according to the IEC standard as the 10 cycles for a 50Hz while 12 cycles for a 60Hz power supply system [5].

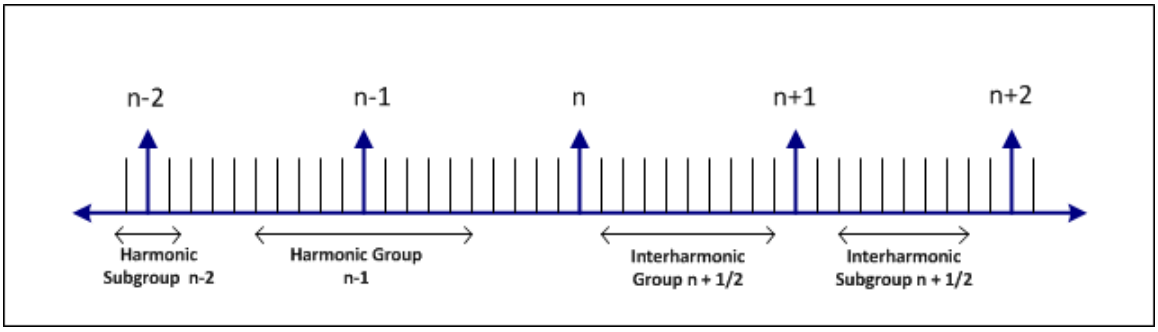

Figure 2.3 Illustration of the Harmonics and Interharmonics Group As Defined in the IEC Standard

IEC standard includes DFT as a signal processing technique to measure the harmonic distortion using 5 Hz frequency resolution. The standard states that the sampling frequency should be kept large enough so that harmonic components can be detected up to 9 kHz.

2.4.2 IEEE Standard 519-1992

The IEEE standard 519 defines the permissible voltage distortion limits that a utility company should comply and current distortion limits that customers should follow for a successful and reliable operation of power system. The standard explains that the harmonic

problem is a responsibility of both utility as well as consumers. The admissible limits of voltage and current distortion are listed in Table 2.2 and Table 2.3. The allowable individual and total harmonic distortions are reducing as the voltage level is increasing as shown in Table 2.2.

Table 2.2 Voltage Distortion Limits

Bus Voltage at PCC	**Individual Voltage Distortion (%)**	**Total Voltage Distortion THD (%)**
69 kV and below	3.0	5.0
69.001 kV through 161kV	1.5	2.5
161.001 kV and above	1.0	1.5

Table 2.3 Current Distortion Limits for General Distribution Systems

(120 V Through 69 000 V)

I_{sc}/I_L	**h<11**	**11≤h<17**	**17≤h<23**	**23≤h<35**	**35≤h**	**TDD (%)**
<20	4.0	2.0	1.5	0.6	0.3	5.0
20-50	7.0	3.5	2.5	1.0	0.5	8.0
50-100	10.0	4.5	4.0	1.5	0.7	12.0
100-1000	12.0	5.5	5.0	2.0	1.0	15.0
>1000	15.0	7.0	6.0	2.5	1.4	20.0

I_{sc}: Maximum short-circuit current at the Point of Common Coupling (PCC).

I_L: Maximum demand load current (fundamental) at the PCC.

The standard defines the limits for individual current harmonics along with the other parameters like TDD and system capability to withstand the harmonic distortion using the ratio of short circuit current to the load current at the point of common coupling. Power systems with higher short circuit capacity to the load current ratio can withstand with the higher harmonic distortions. Table 2.3 shows the acceptable ratios of (I_{sc}/I_L) along with the limits of individual harmonic distortion and TDD.

2.5 Harmonics Measurement Techniques

Harmonic distortion is one of the major PQ problem in electrical networks that can deteriorate the performance of the power systems. The major sources of the harmonics are the power electronics equipment and the connection of nonlinear loads at the PCC. The potential effects of harmonics can substantially reduce the electrical equipment efficiency and useful life. Therefore, in order to obtain a suitable control strategy for harmonic suppression, the amplitude of individual harmonics should be estimated accurately.

2.5.1 Discrete Fourier Transform

Fourier Transform (FT) decompose the signal into a family of complex sinusoids which are symmetrical, smooth and regular. DFT is widely used as the signal processing techniques for the measurement of harmonic distortion. DFT is used to represent the signal magnitude on their respective frequency components.

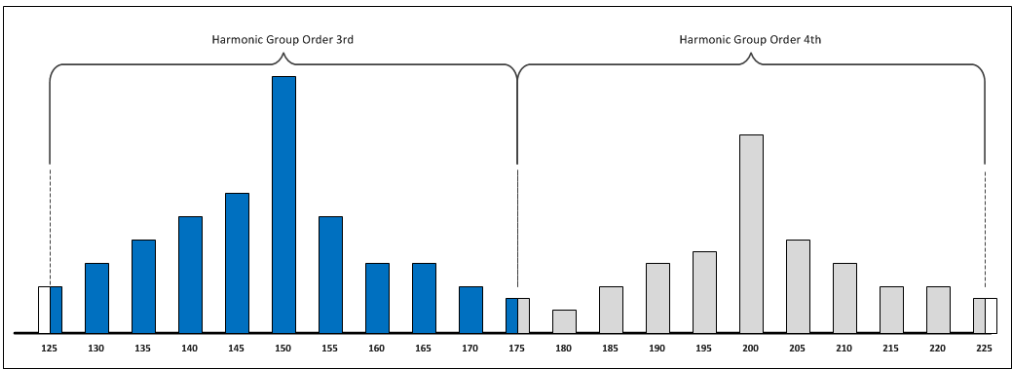

Figure 2.4 Harmonic and Interharmonic Groups [22]

According to the IEC standard Eq (2.10) is used to calculate the harmonic groups of order *n* using the DFT bins keeping the harmonic frequency as the center frequency. Harris [23] presented a comprehensive analysis on the selection of window for the analysis of harmonics using DFT in the presence of broadband noise. In [24] , the author presented an algorithm that computes the necessary constraints for window coefficients to measure the amplitude of the sine wave using DFT. The derived constraints ensure that the quantization error does not exceed the certain threshold level and does not influence the measurement of harmonics. Nyarko and Strsmsmoe [25] proposed asynchronous sampling as a tool to modify the spectral leakage using DFT coefficients. The modified algorithm gives approximately same results, but it is more practical then the synchronous sampling for the measurement of harmonic components.

For the harmonic analysis using DFT, apart from the other problems associated with the DFT analysis like aliasing and picket fence effect, leakage is considered to be as the most challenging problem. The leakage is introduced in the DFT process when the synchronization error occurred between the sampling process and the signal to be analyzed. The effect of leakage can be characterized based on its location as short range leakage is

the leakage to the adjacent frequency bins while long range leakage is the leakage to the far frequency bins. The effect of leakage can be effectively reduced by two main techniques namely the windowing and interpolation. In the first approach, various types of windows can be introduced to reduce the leakage like Hanning window, Hamming window, Blackman window and Kaiser window. The selection of window may affect the particular type of leakage like Hamming window can reduce the short range leakage more affectively while Hanning window is fruitful in order to reduce the long rage leakage [23]. However, the leakage in the adjacent frequency bins cannot be controlled by using the windows other than rectangular window due to the fact that, their passband width is more as compared to the rectangular window. The second approach to reduce the leakage is the interpolation between the frequency bins. The interpolation can work effectively in case of leakage to the adjacent frequency bins and is unable to detect the leakage in the far frequency bins [26], [27]. A combination of both techniques windowing for long range leakage and the interpolation for the short range leakage is considered to be a good solution to tackle the leakage as whole [28]. Interharmonic distortion is also measured quite effectively using the same technique of interpolation window FFT [29].

S.-L. Lu [30] proposed an algorithm that reduces the shortcomings of DFT using Filter Banks. A combination of Finite Impulse Response (FIR) filters with the center frequency shifted to the harmonic frequency is used to isolate and measure the harmonic contents in the signal. The practicality of the proposed algorithm is limited due to the higher order of FIR filter to be used for acceptable accuracy. Another maximally flat filter bank based technique is presented in [31]. The technique is named as Taylor–Fourier Transform (TFT)

due to the expansion of McLaurin series expansion at each harmonic frequency. The time varying harmonics can be estimated accurately using TFT [32].

Iterative DFT (IDFT) based algorithm is proposed in [33] that extrapolates the signal. The frequency resolution can be adjusted adaptively by adjusting the number of samples in time and frequency domain. The proposed algorithm can measure the interharmonic distortion accurately inside the IEC defined window but the performance is not consistent in the presence of noise. To overcome the shortcomings of DFT, Piecewise-overlapped Group-harmonic Energy Restoring (PGER) [34] was proposed to track the harmonic and interharmonic distortion for both the stationary and non-stationary signals. The proposed algorithm restores the energy leaked to the neighboring frequency bins by piecewise overlapping method.

2.5.2 Short Time Fourier Transform

The limitation of DFT was somehow covered by the introduction of Short Time Fourier Transform (STFT). STFT uses a fixed window size to compute the Fourier transform which insures that at what time interval certain frequency band exists keeping the window width small enough to assure that the signal is stationary inside the sampling window. STFT maps the one dimensional time domain signal into two dimensional time and frequency domains by using a fixed window size [35]. The time domain signal *x(τ)* is multiplied with a short duration window function $\gamma(\tau - \mathrm{t})$ as:

$$X(\mathrm{t}, \omega) = \int_{-\infty}^{\infty} x(\tau)\gamma(\tau - \mathrm{t})\, \mathrm{e}^{-j\omega\tau}\, d\tau \tag{2.14}$$

The small duration window function is shifted to cover the whole signal. The computational complexity of STFT is reduced by applying the multiple pole window which updates the STFT at each N^{th} sample [36]. The multiple pole STFT does not possess any side lobe. STFT inherits the resolution problem as narrow window size gives good time resolution but worst frequency resolution and increasing the window size acts other way around as shown in Figure 2.5. The time frequency resolution problem is goes back to the Heisenberg uncertainty principle which states that it is impossible to at what time a particular frequency exist but it is possible to obtain a frequency band exist at a particular time interval.

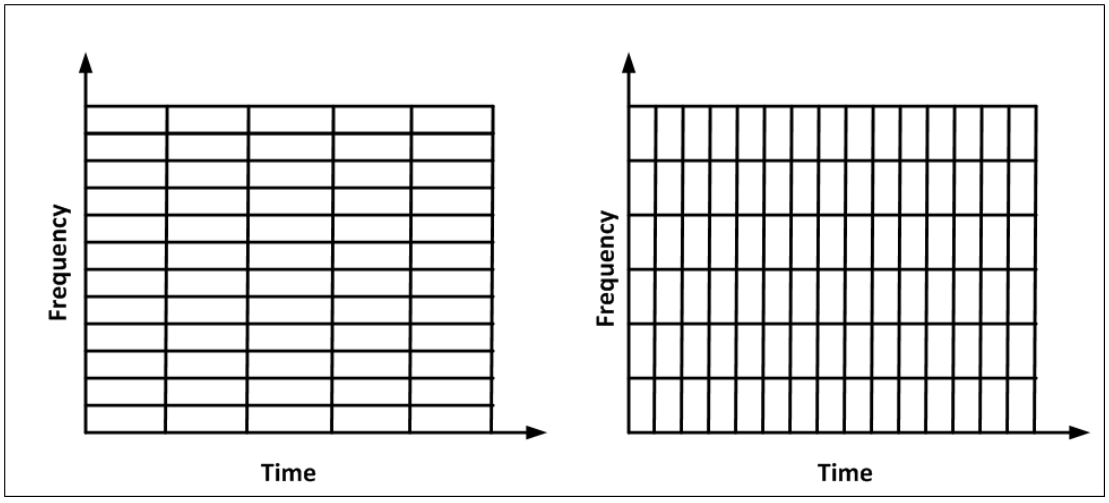

Figure 2.5 Time and Frequency Resolution of Short Time Fourier Transform

2.5.3 Wavelet Analysis

The introduction of Wavelet Transform (WT) overcomes the issues associated with FT and STFT. Wavelet Transform provides the time frequency representation of the signal. The wavelet transform is a mathematical tool that divides data into different frequency bands by passing through low pass and high pass filters. WTs uses the variable scales to dissect a signal into its frequency components [37], [38].

In electrical systems, the voltage and current signals need to be constantly monitored and analyzed for the control and protection of power system. For a proper control action, the signals need to be accurately located in time and frequency, simultaneously. The WT has become an interesting and useful computational tool for evaluating the signal characterization both in the time and frequency domains simultaneously. Continuous Wavelet Transforms (CWT) operates over every possible scale and translation, which limits its usage for real time applications. Apart from that, CWT decomposition is not compatible with the harmonic groups [38]–[41].

Discrete Wavelet Transform (DWT) is widely used in literature to detect and measure the harmonics in power systems. DWT uses a specific set of scale and translation values. In [42], a technique is presented to measure the harmonic and interharmonic distortion using DWT detail coefficients from *d1-d15*. The practicality of DWT is investigated to measure the harmonic distortion in three phase transformers, [43] and harmonic analysis of Electromagnetic transients of single circuit transmission lines, [44]. In [45], harmonic source is detected by computing active power measurement using DWT. The detail coefficients at lower level of decomposition have been compared to identify the harmonic source if only one harmonic source is available in the system or isolate the dominant harmonic source if more than one nonlinear loads are present in the system.

Most of the DWT applications focus on the localization of the power quality disturbance by taking the advantage of time frequency measurement of wavelet transforms. The applicability of DWT for harmonic detection is limited due to its non-uniform frequency decomposition. The first approximation band consists of almost half of the measurable harmonics and gradually reduces the number of harmonics with the higher level of

decomposition. All harmonic contents or groups cannot be isolated using DWT. Other applications of DWT include the signal analysis and signal processing such as peak detection, noise reduction and power quality problems identification and localization.

Pham & Wong [46] implemented CWT to measure the harmonic contents in the voltage and current signals. Input signal was first decomposed to the subbands using wavelet packet transform, after that CWT was applied to measure the effective rms in the subbands. A new technique was also developed to mitigate the image effect of up and down sampling of the signal. The major drawback of this method is the computational complexity, which limits the usage of presented technique in real time systems. DWT decomposition is not compatible with the harmonic standards due to the non-uniform frequency decomposition. Therefore, the DWT based algorithms are not suitable for harmonics and interharmonics measurement.

The limitations of CWT and DWT based algorithms are efficiently covered with the aid of Wavelet Packet Transform (WPT). WPT decomposes a signal into uniform frequency bands. The WPT based decomposition can be made compatible to the harmonic groups defined in the IEC standard.

A new technique based on WPT was presented to find the rms value of the harmonic components [47]. Two level wavelet packet decomposition was used to find the harmonic components and power of the signal. The presented algorithm is only capable to investigate the harmonic distortion.

In [48], a hybrid wavelet-Fourier approach is proposed for the analysis of harmonics. The proposed algorithm first decomposes the signal into uniform frequency bands using WPT

and then applies FT to extract the spectral features in each wavelet band with reduced computational complexity. The proposed method only computes the odd harmonics and does not include interharmonic distortion. Vatansever [49] proposed another hybrid approach using Hilbert Transform (HT) & WPT for the measurement of rms value of fundamental harmonic. WPT level one decomposition was used for fundamental and phase measurements. The limitation of the presented algorithm is that, the measurements are limited to fundamental component only.

Diego and Barros [6], [50], [51] developed techniques for the measurements of harmonic groups, interharmonic groups and subharmonic groups using the IEC-61000-4-7 specified standards. The limitation of the developed algorithms is addressed in [52]. The same reference model with discrete mayer as the mother wavelet instead of vaidyanathan was used. The efficiency of Diego's method is improved using successive filtering technique. In [52], a higher energy component is estimated and then filtered out from the input signal. The iterative filtering approach promises less spectral leakage in adjacent harmonic groups as compared to the previous methods. A mechanism for estimating the even harmonics along with odd harmonics has been introduced.

2.5.4 Kalman Filtering Approach

Kalman Filter (KF) is an optimal estimator that infers parameters of interest from inaccurate and uncertain observations. It operates recursively so that the information can be processed as they arrive. KF estimates the desired parameters from noisy and uncertain stream of inputs as it filters out the noise from the input signal. The Kalman filter is a dynamic estimator suitable for systems described by a state variable form. The generic Kalman filters formulation can be represented as

State Equation : $$X_{k+1} = \phi_k X_k + W_k \quad (2.15)$$

Measurement Equation: $$Z_k = H_k X_k + V_k \quad (2.16)$$

Where X_k represents the states of the system that can be considered as the injected current in case of harmonic measurement at each bus. Φ_k is the state transition matrix whereas V_k and W_k can be obtained from the system transition matrix. The initial covariance matrix depends on the prior knowledge of the system. The covariance matrix can be made diagnol assuming that the current injection at aparticular bus is independent to the others, this may results in a wrong assumption and ultimately affects the system performance. So the covariance matrix is not a completely diagnol matrix.The complete formulation of Kalman Filter is described in [53].

Kalman Filter Gain : $$K_k = P_k H_k^T (\mathrm{H}_k \mathrm{P}_k^- \mathrm{H}_k^T + \mathrm{R}_k)^{-1} \quad (2.17)$$

Update harmonic Estimate: $$X_k = X_{\bar{k}} + K_k(\mathrm{z}_k - H_k X_{\bar{k}}) \quad (2.18)$$

Error Covariance: $$P_k = (\mathrm{I} - \mathrm{K}_k \mathrm{H}_k)\mathrm{P}_{\bar{k}} \quad (2.19)$$

Project ahead: $P_{k+1}^- = \phi_k P_k \phi_k^T + Q_k$ and $X_{\bar{k}+1} = \phi X_k$

where,

P_k	Error covariance matrix
H_k^T	T order harmonic estimationmatrix at step k
K_k	Kalman filter gain at step k
z_k	Harmonic measurement vector at step k

R_k	Measurement of noise variance
Φ_k	State transition matrix
Q_k	System covariance matrix

Kalman Filters were presented to detect, identify and measure the harmonic distortion in power systems [54]. State variables are used as harmonic injection at each buses in unbalanced three phase power system. However, KF cannot track sudden or dynamic changes of signal and its harmonics. To overcome this deficiency, adaptive KF has been proposed for dynamic estimation of harmonic signals to track dynamic and sudden changes of harmonics amplitudes [55]. The proposed adaptive Kalman filter uses two basic models of noise covariance matrix for steady-state and transient estimation. Extended KF was proposed to include the nonstationay behavior of signals [56], [57]. The proposed algorithm is capable of tracking and estimating the harmonics having time varying amplitude and frequency. The basic problem associated with the KF approach is the requirement of previous knowledge of all harmonic component of the system as any component previously not provided in the model may be considered as a noise.

2.5.5 Intelligent Techniques

Harmonic estimation using artificial intelligent techniques is thoroughly investigated in the literature. Linear least square method is proposed to estimate the amplitude and phase of harmonic components in the presence of noise using singular value decomposition (SVD) [58]. Application of Genetic Algorithm (GA) is inspected for detection and estimation of harmonics in distribution system [59], multilevel inverter [60], [61] , Grid connected distributed generation [62] and harmonic elimination in PWM chopper [63]. GA based techniques work well for the measurements of harmonics for nonlinear loads, but the

performance of GA is limited due to the large convergence time and the simultaneous measurement of phase and amplitude is difficult due to the completely different nature of the measured quantities [64].

A hybrid technique of least square method and GA was proposed [65] to address the aforementioned issues. Another hybrid approach using particle swarm optimizer with passive congregation (PSOPC) and least square method was presented in [66]. The presented algorithm uses PSOPC for harmonic phase detection and least square method for harmonic amplitude estimation. Ray and Subudhi [67] proposed an improved hybrid harmonic estimation strategy based on Recursive Least Square (RLS) and Bacterial Foraging Optimization (BFO for determining amplitude and phase of harmonic components using known and estimated parameters respectively.

2.6 PQ Disturbance Classification

There are numerous types of PQ problems, which might have varying and diverse causes such as impulses, oscillations, sags, swells, interruptions, under-voltages, over-voltages, DC offset and harmonics [68]. According to IEEE Std-1159, the short-duration voltage variations are variations of the root mean square (RMS) value of the voltage over short time intervals.

Short duration voltage variations are mainly divided into three categories namely voltage sag, voltage swell and interruption. These disturbances are caused by the switching of the loads and capacitor banks, starting of the loads having large input current and faults. Voltage interruption can be categorized as the drop of voltage to 10% or less from the nominal RMS value due to the switching of loads. Voltage interruption last only for less

than a minute. If it sustains more than a minute with voltage magnitude ranges from 90% to 10%, the disturbance is named as voltage sag. Voltage swell is categorized as the voltage exceeds from 110% to 180% of its nominal value and last from 0.5 cycles to 1 minute [69]–[71]. The classification of the PQ disturbances is entirely dependent on the calculation of the voltage RMS value and its accuracy is highly dependent on the window length used to compute the voltage RMS value [72].

Previously, Fourier Transform (FT) [73] and Short Time Fourier Transform (STFT) [74] were presented as signal processing techniques for the analysis of PQ disturbances. FT is more suitable for the steady state analysis of stationary signals. However, PQ disturbances are usually non-stationary and transient in nature which limits the usage of FT for PQ disturbances analysis. STFT provides the time frequency analysis of signals using a fixed time window. The performance of STFT is highly dependent on the selection of window length. Point by point comparison was used to detect the power quality disturbance between successive cycles [75]. However, this technique was insensitive to the instantaneous power quality problems like harmonic and inter-harmonic distortion and only responds to the system when a certain threshold of disturbance is achieved compared to the previous cycles.

Recently, Wavelet based approaches are considered as a potential candidate for the classification of PQ disturbances by segmenting the received signal into low and high frequency bands with different time scale resolutions [76]–[80]. A continuous wavelet transform based voltage sag and transients detection technique is presented in [76]. A new inductive learning approach based on decision tree was proposed in [77]. The size of decision tree was reduced using wavelet based features. A wavelet based self-organizing

learning array system (SOLAR) is presented in [78] for the classification of PQ disturbances. Dash *et al.,* draw a comparison between wavelet transform and S-transform based PQ classification using time series data [79], where wavelet transform as an efficient tool for PQ classification was presented. A new method based on discrete wavelet norm entropy feature vector and ANN is presented to classify the PQ disturbances [80]. Present automatic classification techniques for multiple PQ disturbances need much improvement in terms of their computational complexity, accuracy, flexibility and consistency.

2.7 Harmonics Mitigation Techniques

There are several harmonic mitigation strategies developed in the literature. Among them, passive and active harmonic filters are the most popular. These filters can be modeled as voltage or current source inverter. Passive filters provide a low impedance path to the harmonic current and trap the harmonics while the active filters inject the same current as the harmonic current but opposite in direction to cancel the effect of the harmonics and block the possible flow in the system.

2.7.1 Passive Harmonic Filters

Passive harmonic filters present low impldance to the nonlinear load current harmonics as compared to the source impedance . Harmonics are likely flowing to the lower impedance of passive filters and they are ultimately trapped. There are many different types of passive harmonic filters designed for a particular type of application. The basic types are notch filter (single tuned) and high pass filter with first second and third order charactrisitics as shown in Figure 2.6. The notch filter is connected in shunt with the load to provide an alternative path to the harmonic current. The optimal location and size of the harmonic

filter is a crucial issue and throughly investigated in the literature. [81] presents the optimal size and location of passive harmonic filters in distribution system.

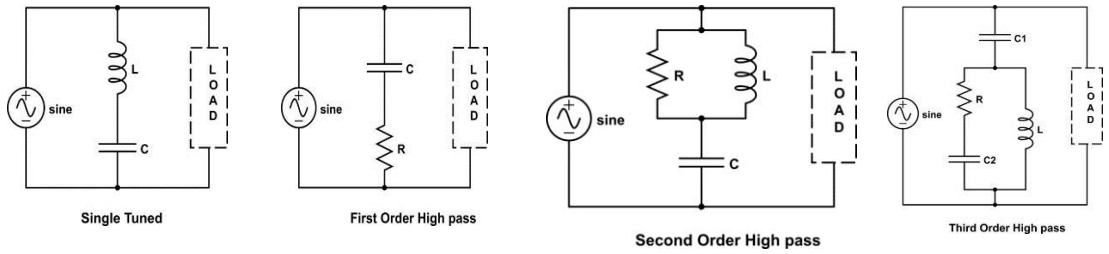

Figure 2.6 Single Tuned and High Pass Passive Filters [82]

High pass passive filters are used to eliminate more than one harmonics from the system. The use of the first order high pass harmonic filter is limited because it distorts the fundamental component as well. Second order harmonic filters are widely used to eliminate the harmonic contents higher than the cutoff frequency and reduce the limitation of the first order filters [83], [84]

Passive filters are not suitable for changing power systems conditions as once they are installed it is not easy to change their tuning frequency. Passive harmonic filters provide alternative path to trap the harmonics providing less impedance path to flow the harmonic current as compared to the source. If the source impedance changes the performance of passive filters is degraded. Outage of a parallel branch can also increase the impedance of the systems and detune the passive filter [85].

2.7.2 Active Power Filters

Active Power Filters (APF) are power electronic based devices that inject current in the system equals but opposite to the harmonic current generated by the nonlinear loads. The main advantage of active power filters is their capability to mitigate more than one

harmonic components at the same time. As APFs are power electronics based devices, they can mitigate selective harmonic or group of harmonics as well. APF can be divided into three main categories as shown in Figure 2.7, namely, shunt, series and hybrid configuration.

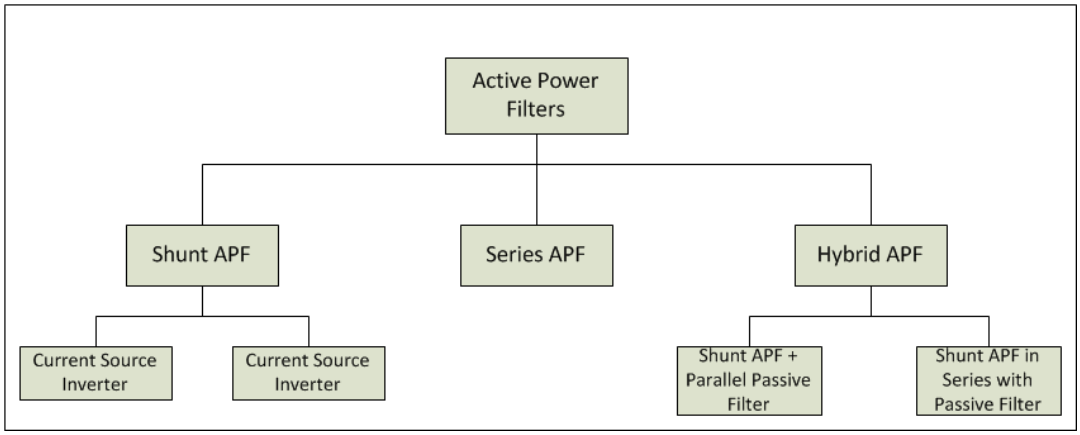

Figure 2.7 Active Power Filters [86]

Series Active Filters are connected in series with the load. They can be modeled as voltage control source to mitigate the harmonics in power system. The impedance of series active filters is increased at harmonic frequency as the voltage is increased and block the harmonic currents to flow in the power system. The major drawback of series active filters is the requirement of a transformer to inject the voltage to compensate the harmonic currents. During short circuit, a high current is passed through the secondary of the transformer and cause a potential damage which ultimately results the isolation of the system [87]. Due to the series connection of active power filter with the load, malfunction may disturb the whole power system. Jacobina [88] proposed a series active filter without dc source and isolation transformer for harmonic mitigation.

Shunt Active Power Filters **(SAPF)** are the most commonly used active filters for harmonic elimination. SAPF can be modeled as controlled current source which injects current in the power system equals to the harmonic current but opposite in direction to suppress the harmonics [89]. The basic configuration of SAPF consists of DC-bus capacitor, power electronic switches and interfacing inductors. The harmonic compensation current is achieved by shaping the compensation harmonic waveform using voltage source inverter switch. The shape of the distorted waveform is estimated by subtracting the load current from the pure sinusoidal current waveform. The load extracts the sinusoidal current from source and the remaining non-sinusoidal component is provided by SAPF [90], [91].

A new control method based on instantaneous reactive power is developed in [92] for SAPF. Machmoum [93] presented a DSP based algorithm for the selective harmonic elimination using SAPF. The presented algorithm uses the fundamental positive sequence voltage along with the phase lock loop (PLL) to reduce the time delay and improve the dynamic characteristics of the filter. The effect of the control strategy using frequency domain (Fourier transform) [94] and time domain using p-q theory to observe the performance of SAPF under different conditions is investigated in [95], [96].

The major advantages of SAPF are the capability of mitigating more than one harmonic component selectively or all available harmonic contents. Since the SAPF works in parallel, so malfunctioning does not create any problem for the whole system.

2.8 Harmonic Detection and Measurement Based On LabVIEW and Embedded Systems

LabVIEW (Laboratory Virtual Instrumentation Engineering Workbench) is used for system design using higher-level graphical programming language. LabVIEW is the property of National Instruments used to implement the sophisticated systems. The compatibility of LabVIEW with reconfigurable hardware along with its data capturing/logging system makes it an eye-catching tool for real time development.

LabVIEW is extensively used in literature for PQ disturbance detection and analysis [97]–[101]. Real-time monitoring and analysis systems based on LabVIEW software and NI hardware have been developed for frequency monitoring, voltage and current waveforms readings, and harmonics analysis. The requirements of software and hardware for automatic measurements of electrical voltage and current based on virtual instruments have been described in [102].

In this work, LabVIEW is used and implemented to measure the real time voltage and current signals, detect the harmonic and interharmonic distortion. The developed prototype is also used for harmonic mitigation.

2.9 Discussion

This literature survey has revealed the following limitations for the detection, measurement and mitigation of harmonics and interharmonics distortion in voltage and currents signals:

- Analysis of stationary signal is performed quite accurately using DFT, however the DFT is is unable to track the sudden changes in signals and large errors are expected in measurements due to its inability to consider the nonstationarity in the signals during analysis.
- KF cannot track the interharmonics distortion correctly, as it requires the prior knowledge of the system for accurate measurement.
- The accuracy of artificial intelligent techniques is highly dependent on the initial population size and training data. The large convergence time and finite set of training data limits their usage for real time applications.
- Performance of conventional passive filters are strongly affected by source impedance and resonance phenomena between filter and source. Passive filters can easily detuned in changing power system conditions.

This thesis addresses these limitations through the development of new techniques for accurate detection, analysis and mitigation of power system harmonics as follows:

- A new technique based on wavelet packet transform is proposed for the measurement of harmonics and interharmonics group distortion according to the standard IEC-61000-4-7.
- New infinite impulse response filter bank is proposed and designed to overcome some limitations of WPT. The proposed algorithm utilizes half number of filters as compared to the WPT based techniques, which reduced the computational complexity as well as improve the processing time. The proposed method is best suitable for real-time detection and monitoring applications.

- A harmonic mitigation strategy is developed using shunt active power filter to mitigate the harmonics and interharmonics distortion.
- A laboratory scale prototype is also developed for the accurate detection, measurement and mitigation of PQ disturbances using proposed techniques.

CHAPTER 3

MEASUREMENTS OF HARMONICS AND INTERHARMONICS USING WAVELET PACKET TRANSFORM

The IEC 61000-4-7 specifies the use of the DFT in the reference instrument for the measurement of harmonic components of voltage and current signals. The standard itself states that, the use of DFT does not preclude the use of other signal processing techniques. This chapter presents a wavelet packet transform based technique for the accurate detection and estimation of harmonics and interharmonics groups defined in the IEC standard. Several case studies are presented to measure the harmonic and interharmonic distortion in the voltage and current signals.

3.1 Wavelet Analysis

The introduction of Wavelet Transform overcomes the issues associated with FT and STFT. Wavelet transform uses short window length at high frequency and long window length at lower frequency to rectify the problems associated with the fixed window length at all frequencies used in STFT. The use of variable window length solves the issues mentioned in the Heisenberg uncertainty principle to certain extent due to the fact that the

high frequency component can be localized well in time while the low frequency component can be localized well in frequency as shown in Figure 3.1.

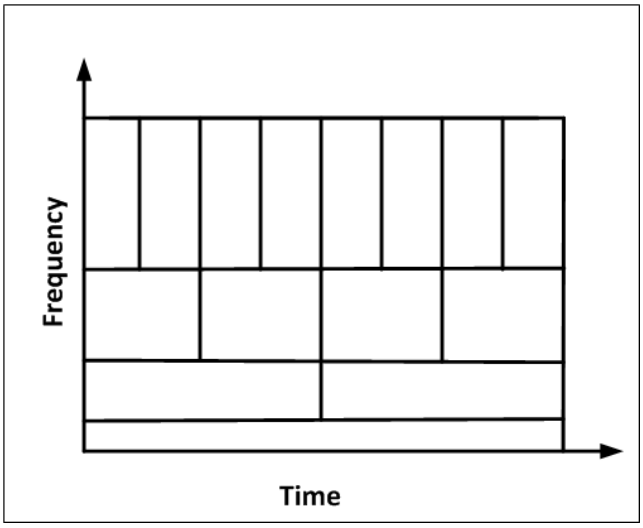

Figure 3.1 Time and Frequency Resolution of Wavelet Transform

3.1.1 Continuous Wavelet Transform

Wavelet transform decomposes a signal into family of finite duration wavelets that can be symmetrical or asymmetrical, regular or irregular, smooth or sharp. Wavelet Transform computes the inner product of a signal with the family of wavelets. The family of wavelets are the dilated and translated versions of mother wavelets such as:

$$X_{\omega}(a,b) = \frac{1}{\sqrt{|a|}} \int_{-\infty}^{+\infty} x(t)\psi^{*}(\frac{t-b}{a})dt \qquad (3.1)$$

Where $\psi(t)$ is the mother wavelet which is continuous in both time as well as frequency. $x(t)$ is the input signal and a ,b are the scaling and translation factors respectively. X_{ω} represents the similarity between the mother wavelet scaled at a and shifted at b with the input signal $x(t)$. Careful selection of the mother wavelet reduces the distortion in each

output band. The distortion between the adjacent frequency bands can be reduced by increasing the number of wavelet coefficients.

Application of CWT includes the signal analysis, self-similarity and time frequency relationship.

3.1.2 Discrete Wavelet Transform

CWT is obtained through integration of mother wavelet and input signal while the DWT can be obtained by discretizing the CWT. The DWT represents the input signal *x(n)* with respect to the versions of mother wavelet *g(n)* scaled by *'a'* and shifted by *'b'* as given in Eq (3.2).

$$DWT(m,k) = \frac{1}{\sqrt{a^m}} \sum_n x(n) g(\frac{k - nba^m}{a^m}) \tag{3.2}$$

Mallat [103] proposed a method for obtaining Discrete Wavelet Transform by taking the advantage of CWT similarity with filters equation. Input signal is passed through a number of low pass and high pass filters defined in equations (3.3) and (3.4) to get the required frequency resolution as follows:

$$c(n) = \sum_k h(k - 2n)\, \mathrm{x}(k) \tag{3.3}$$

$$d(n) = \sum_k g(k - 2n)\, \mathrm{x}(k) \tag{3.4}$$

where, $c(n)$ and $d(n)$ are the coefficients of quadrature mirror filters. In DWT, the input signal is decomposed into non-uniform frequency bands in such a way that higher frequency bands contain more harmonics as compared to the lower frequency bands as shown in the Figure 3.2.

High Pass (HP) filter produces the detail coefficients *d(n)* while the Low Pass (LP) filter produces the approximation coefficients *a(n)* as shown in Figure 3.2. The detail coefficients are passed again through LP and HP filters to produce the approximation and detail coefficients at second stage. Each time the input signal is passed through LP and HP filters, the frequency bands is reduced to half and ultimately half number of samples are required by sampling theorem to accurately represent the signal. The reduction of samples at each stage ultimately reduces the time resolution by half as the complete signal is now represented by half number of samples and the signal can be localized accurately in time at higher stages as compared to the lower ones.

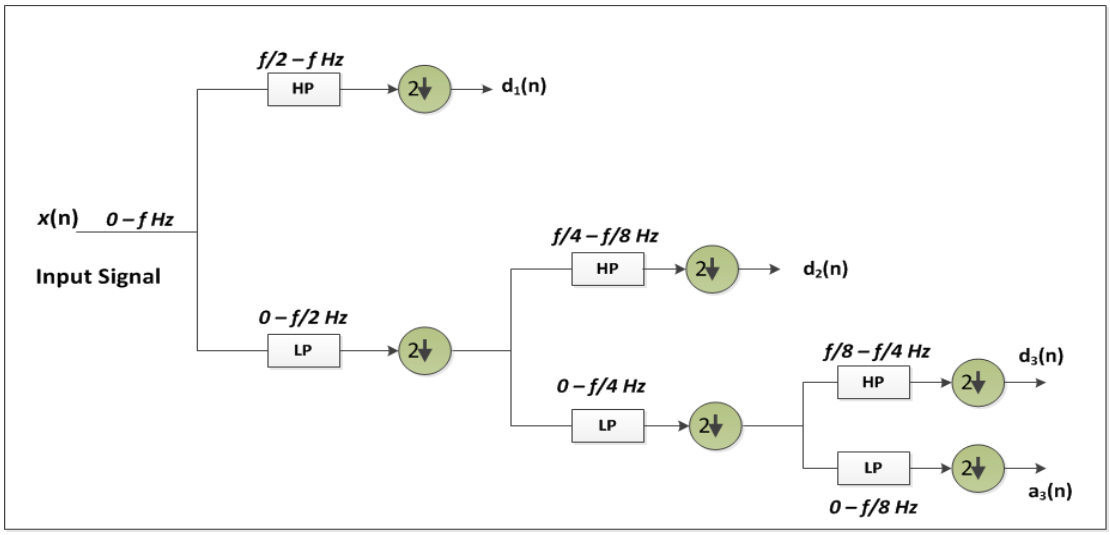

Figure 3.2 Decomposition Tree of Discrete Wavelet Transform [50]

3.1.3 Wavelet Packet Transform

In WPT, a complete binary tree decomposition is obtained by successively passing the input signal to high pass and low pass filters. Due to the uniform frequency bands WP decomposition can be used to measure the harmonic groups defined in the standard. Figure 3.3 shows the three level WP decomposition in which an input signal is passed

through a series of LP and HP filters. The required frequency resolution can be obtained by passing the obtained signal to next level of WP decomposition.

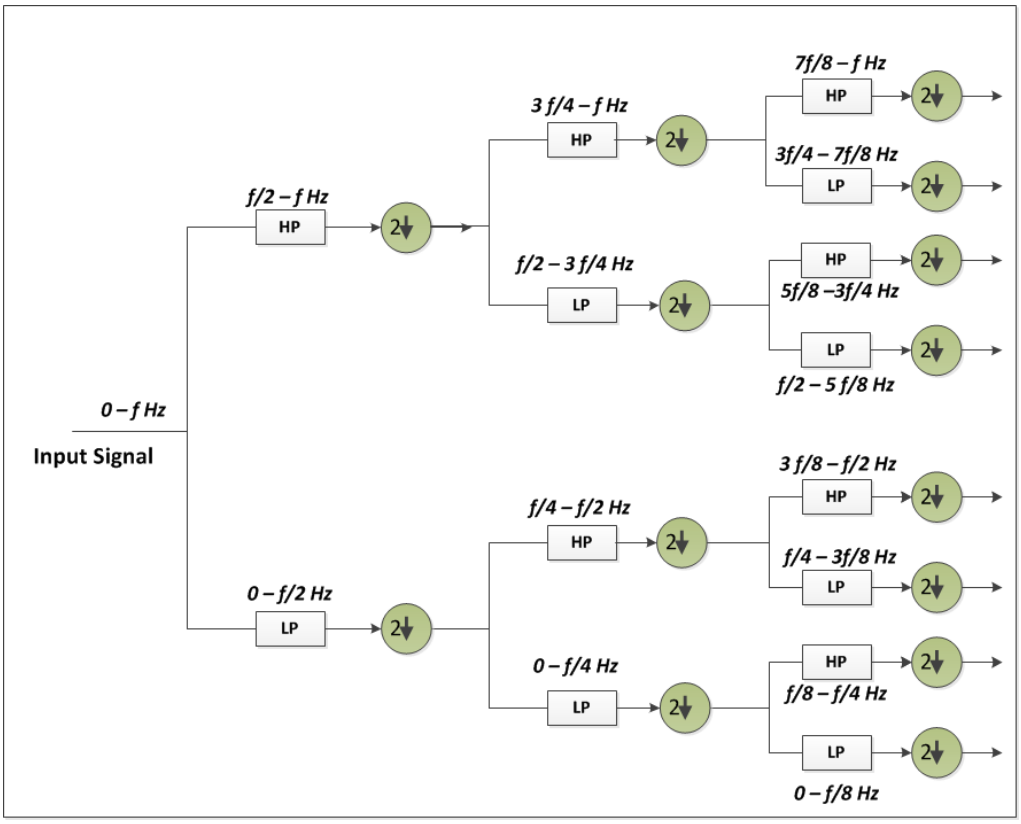

Figure 3.3 Decomposition Tree of Wavelet Packet Transform

3.2 Wavelet Scaling Function and Filters

Wavelets are defined by the wavelet function and scaling function in the time domain. Wavelet function can be defined as a bandpass filter which halves the bandwidth at each level. An infinite number of levels are required to cover the entire spectrum. Therefore, scaling functions are used, which filters the lowest level of transform using finite impulse response (FIR) filter to ensure that the whole spectrum is covered. The width of the scaling function is an important design parameter in wavelet analysis. A large number of wavelet coefficients and scale information is required for shorter spectrum of scaling functions.

Therefore, the selection of the scaling function width directly affects the accuracy of wavelet analysis. Figure 3.4 represents the Daubechies wavelets with different number of vanishing moments. As the number of vanishing moments increases, the response of the wavelet analysis improves due to the shorter and smoother wavelet scaling function. Daubechies *db8* has much shorter and smoother wavelet scaling function as compared to the *db2* wavelet scaling function as shown in Figure 3.4.

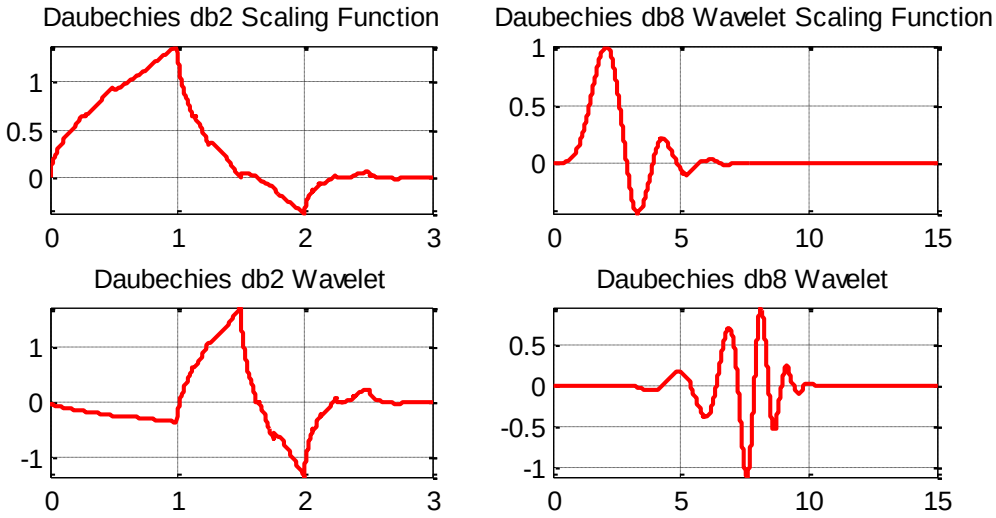

Figure 3.4 Comparison of Daubechies db2 and db8 Wavelets

Figure 3.5 shows the orthogonal Daubechies db4 scaling and wavelet functions along with their associated lowpass and highpass quardrature mirror filters. The analysis filter is used to decompose a signal for analysis purpose, while reconstruction filter is used to construct back the original signal. The length of these FIR filters are *2N* for *dbN* wavelets.

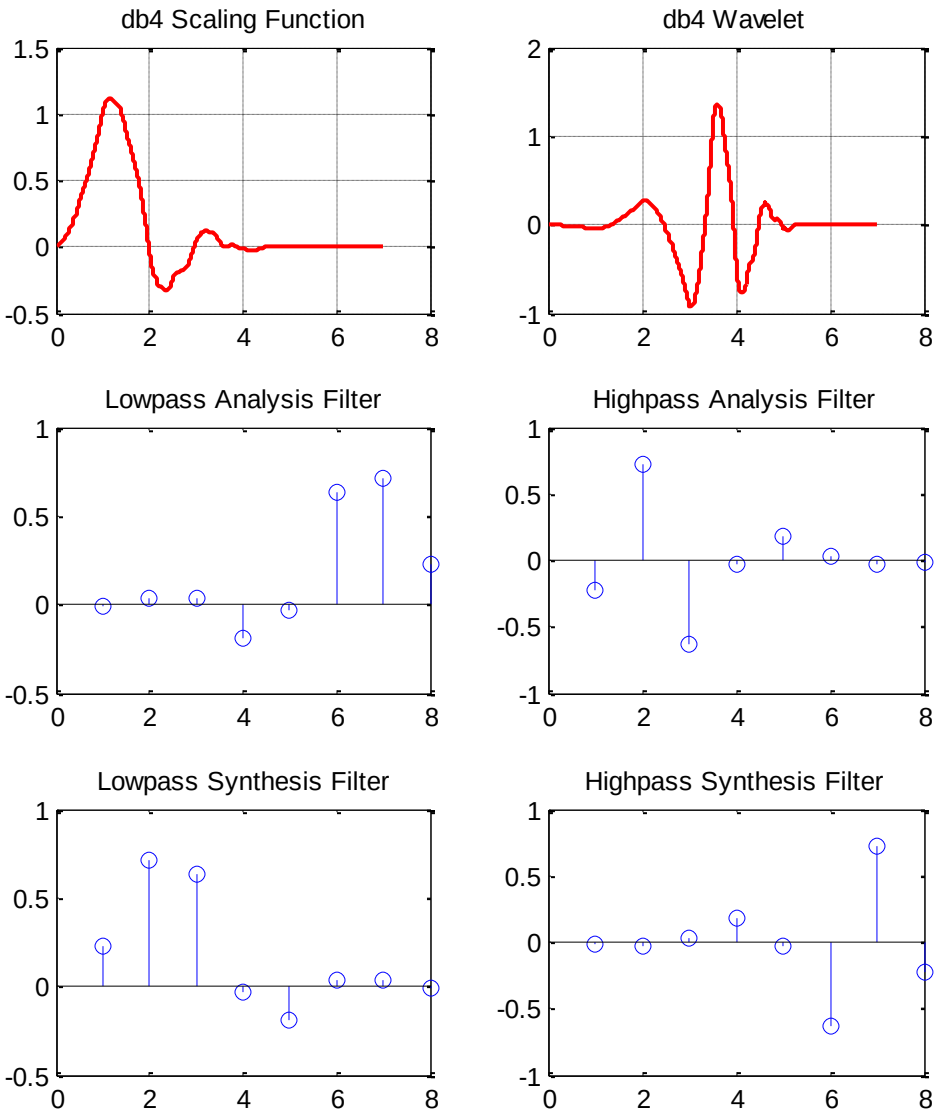

Figure 3.5 Daubechies db4 Wavelets and Filters

3.3 WPT Based Proposed Algorithm

The use of WPT permits the measurements of harmonic groups by decomposing the input signals into uniform frequency bands. Wavelet tree is decomposed in such a way that harmonic frequency is adjusted in the center of the wavelet band. This will help in compensating the spectral leakage to the adjacent frequency bands.

Generally, a signal *f* can be decomposed into approximation and detail components, as follows:

$$f = \sum_{k} a_{j_0 k} \varphi_{j_0 k} + \sum_{j \le j_0} \sum_{k} d_{jk} \psi_{jk} \tag{3.5}$$

where,

$$\psi_{jk}(t) = 2^{-j/2} \psi\left(2^{-j} t - k\right) \tag{3.6}$$

$$\varphi_{j_0 k}(t) = 2^{-j_0/2} \varphi\left(2^{-j_0} t - k\right) \tag{3.7}$$

$\psi(t)$ and $\varphi(t)$ represent the mother wavelet and the scaling function respectively. The approximation coefficients, $a_{jok,}$ and detail coefficients, $d_{jk,}$ can be computed as:

$$d_{jk} = \int f(t) \psi_{jk}(t) dt \tag{3.8}$$

$$a_{j_0 k} = \int f(t) \varphi_{j_0 k}(t) dt \tag{3.9}$$

The root mean square (RMS) of electrical quantities like voltage and current can be measured using instantaneous voltage and currents using equation (3.10)

$$V_{rms} = \sqrt{\frac{1}{T}\int_0^T v^2(\mathrm{t})\,\mathrm{dx}}, \qquad I_{rms} = \sqrt{\frac{1}{T}\int_0^T i^2(\mathrm{t})\,\mathrm{dx}} \tag{3.10}$$

The time domain RMS calculation can be computed using wavelet coefficients at node *n* and level *j* decomposition using equation (3.11).

$$V_{rms} = \sqrt{\frac{1}{2^N}\sum_{k=0}^{2^{N-j}-1}\left(a_{jo}(k)\right)^2 + \frac{1}{2^N}\sum_{n=1}^{2^j-1}\sum_{k=0}^{2^{N-j}-1}\left(d_{jn}(k)\right)^2}$$

$$I_{rms} = \sqrt{\frac{1}{2^N}\sum_{k=0}^{2^{N-j}-1}\left(a'_{jo}(k)\right)^2 + \frac{1}{2^N}\sum_{n=1}^{2^j-1}\sum_{k=0}^{2^{N-j}-1}\left(d'_{jn}(k)\right)^2} \tag{3.11}$$

Where d_{jn} and a_{jo} represents the wavelet detail and approximation coefficients at level *j* and node *n* for voltage signals, while d'_{jn} and a'_{jo} are the wavelet detail and approximation coefficients for current signals respectively.

The imperfect frequency response of the filters may result in spectral leakage to the adjacent harmonics. So a two-stage process is proposed and adopted in this work. In the first stage, five level wavelet packet decomposition is applied to the sampled signal.In the second stage, a grouping mechanism is applied on the resultant WP decomposition as the fifth level decomposition frequency bands does not correspond to the harmonic groups. Figure 3.6 presents the block diagram of the proposed algorithm.

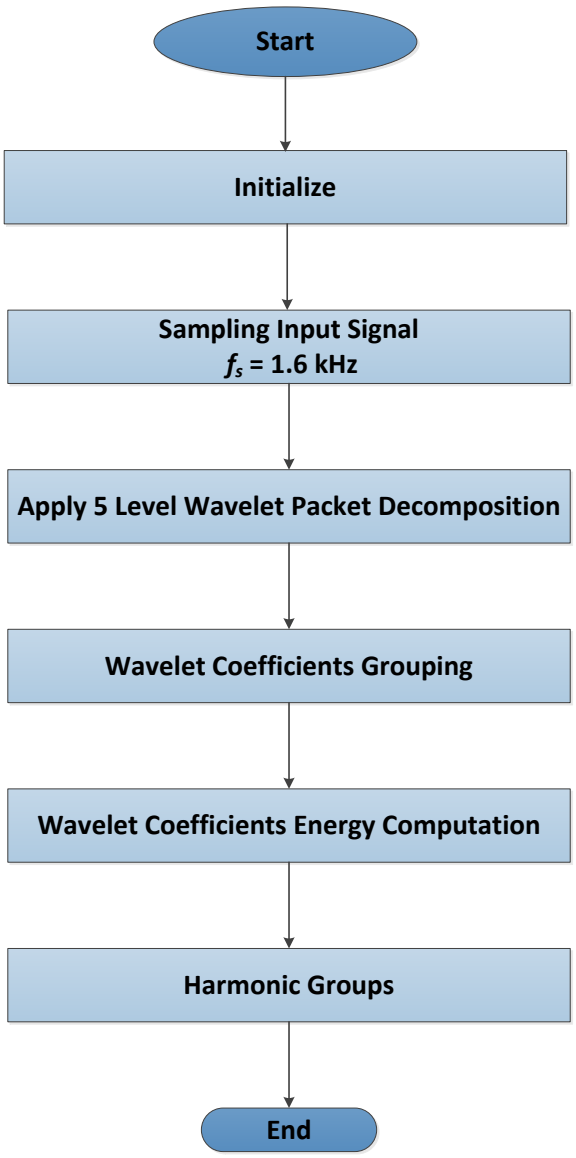

Figure 3.6. Block Diagram for Harmonic Groups Computation using WPT

The proposed algorithm samples the input signal using sampling frequency of 1.6 kHz as it can easily cover the small harmonic group measurement defined in the IEC standard [6]. The small harmonic group represents the measurement of first fifteen harmonic groups. The sample signal passes through the 5-level wavelet packet decomposition. The resultant sub frequency bands after decomposition consist of 25 Hz bandwidth each. So a two-level grouping is assumed in which 25-50 Hz and 50-75 Hz bands are grouped together to form

a 50 Hz band from 25-75 Hz, this will insure the fundamental frequency as the center frequency of the first harmonic group which ultimately results in the minimum spectral leakage to the adjacent bands as shown in Figure 3.7. The grouped frequency bands are used to measure the harmonics group distortion, the group (25-75 Hz) corresponds to the first harmonic group and the group (75-125 Hz) corresponds to the second harmonic group with group order specified by center frequency of each group as:

$$G_{g,h} = \sqrt{\frac{1}{M}\sum_{j}[(d_{i,5}(k))^2 + (d_{(i+1),5}(k))^2]} \tag{3.12}$$

Where G represents the harmonic group of order *'h'* evaluated at 5th level, '*j*' is the WP decomposed sub band identifier while *'M'* represents the total number of samples. The proposed algorithm uses discrete mayer as a mother wavelets for the computation of harmonic distortion as shown in Figure 3.8 and Figure 3.9.

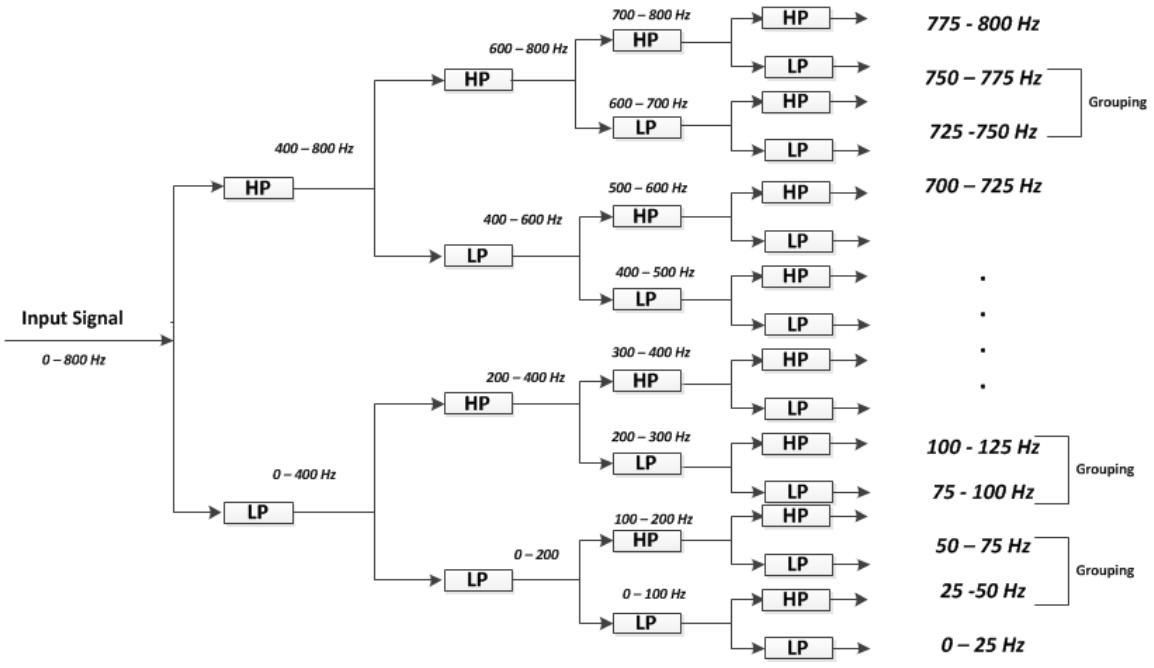

Figure 3.7 WP Decomposition Tree for 1.6 kHz Sampling Frequency

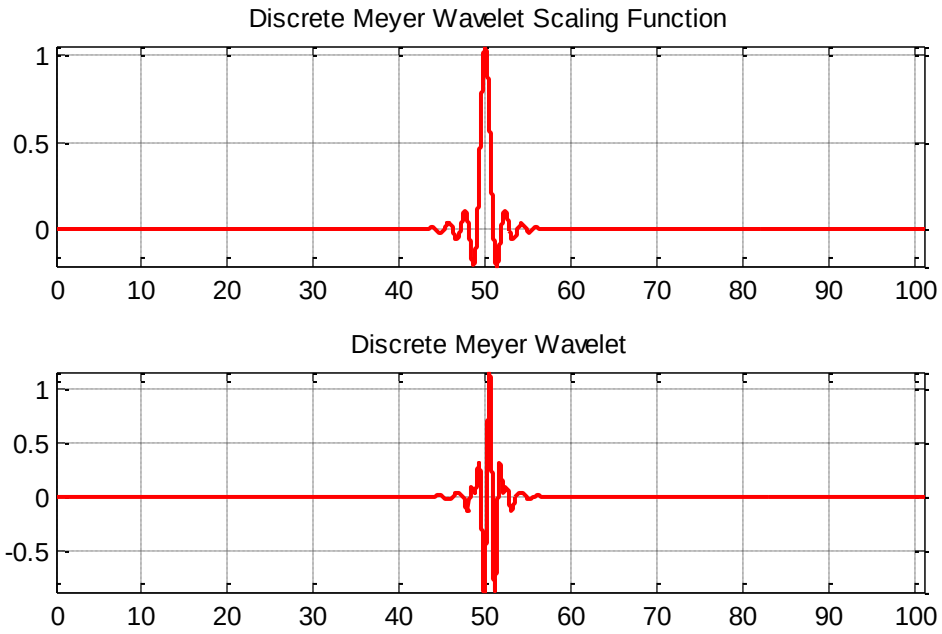

Figure 3.8 Discrete Meyer Wavelets

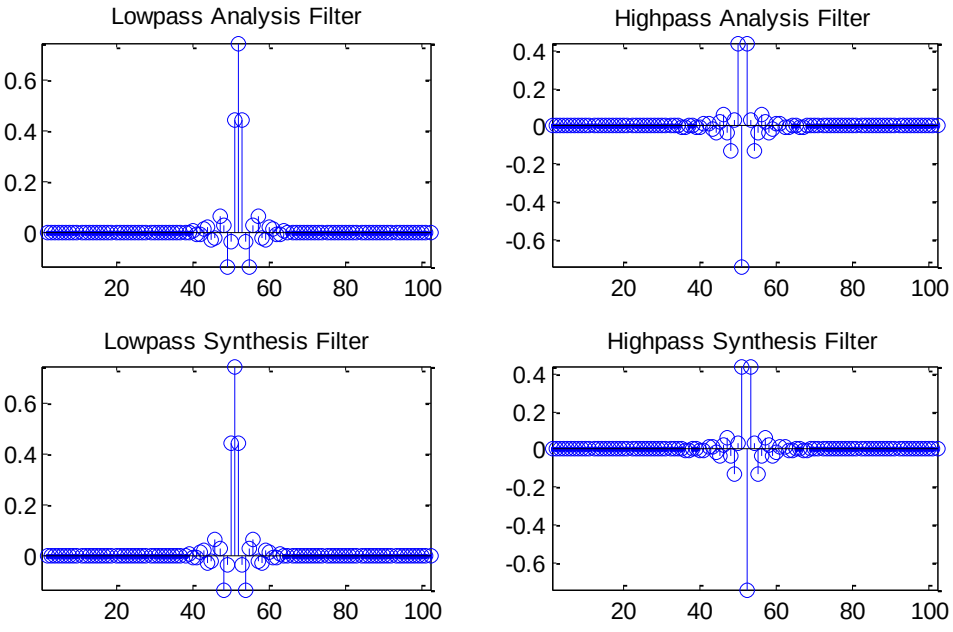

Figure 3.9 Discrete Meyer Filters

3.3.1 Interharmonics Measurement using WPT

The measurement of interharmonics is not a trivial task. An interharmonics waveform may not be necessarily regular. It may be an aperiodic signal and even asymmetric depending upon the observation window. The IEC standard 61000-4-7 defines interharmonic groups as the all frequency bins of DFT between two successive harmonic frequencies as shown in Figure 3.10.

For DFT analysis, sampling window should be wide enough so that it may become synchronous with the signal to be analyzed. These wide window lengths might not be suitable for the non-stationary signals. So, a new method is required to overcome the issues associated with the DFT based algorithms.

To compute the first fifteen interharmonics groups, a WPT based interharmonics groups measurement strategy is developed as shown in Figure 3.11. The input signal is sampled using IEC defined window of 0.2 sec. The signal is sampled using the sampling frequency f_s = 1.6 kHz. The sampled signal is passed through a high pass filter to reduce the distortion introduced by the high power fundamental component in the neighboring bands. The filtered signal is passed through a four level WP decomposition. Finally, the energy content in each subband is computed to find the interharmonics groups distortion.

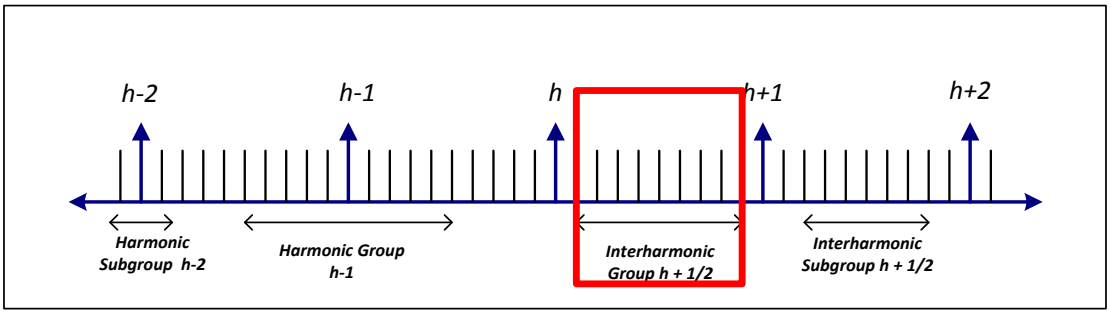

Figure 3.10 Interharmonic Groups Defined in IEC Standard

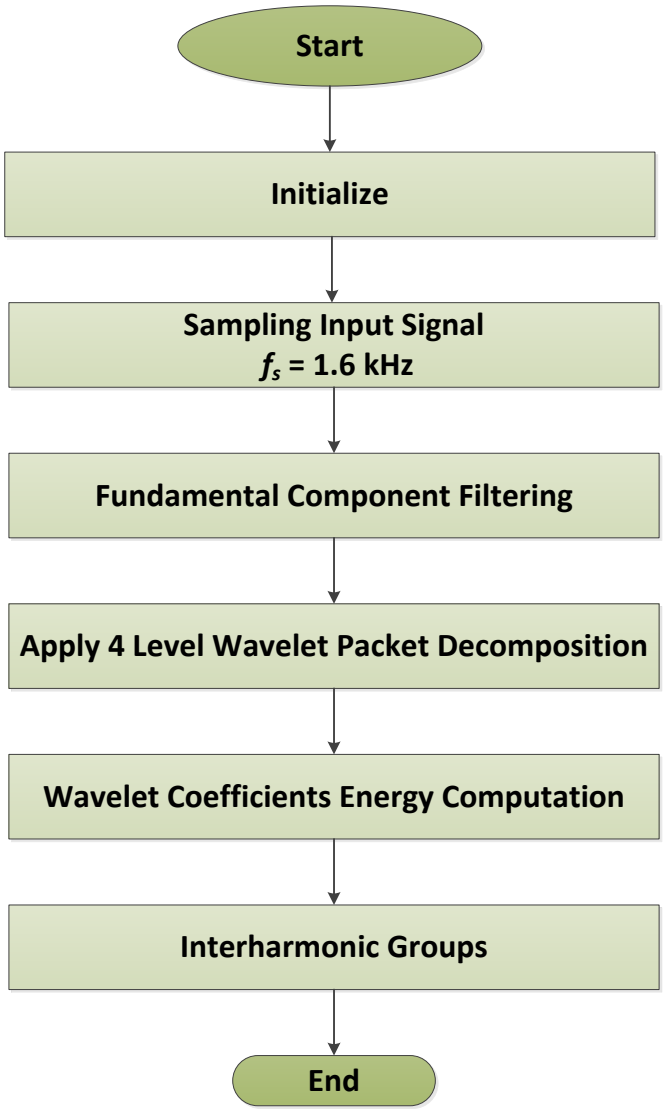

Figure 3.11 Block Diagram for the Measurement of Interharmonic Groups using WPT

3.4 Results and Discussion

Wavelet packet transform is applied to the stationary and non-stationary signals to measure the harmonic and interharmonic distortion in voltage and current signals. Different test cases are applied to investigate the applicability of the proposed WPT based algorithm. The test cases include single tone analysis, harmonic groups measurement in stationary signals, harmonics groups measurement in non-stationary signals and finally the interhamonic groups measurement.

3.4.1 Single Tone Analysis

In this test, the analysis of a single tone signal consisting of the fundamental frequency 50 Hz and harmonic frequencies of third, fifth, seventh, ninth and eleventh harmonic signal is presented in Table 3.1. A single tone of 1 pu is applied and the rms values are calculated against the grouped harmonic frequency bands. It can be seen from Table 3.1 that, moving towards the center of the decomposition tree leads to an increase in the leakage introduced by the WP decomposition. This can be due to the imperfect filtering response of the analysis filter. The seventh harmonic frequency has the maximum leakage as it results in 0.9569 by applying a 1 pu tone signal at 350 Hz. The result shows that an error of 4.31 % is observed in the calculated rms value.

3.4.2 Harmonic Analysis using Stationary and Non-Stationary Signals

This section presents the harmonic analysis using stationary and non-stationary harmonically distorted voltage and current signals. The test cases I analyses the harmonics present in a six-pulse diode rectifier current waveform, while the test case II analyses the occurrence of a non-stationary harmonic distortion present in the supply voltage.

Figure 3.12 and Figure 3.13 show the harmonically distorted current waveform and its corresponding spectra obtained by WPT. The test signal I consists of fundamental current waveform along with third, seventh and eleventh harmonics with different amplitudes.

Table 3.1 Single Tone Analysis using WPT

Harmonic Order	50 Hz	150Hz	250Hz	350Hz	450Hz	550Hz
1	***0.9808***	0.1525	0.0658	0.0567	0.0287	0.0187
2	0.1461	0.2211	0.0878	0.0746	0.0347	0.0195
3	0.0659	***0.9799***	0.1135	0.0796	0.0362	0.0205
4	0.0284	0.1880	0.2069	0.0877	0.0374	0.0216
5	0.0158	0.0750	***0.9647***	0.1447	0.0505	0.0233
6	0.0115	0.0385	0.1869	0.2005	0.0594	0.0261
7	0.0064	0.0235	0.1058	***0.9569***	0.2208	0.0319
8	0.0053	0.0167	0.0556	0.1783	0.1726	0.0546
9	0.0039	0.0131	0.0283	0.2341	***0.9772***	0.0945
10	0.0028	0.0090	0.0177	0.0430	0.1219	0.1605
11	0.0021	0.0066	0.0124	0.0233	0.0708	***0.9883***
12	0.0015	0.0048	0.0088	0.0167	0.0403	0.1588
13	0.0011	0.0034	0.0061	0.0119	0.0299	0.0944
14	0.0007	0.0022	0.0039	0.0075	0.0258	0.0550
15	0.0003	0.0011	0.0019	0.0060	0.0214	0.0516

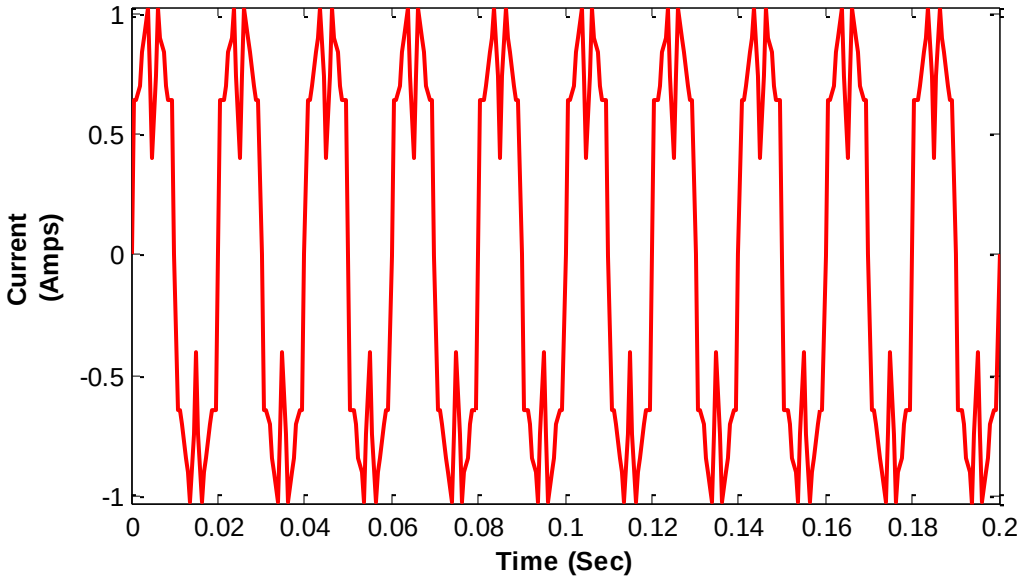

Figure 3.12 Harmonically Distorted Current Waveform

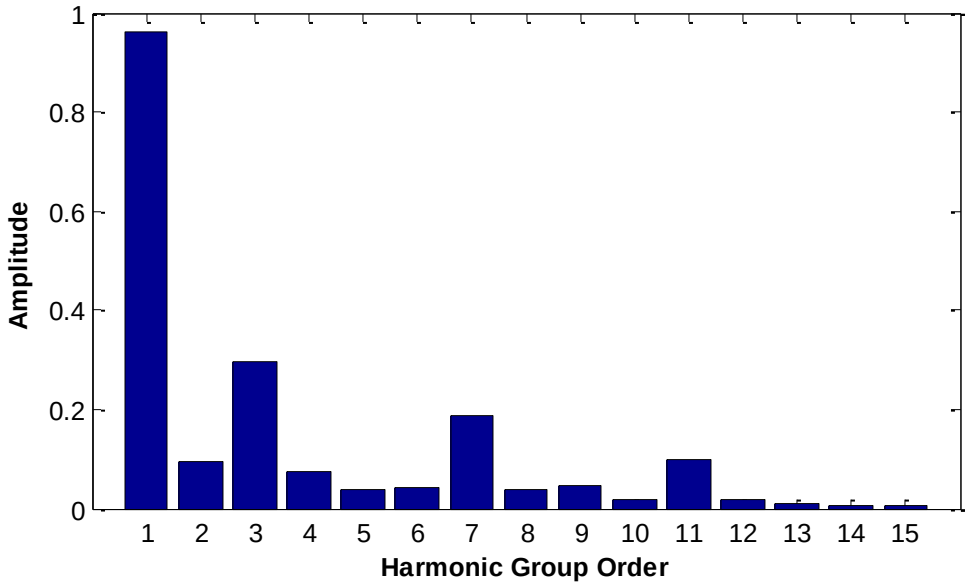

Figure 3.13 Harmonic Groups for the Distorted Current Waveform using WPT

The actual harmonic components along with the obtained results using WPT is presented in Table 3.2. The actual harmonic contents present in the current waveform at 3rd, 7th and 11th harmonic groups are 0.3, 0.2 and 0.1, while the measured harmonic groups using WPT are 0.2967, 0.1866 and 0.0980 respectively. The obtained results show that a percentage of 1.1%, 6.7% and 2% error is observed in the calculated harmonic groups using WPT.

Table 3.2 Harmonic Groups Measurement using WPT

Harmonic Order	**Test Case I**		**Test Case II**	
	Actual Signal	**WPT**	**Actual Signal**	**WPT**
1	***1***	***0.9635***	***1***	***0.9110***
2	0	0.0952	0	0.1187
3	***0.3***	***0.2967***	***0.25***	***0.1691***
4	0	0.0734	0	0.0512
5	0	0.0368	0	0.0243
6	0	0.0406	0	0.0160
7	***0.2***	***0.1866***	0	0.0090
8	0	0.0392	0	0.0073
9	0	0.0483	0	0.0053
10	0	0.0167	0	0.0038
11	***0.1***	***0.0980***	0	0.0029
12	0	0.0175	0	0.0021
13	0	0.0113	0	0.0015
14	0	0.0054	0	0.0009
15	0	0.0048	0	0.0005

The second test case in Table 3.2 consists of a time varying harmonically distorted voltage waveform. Figure 3.14 shows the time domain voltage waveform with a time varying third harmonic component. The third harmonic distortion added in the voltage waveform at the half way of the IEC window starting from 0.1 sec with an amplitude of 0.25 pu. The Test case II in Table 3.2 represents the results obtained using WPT. The obtained results are very much near to the actual harmonic content present in the signal. It is observed that the second harmonic group has high leakage due to the high-energy fundamental component and the occurrence of time varying third harmonic.

3.4.3 Interharmonics Measurement

The performance of the WPT based algorithm is analyzed under the interharmonic distortion present in the supply voltage. Figure 3.15 shows the time domain voltage supply signal consisting of the fundamental 230V, 50 Hz voltage supply along with a 20V interharmonic present at 270 Hz frequency. The interharmonic of 270 Hz falls under the fifth interharmonic group defined in the IEC standard. Table 3.3 shows the interharmonic groups measurement results obtained using WPT. The results show a good aggrement to the actual energy content present in the signal. The measured signal shows that the fundamental 50 Hz high-energy component is successfully filtered from the voltage signal. The resulting groups clearly show the presence of fifth interharmonic group in the signal. The fifth interharmonic group represents the 18.5719 rms voltage obtained using WPT corresponds to the actual 20V, which gives an error of 7.14%.

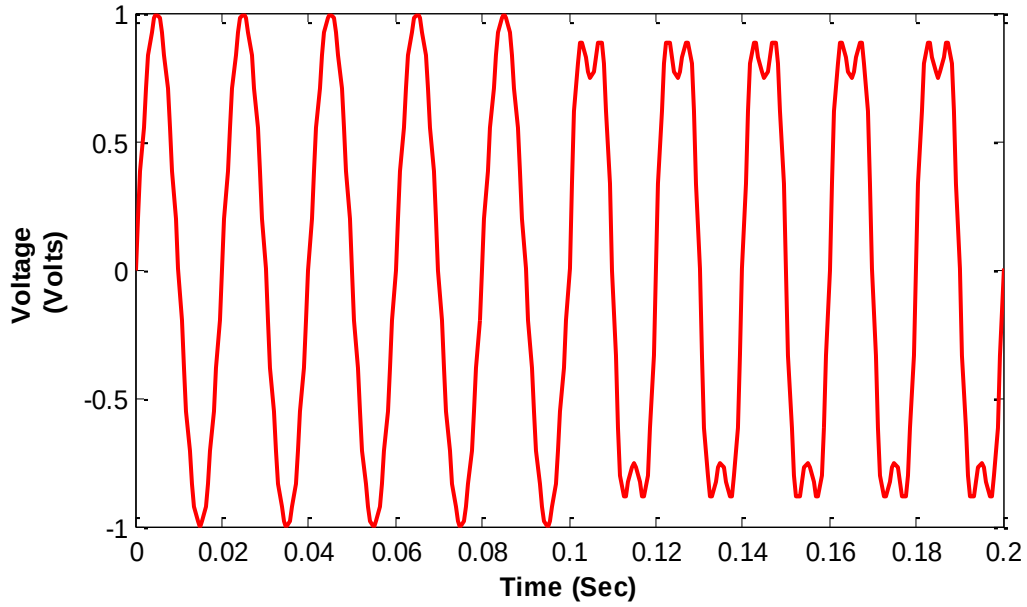

Figure 3.14 Time Varying Distorted Voltage Waveform

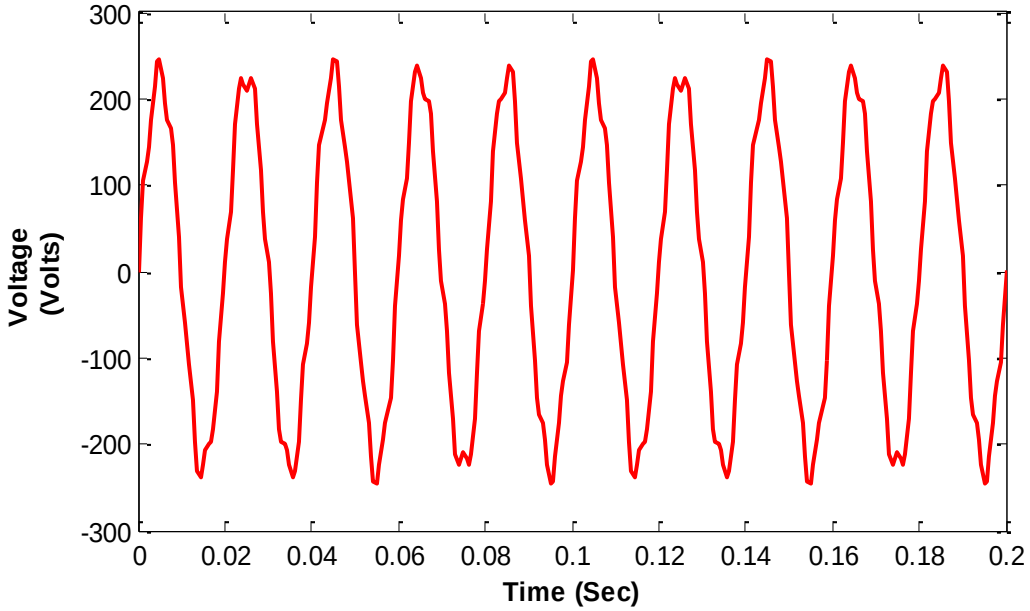

Figure 3.15 Voltage Waveform with Interhamonic Distortion

Table 3.3 Interharmonic Groups Measurement using WPT

Interharmonic Order	**Actual Signal**	**WPT**	**Error %**
1	***230***	***0.1269***	***0.05***
2	0	0.1683	0.073
3	0	0.3741	0.162
4	0	1.9801	0.860
5	***20***	***18.5719***	***7.140***
6	0	0.7733	0.330
7	0	0.1422	0.061
8	0	0.0325	0.014
9	0	0.0147	0.006
10	0	0.0088	0.003
11	0	0.0059	0.002
12	0	0.0043	0.001
13	0	0.0023	0.001
14	0	0.0023	0.001
15	0	0.0028	0.001

3.5 Conclusion

In this chapter, a new approach for the measurement of harmonics and interharmonics is proposed using wavelet packet transform. The proposed approach is capable to automatically detect and measure the harmonics and interahrmonics in voltage and current signals. The performance of the proposed approach is tested under the stationary and non-stationary harmonics and interharmonics distortion. This shows the potential of wavelet packet transform as an alternative tool for the measurement of harmonic distortion in voltage and current signals. The obtained results show a good agreement to the actual harmonic contents available in the test signals. However, the frequency characteristics and spectral analysis reveals some limitations of wavelet based analysis.

The WPT based decomposition has three major drawbacks: firstly, in the WP decomposition a null of wavelet filter is present at the harmonic frequency, which results in a poor filtering and inaccurate measurement obtained by grouping consecutive WP sub bands. Secondly, at each successive filtering stage, a fraction of signal energy is lost as compared to the previous stage due to the imperfect filtering and leakage. Energy leakage is very large particularly at the middle of the sampling frequency due to the roll off factor of the filter. Thirdly, WPT based decomposition is highly sensitive to the source frequency if the fundamental frequency is changed from 50 Hz to 60 Hz, the WP decomposition is no longer applicable for the measurement of harmonic groups. Therefore, a new and more efficient harmonic measurement method is needed to address the limitation of WPT based algorithms.

CHAPTER 4

MEASUREMENTS OF HARMONICS AND INTERHARMONICS USING IIR FILTER BANK

In this chapter, a novel harmonic and interharmnic groups measurement approach is proposed using IIR filter bank. This chapter also compares the results of the proposed method with those of wavelet packet transform based methods in terms of measurement accuracy. Furthermore, the experimental results of the proposed method are discussed.

4.1 Harmonic Estimation using IIR Filter

IIR filter was previously used as a notch filter for single harmonic frequency measurement and filtering [104]–[109]. To the best of our knowledge, the potential of IIR filters for harmonic and interharmonic groups measurement is not being evaluated so far in the literature.

4.1.1 Filter Design

There are several methods for design of digital IIR low pass filters. The technique used here is to convert an analog filter into a digital one using frequency transformation. A typical analog bandpass filter response is described by the input output relationship as:

$$y(p)+\sum_{k=1}^{n} a_k y(p-k)=\sum_{k=0}^{m} b_k x(p-k) \tag{4.1}$$

where *x(p)* and *y(p)* are the input and outputs while a_k and b_k are the coefficients of numerator and denominator respectively. The input output response of the above analog filter can be written as:

$$H(\Omega) = \frac{\sum_{k=0}^{m} b_k e^{-jk\Omega}}{1 + \sum_{k=1}^{n} a_k e^{-jk\Omega}} \tag{4.2}$$

Where $\Omega = 2\pi(f/f_s)$ is the normalized angular frequency represented in [-∞,∞] and f_s is the sampling frequency of the signal. The infinite frequency range for the variable Ω is transformed into a finite frequency range variable ω [-π, π] using periodic sampling of the continuous time signal. Thus, a bandpass filter response in discretized form can be written as:

$$\left|H(\mathrm{e}^{j\omega})\right| = \begin{cases} 1, & \omega_p \le \omega \le \omega_s \\ 0, & \omega > \omega_s, \omega < \omega_p \end{cases} \tag{4.3}$$

The typical response of IIR bandpass filter is obtained using (4.3), where ω_p and ω_s are the passband and stopband frequencies of the desired bandpass IIR filter in rad/sec. The transfer function of the above filter can be obtained as:

$$H(\mathrm{s}) = \frac{\sum_{k=0}^{M} \beta_k s^k}{\sum_{k=0}^{N} a_k s^k} \tag{4.4}$$

where α_k and β_k are the filter coefficients namely poles and zeros of the filter. For a stable IIR filter, all poles α_k must lie inside the unit circle. *M* and *N* are the total number of zeros and poles respectively. The number of zeros are usually less than the number of poles in an IIR filter *(M<N)*. If the number of zeros in an IIR filter is larger than poles, the filter

can be decomposed into an FIR filter of order *(N-M)* and IIR filter of order *N*. There are several methods for frequency transformation that can be used to transform an analog filter to digital one like impulse invariance, step invariance and bilinear transform. In this study, the bilinear transform is selected due to its several advantages such as it ensures the stability of the filter and preserves the maxima and minima of the analog filter response. The transformation is carried out to map all the poles inside the unit circle to ensure the stability of the system as follows:

$$H(z) = H(s)\Big|_{s=\frac{2}{T}\left(\frac{1-z^{-1}}{1+z^{-1}}\right)} \tag{4.5}$$

4.1.2 The Proposed Approach

The proposed algorithm consists of two stages of filtering presented in Figure 4.1. First the input signal is sampled using 1.6 kHz sampling frequency and pass through the pre-filtering stage which results a bandlimited signal ranging from 25-775 Hz which is suitable for the measurement of first 15 harmonic groups represented by *'K'*. The resulting bandlimited signal is passed to the next stage of IIR filter which decomposes the signal into its respective harmonics groups using IIR bandpass filter having center frequency as the harmonic frequency itself.

The proposed approach will not only help to reduce the leakage of harmonic contents to the neighboring bands but also reduces the complexity introduced by WPT due to the next stage of filtering (32 more filters required to implement the 5^{th} level of WP decomposition). It reduces the distortion introduced by the grouping as well.

The first harmonic group defined in IEC-61000-4-7 using 50 Hz fundamental frequency is estimated using ω_p = 25 Hz and ω_s = 75 Hz. Figure 4.2 shows the IIR butterworth filter

for order N=2, 3, 4 and 6 for 7th harmonic group with passband frequency ω_p = 325 Hz and stopband frequency ω_s = 375 Hz having 7th harmonic frequency 350 Hz as a center frequency of the filter. The increased filter order results in a better frequency response with reduced transition band at the expense of increased computational complexity. A tradeoff between filter frequency response and computational complexity is made to obtain the desired results. Butterworth IIR third order filter is used to implement a bandpass filter with passband bandwidth ranging from 25 to 775 Hz with 50 Hz band in each bandpass filter.

Figure 4.3 shows the frequency response of the bandpass filter covering the complete frequency range of 25 Hz to 775 Hz to compute the first 15 harmonic groups.

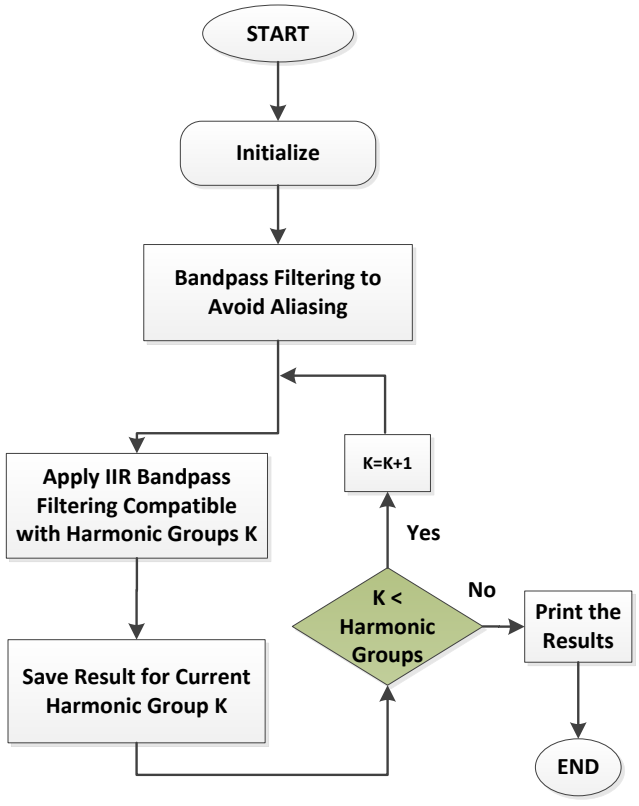

Figure 4.1 Block Diagram of Proposed Multiband Filters Algorithm

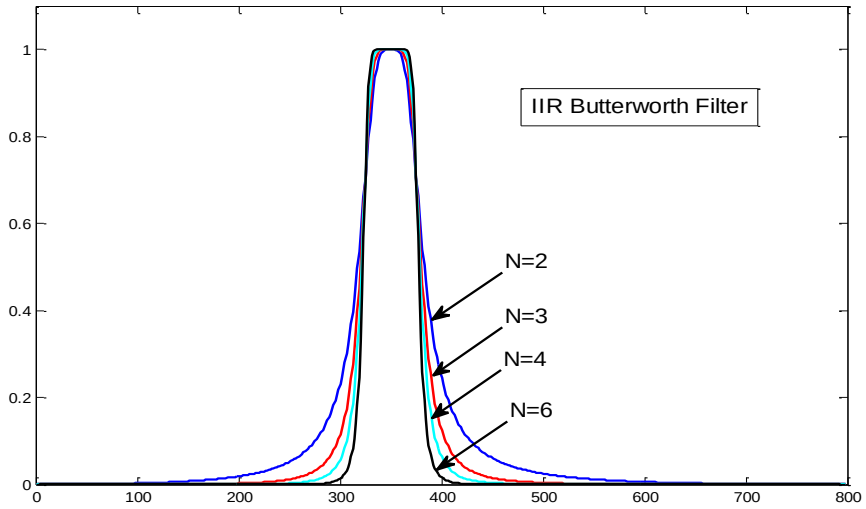

Figure 4.2 IIR Butterworth Bandpass Filter for Different Filter Orders

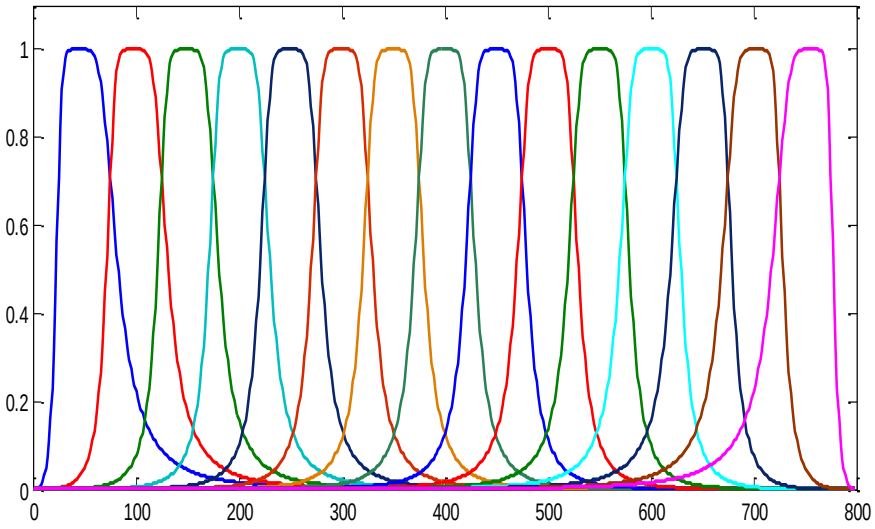

Figure 4.3 Third Order IIR Filters for Harmonic Group Distortion Measurements

4.1.3 Interharmonics Measurement

Interharmonics are the non-integer multiple of fundamental frequency. IEC 61000-4-7 defines interharmonic groups as the all frequency bins of DFT between two successive harmonic frequencies. To compute the first fifteen interharmonics groups, butterworth IIR

bandpass filter bank is designed as shown in Figure 4.4. The proposed bandpass filter bank is designed using third order butterworth filter. The first interharmonic group is evaluated using ω_p = 50 Hz and ω_s = 100 Hz as passband and stopband frequencies respectively, as defined in the IEC standred. Similarly, the second and third interharmonic groups are computed using ω_p = 100 Hz and ω_s = 150 Hz and ω_p = 150 Hz and ω_s = 200 Hz, respectively. The harmonic frequencies are at the edge of the filter so they do not have a larger influence on the filter performance. For comparison purpose and due to the degraded performance of WPT in the presence of fundamental component, a preprocessing stage is applied to filter out the fundamental component. The resulting signal is passed through the butterworth IIR bandpass filters to compute the interharmonic groups.

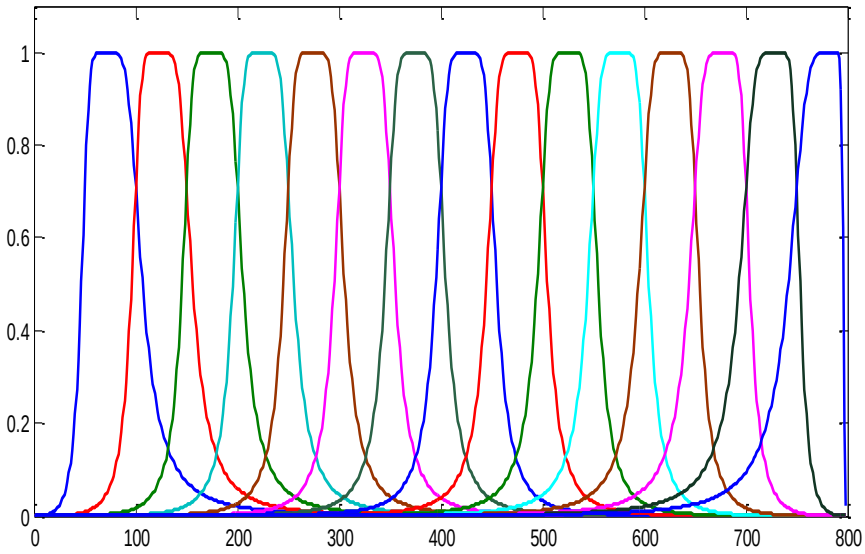

Figure 4.4 Third Order IIR Bandpass Filters for Interharmonic Groups

4.2 Simulation Results

The performance of the proposed approach is tested under the stationary and non-stationary signals to measure the harmonic and interharmonic distortion in voltage and current signals. Different test cases are applied to investigate the applicability of the proposed IIR filter bank based algorithm. The test cases comprise of single tone analysis, harmonic groups measurement and the interharmonic groups measurement.

4.2.1 Single Tone Analysis

In this test, the analysis of a single tone signal consisting of the fundamental frequency 50 Hz and harmonic frequencies of third, fifth, seventh, ninth and eleventh harmonic signal is presented in Table 4.1. A single tone of 1 pu is applied and the rms values are calculated against the harmonic groups. It can be seen from the results that, the performance of the purposed algorithm is pretty much consistent while sweeping through the spectrum. It can be observed that the third harmonic frequency has the maximum leakage as it results 0.9894 by applying a 1 pu tone signal at 150 Hz. The result shows that a 1.06 % error is present in the calculated rms value by the proposed IIR measurement approach.

4.2.2 Harmonic Analysis using Stationary and Non-Stationary Signals

This section presents the harmonic analysis using stationary and non-stationary harmonically distorted voltage and current signals. Figure 4.5 and Figure 4.6 show the harmonically distorted voltage waveform and its corresponding spectra obtained by IIR filter bank. The test signal consists of fundamental voltage waveform along with third, seventh and eleventh harmonic components with different amplitudes.

Table 4.1 Single Tone Analysis using IIR Filter Bank

Harmonic Order	**50 Hz**	**150Hz**	**250Hz**	**350Hz**	**450Hz**	**550Hz**
1	***0.9955***	0.0015	0.0004	0.0106	0.0104	0.0000
2	0.0101	0.0048	0.0005	0.0053	0.0046	0.0000
3	0.0024	***0.9899***	0.0010	0.0044	0.0031	0.0000
4	0.0012	0.0029	0.0041	0.0047	0.0026	0.0000
5	0.0007	0.0005	***0.9894***	0.0063	0.0027	0.0001
6	0.0005	0.0002	0.0033	0.0220	0.0033	0.0001
7	0.0004	0.0001	0.0006	***0.9912***	0.0051	0.0001
8	0.0003	0.0000	0.0002	0.0190	0.0188	0.0002
9	0.0003	0.0000	0.0001	0.0050	***0.9923***	0.0006
10	0.0002	0.0000	0.0001	0.0031	0.0207	0.0033
11	0.0002	0.0000	0.0001	0.0022	0.0050	***0.9894***
12	0.0001	0.0000	0.0000	0.0018	0.0032	0.0041
13	0.0001	0.0000	0.0000	0.0015	0.0023	0.0010
14	0.0001	0.0000	0.0000	0.0013	0.0019	0.0005
15	0.0001	0.0000	0.0000	0.0015	0.0021	0.0004

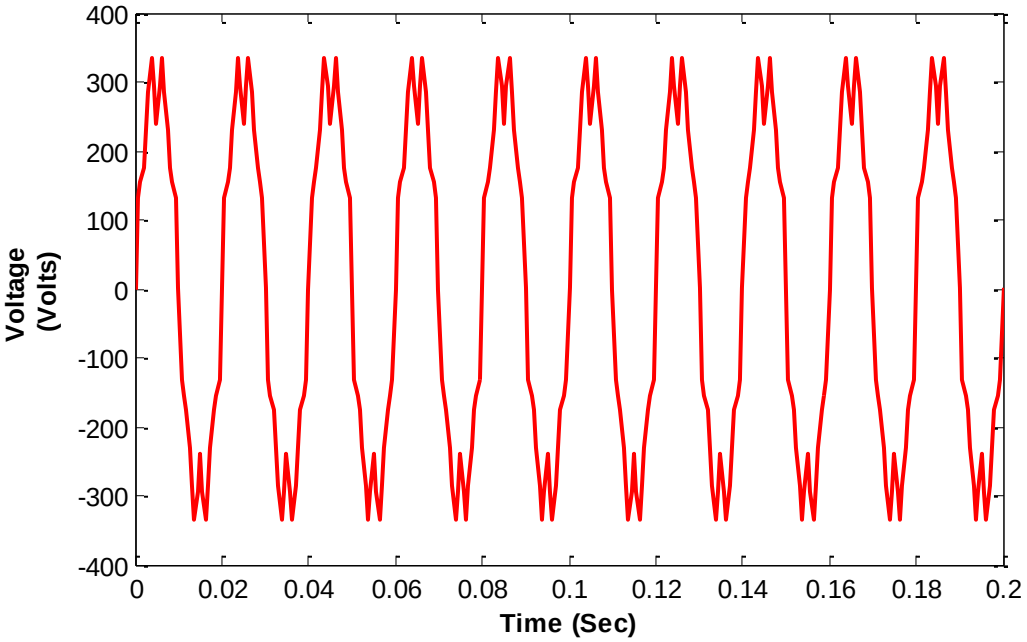

Figure 4.5 Distorted Voltage Waveform

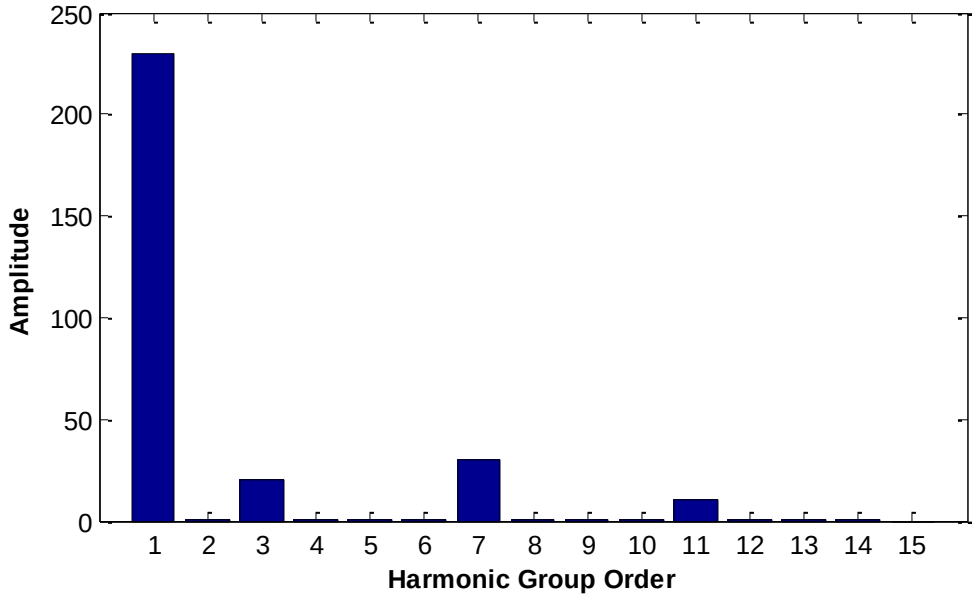

Figure 4.6 Voltage Spectra of Harmonic Groups using IIR Filter Bank

The actual harmonic components along with the obtained results using proposed IIR filter bank is presented in Table 4.2. The obtained results show a good resemblance to the actual harmonic content in the signal. The obtained results show that the maximum error of 0.37% is observed in the calculated harmonic groups using IIR filter bank.

4.2.3 Interharmonics Measurement

The performance of the proposed IIR filter bank based algorithm is analyzed under the interharmonics distortion present in the supply voltage. Figure 4.7 and Figure 4.8 show the time domain voltage supply signal and the corresponding interharmonic group spectra obtained by the proposed approach. The test signal consists of the fundamental 230V, 50 Hz voltage supply along with a 21V interharmonic present at 360 Hz frequency and a 15V interharmonic component present at 520 Hz frequency. The interharmonic of 360 Hz falls under the 8^{th} interharmonic group while 520 Hz interharmonic lies in the 11^{th} interharmonic group defined in the IEC standard. Table 4.3 shows the interharmonic groups measurement results obtained by the proposed IIR filter bank approach. The results show a good comparison to the actual energy content present in the signal. The measured signal shows that the fundamental 50 Hz high-energy component is successfully filtered from the voltage signal. The resulting groups clearly shows the presence of 8^{th} and 11^{th} interharmonic group in the signal. An error of 2.12% is observed at the 8^{th} interharmonic group while the 11^{th} interharmonic group reflects an error of 2.1% as compared to the actual values of 21V and 15V, respectively.

Table 4.2 Harmonic Groups Measurement using IIR Filter Bank

Harmonic Order	**Actual Signal**	**Prop. IIR**	**Error %**
1	***230***	***229.4650***	***0.2326***
2	0	0.8735	0.3797
3	***20***	***19.9534***	***0.233***
4	0	0.1539	0.0691
5	0	0.0172	0.0074
6	0	0.6493	0.2823
7	***30***	***29.9302***	***0.0023***
8	0	0.3426	0.1489
9	0	0.0053	0.0023
10	0	0.1913	0.0831
11	***10***	***9.9767***	***0.0023***
12	0	0.1279	0.0556
13	0	0.0015	0.0006
14	0	0.0001	0.0000
15	0	0.0000	0.0000

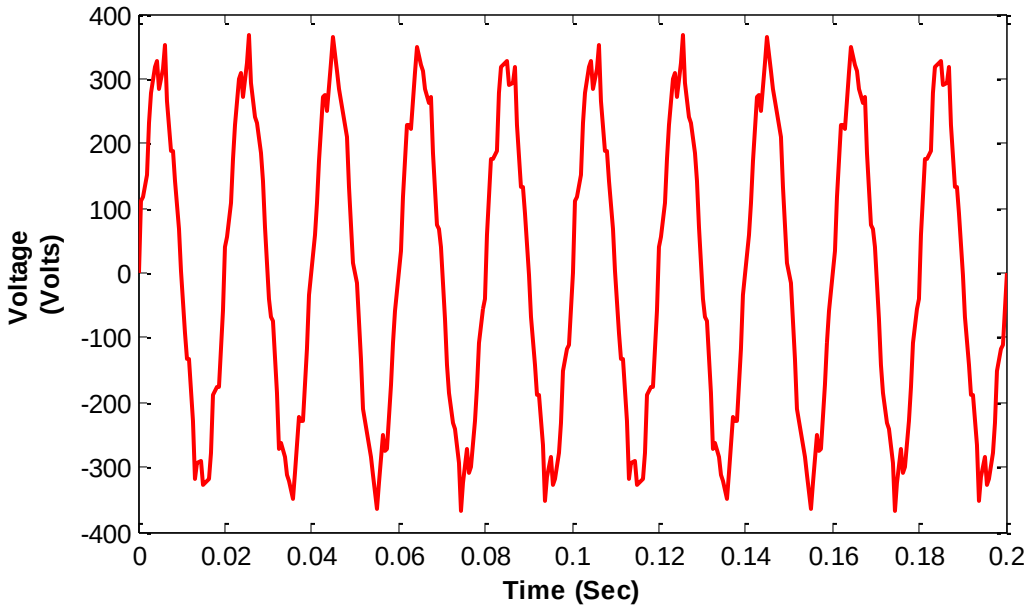

Figure 4.7 Voltage Waveform with Interharmonic Distortion

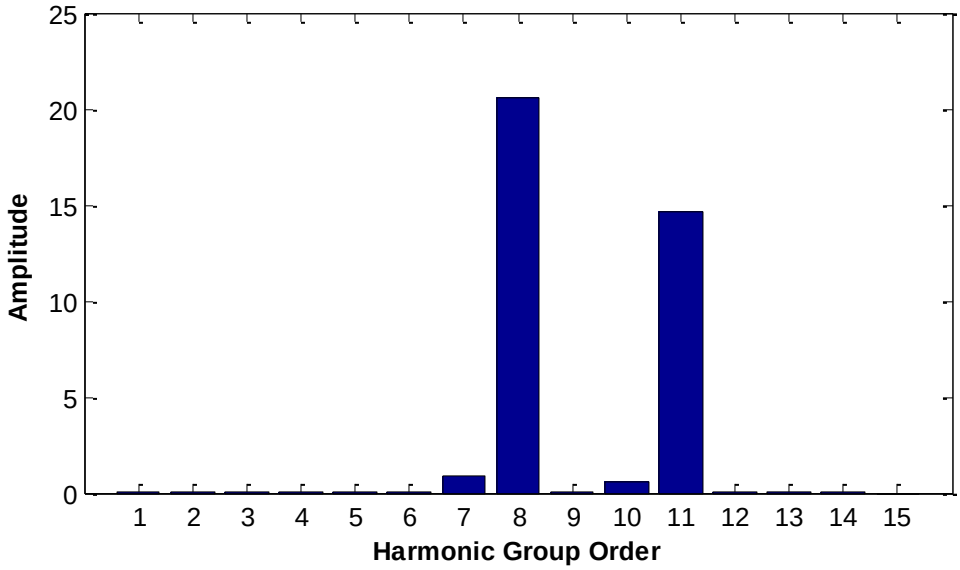

Figure 4.8 Interharmonic Group Spectra using IIR Filter Bank

Table 4.3 Interharmonic Group Distortion using IIR Filter Bank

Interharmonic Order	**Actual Signal**	**Prop. IIR**	**Error %**
1	***230***	***0.00003***	***0.0000***
2	0	0.00004	0.0000
3	0	0.00008	0.0000
4	0	0.00019	0.0000
5	0	0.00073	0.0003
6	0	0.00716	0.0031
7	0	0.88409	0.3843
8	***21***	***20.5743***	***2.0271***
9	0	0.01181	0.0051
10	0	0.59479	0.2585
11	***15***	***14.6847***	***2.1020***
12	0	0.00906	0.0039
13	0	0.00022	0.0000
14	0	0.00001	0.0000
15	0	0.00000	0.0000

4.3 Comparative Analysis of WPT and IIR Filter Bank Approach

A comparative analysis of the proposed harmonics measurement algorithms is presented in this section using different test cases. Firstly, a single tone analysis is performed using the proposed IIR filter bank algorithm and the results are compared with the WPT based algorithm. Secondly, the performance of both algorithms is analyzed using stationary and non-stationary signals and finally, different test cases for time varying harmonics and interharmonics are considered.

4.3.1 Single Tone Analysis

In this test, the analysis of a single tone signal consisting of the fundamental frequency 50 Hz and harmonic frequencies of third, fifth, seventh and ninth harmonic signal is presented in Table 4.4. The results obtained using WPT and proposed IIR filtering approach show that the performance of proposed IIR filter bank is quite accurate and consistent as compared to the WPT, especially when the 350 Hz tone signal is applied. It can be seen that the voltage rms value obtained using WPT is 0.9569 compared to 0.9912 using IIR. The corresponding errors are 4.31% with WPT and 0.0088% with IIR. It can be seen that the performance of IIR is superior and the error is substantially reduced.

Table 4.4 Comparative Analysis of Single Tone Harmonic Measurement

Harmonic Order	50 Hz		350 Hz		450 Hz	
	Prop. WPT	**Prop. IIR**	**Prop. WPT**	**Prop. IIR**	**Prop. WPT**	**Prop. IIR**
1	***0.9808***	***0.9955***	0.0567	0.0106	0.0287	0.0104
2	0.1461	0.0101	0.0746	0.0053	0.0347	0.0046
3	0.0659	0.0024	0.0796	0.0044	0.0362	0.0031
4	0.0284	0.0012	0.0877	0.0047	0.0374	0.0026
5	0.0158	0.0007	0.1447	0.0063	0.0505	0.0027
6	0.0115	0.0005	0.2005	0.0220	0.0594	0.0033
7	0.0064	0.0004	***0.9569***	***0.9912***	0.2208	0.0051
8	0.0053	0.0003	0.1783	0.0190	0.1726	0.0188
9	0.0039	0.0003	0.2341	0.0050	***0.9772***	***0.9923***
10	0.0028	0.0002	0.0430	0.0031	0.1219	0.0207
11	0.0021	0.0002	0.0233	0.0022	0.0708	0.0050
12	0.0015	0.0001	0.0167	0.0018	0.0403	0.0032
13	0.0011	0.0001	0.0119	0.0015	0.0299	0.0023
14	0.0007	0.0001	0.0075	0.0013	0.0258	0.0019
15	0.0003	0.0001	0.0060	0.0015	0.0214	0.0021

4.3.2 Comparative Analysis for Harmonics Measurement

The performance of the proposed algorithms is also investigated using the time varying harmonic distortion test cases. These test cases include the harmonic distortion inside the sampling window. In test case I, a large fluctuation of voltage harmonics inside sampling window is discussed, while test case II discuss the momentary high current distortion due to the switching OFF/ON of large loads.

In test case I, the analyzed signal is consisted on the fifth harmonic amplitude fluctuation inside the sampling window. Figure 4.9 presents the time domain signal in the sampling window of 0.2 seconds. In Test Case I, Table 4.5 summarizes the results of the investigated signal. The results shows that, both algorithms successfully identify the maximum energy at the fifth harmonic groups. The actual rms value of the signal inside sampling window was 2.36, while the obtained rms values using WPT and proposed IIR approaches are 2.3229 and 2.2916 respectively. The percentage of error in rms values are 1.86% and 3.18%. The results clearly justifies the ability of WPT to tackle the time varying signals is better as compared to IIR filter bank.

The second test, Test Case II, consists of a non-stationary current signal with 50% duty cycle in the IEC sampling window as shown in Figure 4.10. The signal contains the third harmonic frequency over 5 cycles and fluctuates to zero amplitude for the remaining 5 cycles that gives a total of 50% signal available in the analysis window duration. In Test Case II, Table 4.5 presents the results obtained using wavelet packet transform and proposed IIR filter bank approach. The total rms current of third harmonics calculated over 0.2 s is 0.707 A. The test results show that the measured values using WPT is 0.6822 while for IIR it is 0.7019 much closer to the actual value of 0.707. The corresponding rms error

in case of WPT is 3.5%, while in case of IIR the error is substantially reduced to only 0.72%.

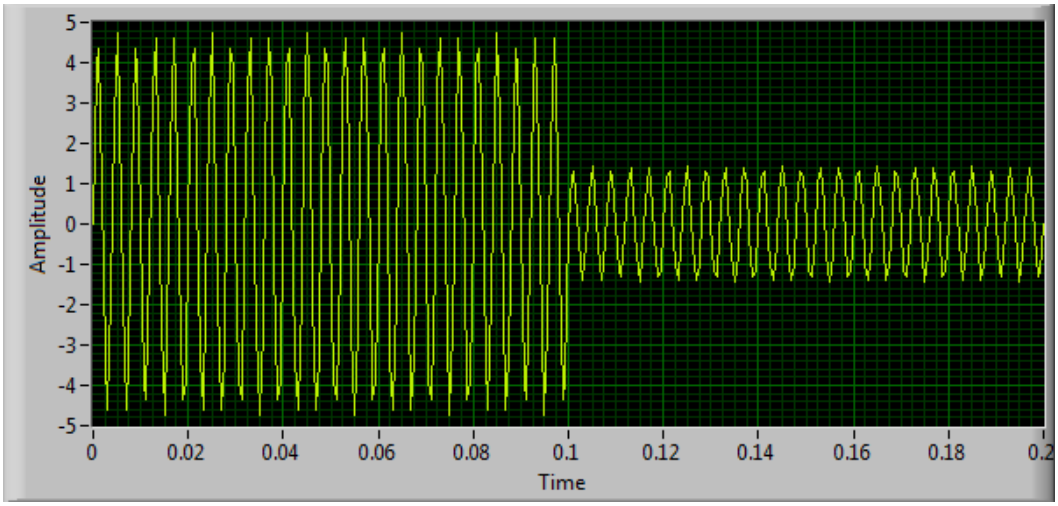

Figure 4.9 Large Fluctuation in Fifth Harmonic Current

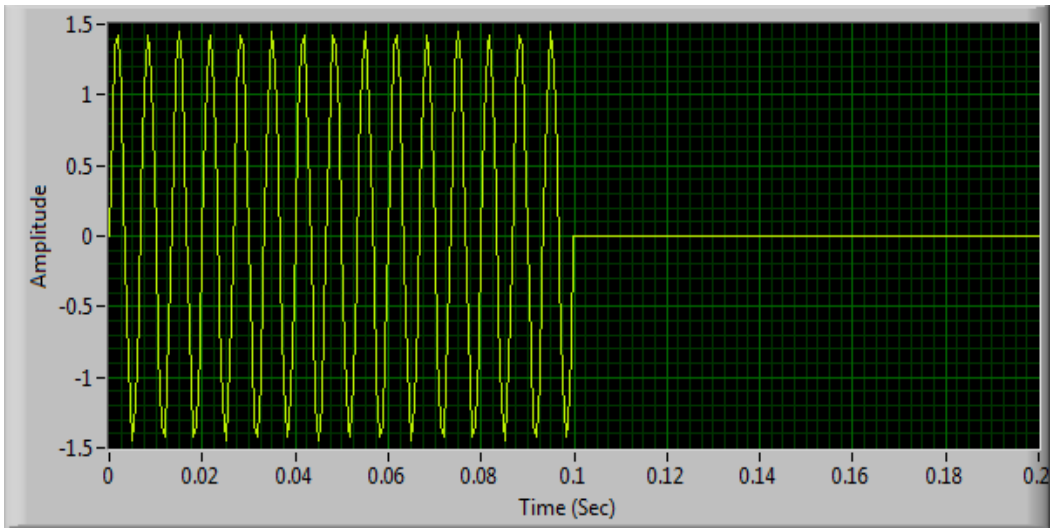

Figure 4.10 Sudden Load Change inside Sampling Window

Table 4.5 Comparative Analysis of Non-stationary Harmonic Signals

Harmonic Order	Actual Signal	Test Case I Voltage Harmonics		Actual Signal	Test Case II Current Harmonics	
		Prop. WPT	Prop. IIR		Prop. WPT	Prop. IIR
1	0	0.1612	0.1007	0	0.1095	0.0440
2	0	0.2153	0.0742	0	0.1712	0.0670
3	0	0.2894	0.0887	***0.707***	***0.6822***	***0.7019***
4	0	0.5115	0.1746	0	0.1324	0.0494
5	***2.36***	***2.3229***	***2.2916***	0	0.0538	0.0194
6	0	0.4587	0.1518	0	0.0283	0.0116
7	0	0.2899	0.0635	0	0.0168	0.0081
8	0	0.1407	0.0401	0	0.0125	0.0062
9	0	0.0695	0.0294	0	0.0095	0.0050
10	0	0.0430	0.0234	0	0.0065	0.0042
11	0	0.0309	0.0197	0	0.0049	0.0037
12	0	0.0227	0.0173	0	0.0037	0.0033
13	0	0.0158	0.0157	0	0.0026	0.0030
14	0	0.0106	0.0147	0	0.0018	0.0029
15	0	0.0080	0.0142	0	0.00131	0.0028

The three phase distorted voltage supply for different harmonic content is shown in Figure 4.11. Phase A contains the fundamental voltage supply with fifth harmonic distortion, phase B contains the multiple harmonic groups having 3^{rd} and 7^{th} while phase C contains 11^{th} and 14^{th} higher order harmonic groups. The harmonic groups measurement results are summarized in Table 4.6. For phase A, the results obtained using WPT is 0.0852

while for IIR it is 0.0869 pu. The actual value of third harmonic was 0.0869 pu. Similarly, for phase B, the harmonic contents available at third and seventh harmonic were 0.043 and 0.0869. The measured harmonic groups using WPT are 0.0413 and 0.0862 pu while IIR gives 0.0428 and 0.0867 pu. The voltage supply for phase C is distorted with the higher order harmonics 11^{th} and 14^{th} with 0.1304 and 0.0896 pu. The measured harmonic groups using WPT are 0.1227 and 0.0851 pu while IIR gives 0.1301and 0.0866 pu.

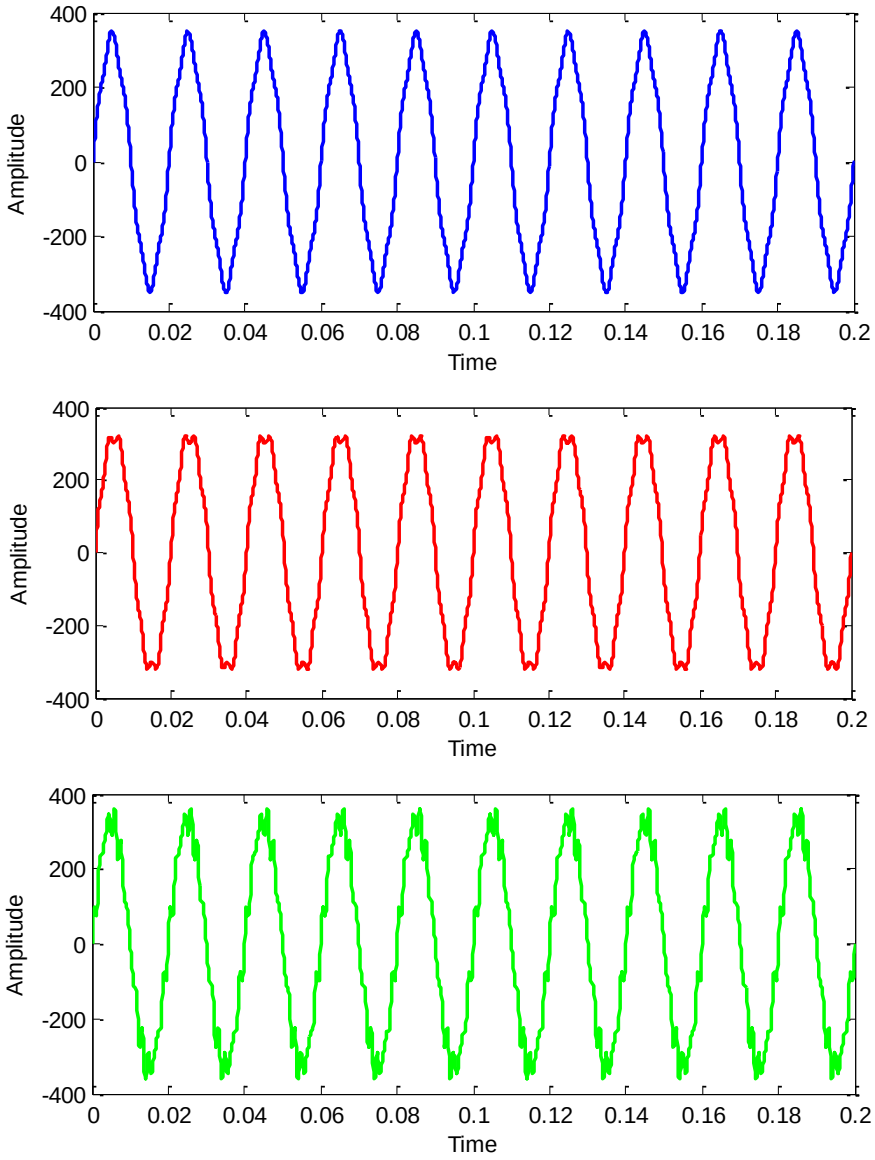

Figure 4.11 Three Phase Voltage Waveforms for Distorted Voltage Supply

Table 4.6 Comparative Analysis of Harmonic Groups Measurement using WPT and IIR for Distorted Voltage Supply

N	Phase A			Phase B			Phase C		
	Actual Value	**Prop. WPT**	**Prop. IIR**	**Actual Value**	**Prop. WPT**	**Prop. IIR**	**Actual Value**	**Prop. WPT**	**Prop. IIR**
1	1	1	1	1	1	1	1	1	1
2	0	0.0006	0.0001	0	0.0026	0.0005	0	0.0001	0.0000
3	0	0.0011	0.0002	***0.043***	***0.0413***	***0.0428***	0	0.0001	0.0000
4	0	0.0037	0.0007	0	0.0010	0.0000	0	0.0001	0.0000
5	***0.0869***	***0.0852***	***0.0869***	0	0.0016	0.0001	0	0.0001	0.0000
6	0	0.0029	0.0005	0	0.0035	0.0006	0	0.0001	0.0000
7	0	0.0009	0.0001	***0.0869***	***0.0862***	***0.0867***	0	0.0002	0.0001
8	0	0.0003	0.0000	0	0.0033	0.0008	0	0.0005	0.0001
9	0	0.0001	0.0000	0	0.0062	0.0002	0	0.0015	0.0002
10	0	0.0000	0.0000	0	0.0002	0.0001	0	0.0036	0.0010
11	0	0.0000	0.0000	0	0.0001	0.0000	***0.1304***	***0.1227***	***0.1301***
12	0	0.0000	0.0000	0	0.0000	0.0000	0	0.0041	0.0008
13	0	0.0000	0.0000	0	0.0000	0.0000	0	0.0024	0.0001
14	0	0.0000	0.0000	0	0.0000	0.0000	***0.0869***	***0.0851***	***0.0866***
15	0	0.0000	0.0000	0	0.0000	0.0000	0	0.0020	0.0014

4.3.3 Comparative Analysis for Interharmonics Measurement

Two different interharmonics case studies are presented to evaluate the performance of the both algorithms.

A 230 V, voltage supply in the presence of 15 V rms interharmonics at 730 Hz is presented in Figure 4.12. The voltage waveform is highly distorted due to the presence of interharmonics corresponds to the 14^{th} group. In Test Case III, Table 4.7 summarizes the results for the interharmonic groups. The rms voltage using WPT corresponding to the 14^{th} interharmonic groups is 14.134 while in case of IIR filters the obtained rms value is 14.8803 resulting in 0.928 % less error as compared to the WPT.

The second interharmonic test case consists of a 50 Hz, 230 V voltage supply contains a non-synchronous interharmonic of 21 volts at 128 Hz. The time domain distorted voltage waveform is shown in Figure 4.13. The interharmonic does not affect the shape of the supply voltage rather it considerably changes the amplitude of the supply voltage. In Test Case IV, Table 4.7 presents the results obtained using WPT and IIR bandpass filters. The 128 Hz interharmonic falls under the second interharmonic group. The second interharmonic groups represents the 20.4985 rms value while IIR bandpass filter rms value 20.791. The percentage error in case of WPT is 2.38 % while the error in case of IIR is 0.99%. This gives an error reduction of 1.39 %.

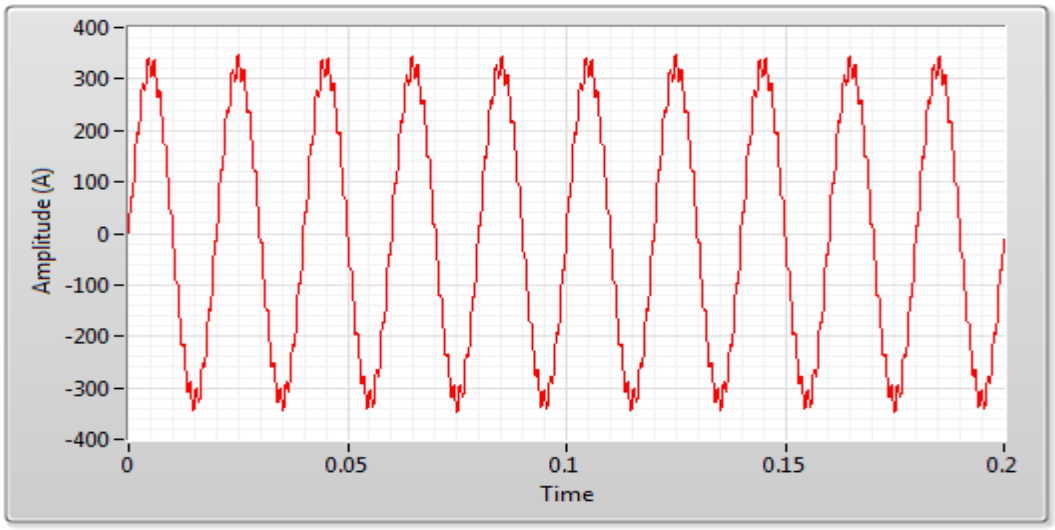

Figure 4.12 Distorted Voltage Waveform in the Presence of Interharmonics

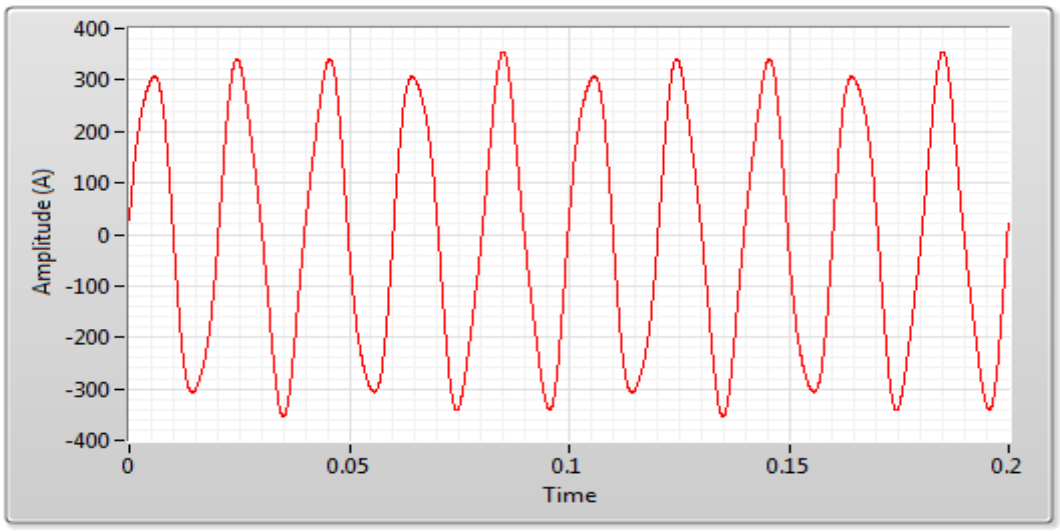

Figure 4.13 Voltage Supply Waveform with Interharmonic Distortion

Table 4.7 Comparative Analysis of Interharmonics Measurement

Interh. Order	Actual Signal	Test Case III		Actual Signal	Test Case IV	
		Prop. WPT	Prop. IIR		Prop. WPT	Prop. IIR
1	0	0.0009	0.2360	0	0.4346	1.5188
2	0	0.0010	0.1135	***21***	***20.4985***	***20.7910***
3	0	0.0010	0.0816	0	1.1489	0.4746
4	0	0.0011	0.0687	0	0.1031	0.1302
5	***2.36***	0.0012	0.0626	0	0.0262	0.0647
6	0	0.0015	0.0596	0	0.0161	0.0391
7	0	0.0019	0.0584	0	0.0159	0.0265
8	0	0.0023	0.0587	0	0.0120	0.0197
9	0	0.0033	0.0606	0	0.0072	0.0160
10	0	0.0052	0.0649	0	0.0057	0.0138
11	0	0.0108	0.0740	0	0.0070	0.0126
12	0	0.0265	0.0966	0	0.0067	0.0118
13	0	0.1782	0.1923	0	0.0040	0.0113
14	***15***	***14.134***	***14.8803***	0	0.0039	0.0109
15	0	1.0623	1.3201	0	0.0057	0.0116

4.4 Discussion

An efficient technique based on IIR filtering approach is proposed to measure the harmonic and interharmonic distortion in the voltage/current signals. The results of the proposed approach is compared with the WPT based technique presented in Chapter 3. The proposed IIR-based technique is insensitive to the source frequency, only a simple delay can adjust the filter bands according to the source frequency. The proposed IIR algorithm utilizes half number of filters as compared to the WPT based techniques, which reduces the complexity as well as improves the processing time. The proposed algorithm shows a sensational improvement as compared to the WPT.

CHAPTER 5

EXPERIMENTAL IMPLEMENTATION OF HARMONIC MEASUREMENT TECHNIQUES

This chapter studies the performance analysis of wavelet packet transform and infinite impulse response filter bank by means of experimental setup. A laboratory scale prototype is developed using digital controller compact RIO, voltage and current transformers, programmable source and controllable loads. This chapter explains in detail the preparation of the experimental setup, implementation of the proposed harmonic and interharmonic measurement strategies and the analysis of the obtained results.

5.1 Experimental Setup

The experimental setup has been built as shown in Figure 5.1 (a) and (b). The setup consists of workstation running LabVIEW 2013, CompactRIO, programmable AC source, programmable electronic loads, and panels housing current transformers. A detailed description of the experimental setup and components is available in Appendix A and Appendix B.

Figure 5.1 (a) represents the block diagram of the hardware setup while Figure 5.1 (b) represents the real time hardware used in this setup. The voltage and current waveforms are acquired using digital signal processor and resampled using the sampling frequency 1.6 kHz. The resampled signal is passed to the particular harmonic detection algorithm for further analysis.

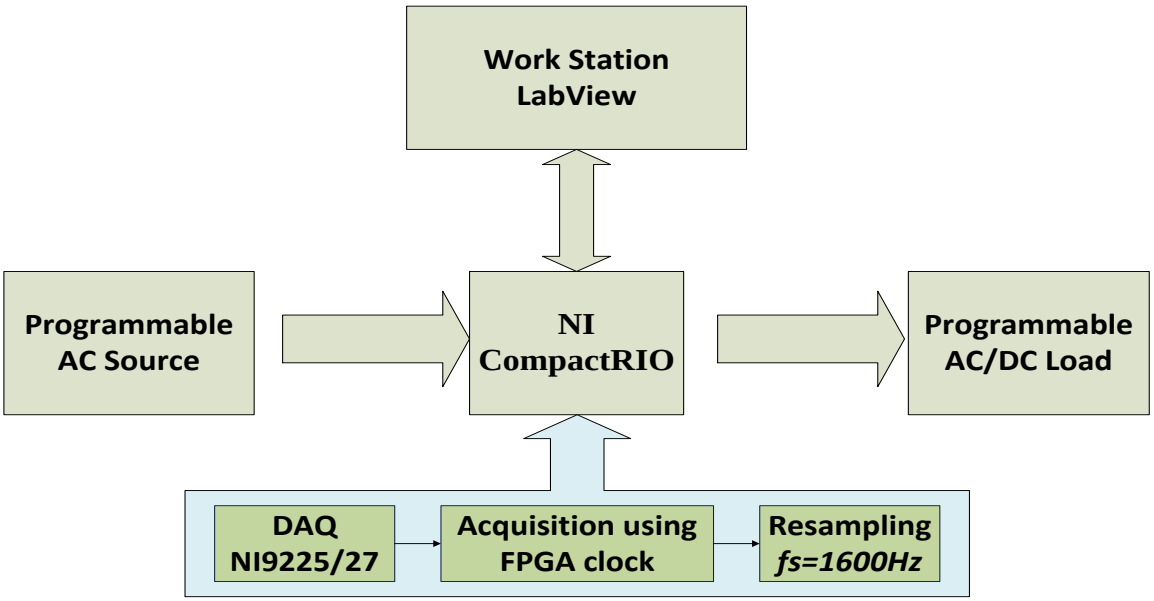

(a)

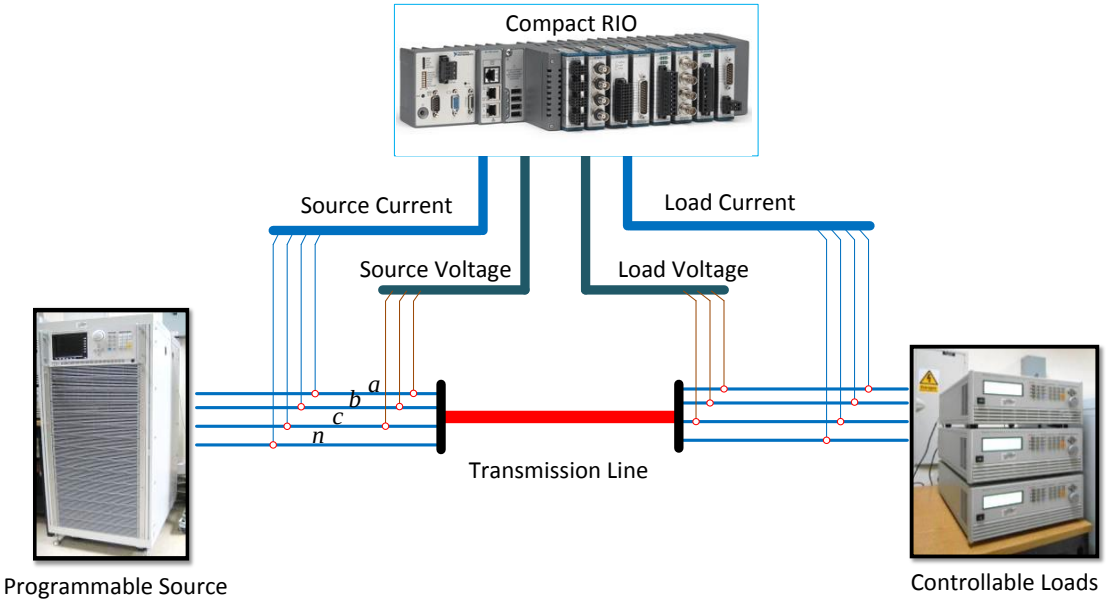

(b)

Figure 5.1 Experimental Setup (a) Block Diagram for Experimental Setup

(b) Hardware Description for Online Monitoring

The experimental setup is shown in Figure 5.1 (b), where programmable source and loads are used to implement a simple distribution system. The current and voltage waveforms of source and load are acquired using NI data acquisition cards. The acquired signals are passed to the digital processor NI CompactRIO for further analysis. A short description of the experimental components used to develop the monitoring and measurement system is given in the following section.

5.1.1 Programmable AC Source

Programmable AC source provides powerful functions to simulate the harmonics and interharmonics. In this work, Chroma 61511 is used as a voltage source. It can provides upto 300 Vrms output voltage and 12 KVA power ratings. It is capable to generate the first forty harmonics and interharmonics ranging from 0.01 Hz to 2400 Hz.

5.1.2 Controllable AC/DC Loads

Programmable electronic loads can simulate non-linear rectified loads and load conditions under high crest factor. In this study, Chroma-63800 is used to simulate different linear and non-linear loads. It can be configured as a constant power source up to 1800W, while as a constant current load up to 45 Arms at the voltage range is 50V – 350 Vrms. Three identical units of chroma-63800 are used separately to simulate the three-phase load.

5.1.3 Compact RIO

CompactRIO (cRIO) consists of three parts, namely an embedded controller, a reconfigurable chassis and I/O modules. The controller part is responsible for communication and processing. A reconfigurable chassis contains the user-programmable FPGA. The hot-swappable I/O modules are used for data acquisition applications.

Voltage Measurement Module: The I/O module NI-9225 is used for the real time voltage measurement. It is a 3-ports module that can measure voltage directly from the line up to 300 V_{rms}.

Current Measurement Module: The I/O module NI-9227 is used for the real time current measurement. It is a 4-ports module that can measure 5 A_{rms} current directly from the line. A Current transformer (100/5 A) is used to measure the load currents greater than 5 A.

5.1.4 LabVIEW Software

LabVIEW 2013 was selected to implement the proposed harmonic detection and measurement strategies in real time setup. It is a graphics based programming language. Algorithms are developed for data acquisition at the specified sampling frequency and processed using the real-time controller to measure the harmonics and interharmonics. The real time data is collected using FPGA clock and then resampled using the specific sampling frequency 1.6 kHz in this study.

5.2 LabVIEW Based Implementation of Proposed Algorithms

The NI LabVIEW software is used to design and develop the real time implementation of wavelet packet transform and IIR filter bank. The proposed strategies are implemented to measure the harmonic and interharmonic distortion in voltage and current signals.

5.2.1 Implementation of Wavelet Packet Transform

LabVIEW based implementation of wavelet packet transform for harmonic measurement is shown in Figure 5.2. The measured voltage and current signals are passed to the wavelet packet subVI implemented in LabVIEW. The wavelet packet VI implements the five level wavelet packet decomposition. The rms value of the wavelet node coefficient is calculated.

The wavelet bands are grouped together to make the decomposition compatible to the harmonic groups defined in the IEC standard. Finally, the results are combined in an array and passed to the main program.

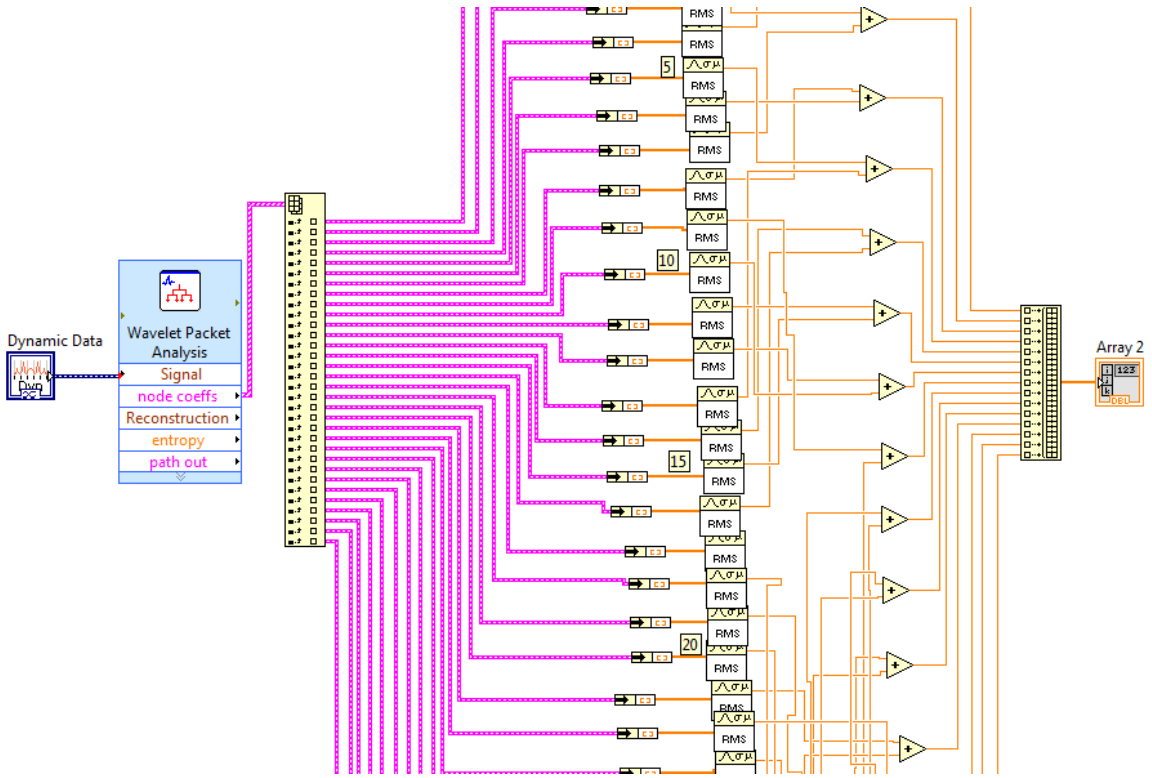

Figure 5.2 LabVIEW Based Implementation of Wavelet Packet Transform

5.2.2 Implementation of IIR Filter Bank

LabVIEW based implementation of IIR filter bank for harmonic groups measurement is shown in Figure 5.3. The dynamic data represents the acquired voltage or current signals input to the IIR filter bank VI. The input signal is passed through an IIR filter bank, whose frequencies are compatible with the harmonic groups. The specifications of the IIR filter developed in LabVIEW are lower and upper band frequencies along with the order of the filter. A six-order butterworth filter is selected for real time implementation. The rms value

of each filtered signal is calculated. Finally, the results are grouped in an array and passed to the main program.

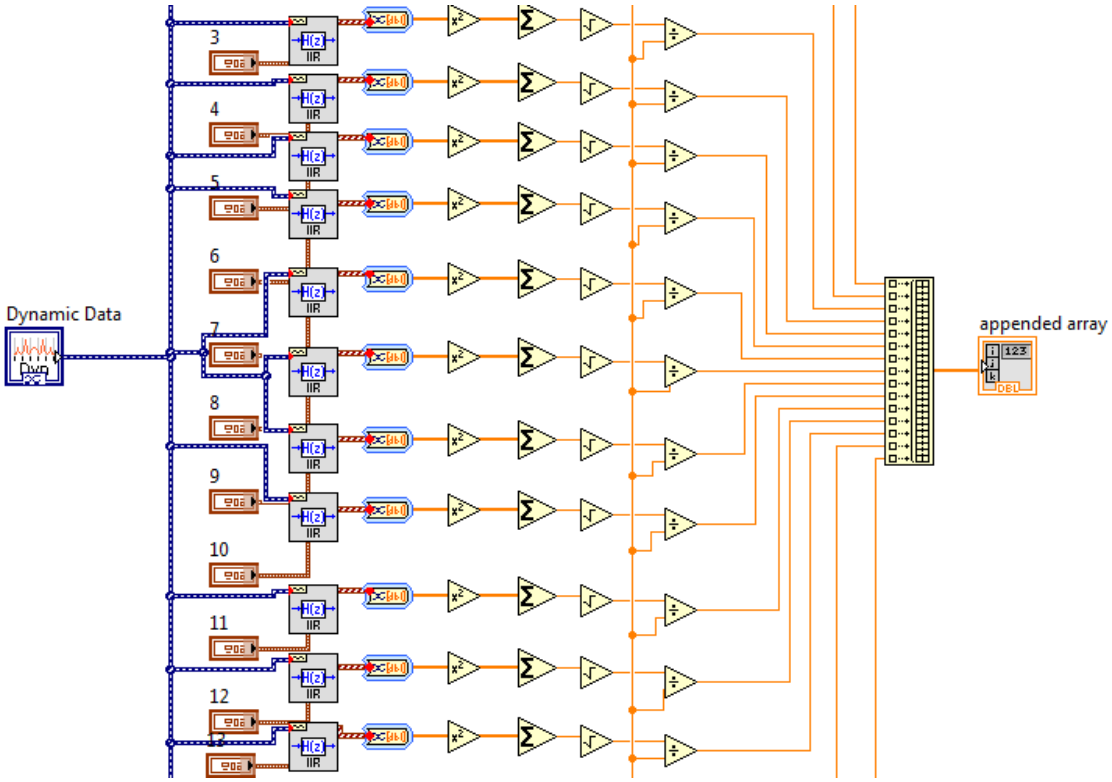

Figure 5.3 LabVIEW Based Implementation of IIR Filter Bank

5.3 Experimental Results

To verify the effectiveness of the proposed methods, the experimental implementation has been carried out using LabVIEW and the setup described above. The test signals utilized to evaluate the experimental real-time performance of the proposed technique are generated by a programmable AC source. Programmable load is used to simulate the linear and non-linear current waveforms. Figure 5.4 and Figure 5.5 represent the graphical user interface and block diagram respectively. The developed program is capable to compute the small harmonic and interharmonic groups measurement using WPT and IIR filter bank.

Figure 5.4 LabVIEW GUI for PQ Monitoring

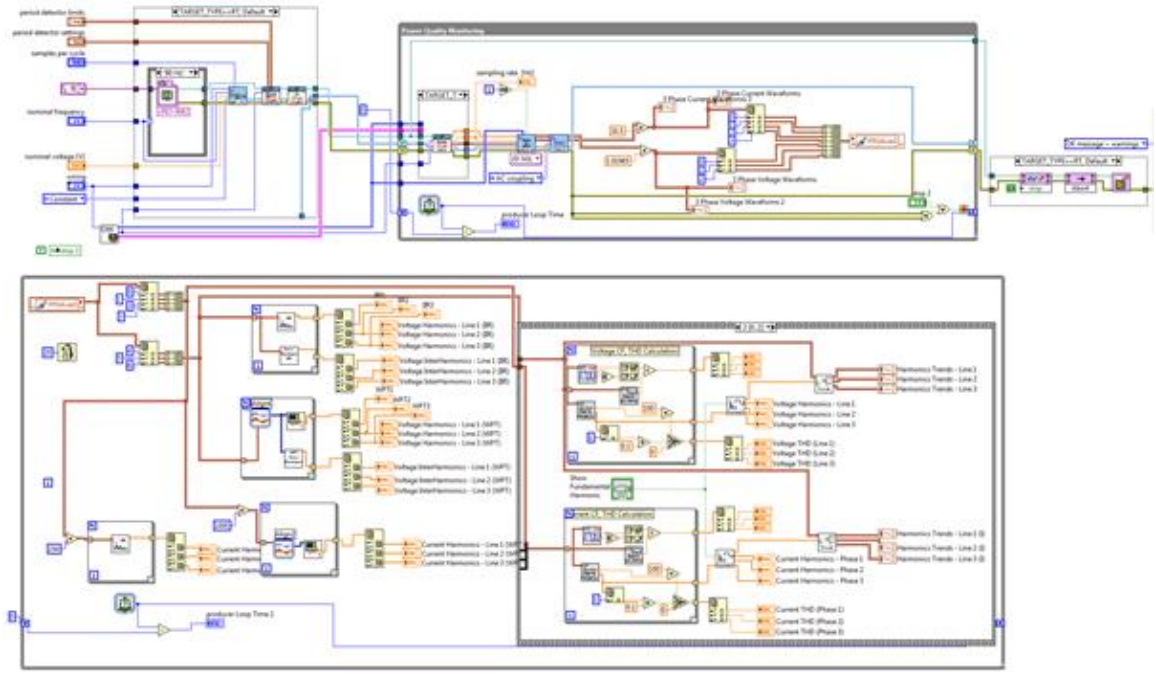

Figure 5.5 LabVIEW Implementation for PQ Monitoring System

Apart from that, other power quality factors like rms voltage and currents, phase angle, three-phase power, power factor, crest factor and total harmonic distortion in voltage and current signals are also calculated in the developed program as shown in Figure 5.4.

A comparative analysis of the proposed harmonics measurement algorithms is investigated using real time experiments. The performance of the WPT and IIR filter bank is tested using different test case. These real time experiments include three-phase voltage distortion measurement and harmonic current measurement under distorted voltage supply and diode rectifier non-linear load.

First experiment comprises of three phase distorted voltage supply produced by programmable source. Three phases have different set of harmonics as shown in Figure 5.6, Figure 5.7 and Figure 5.8. Phase A contains the fundamental component and fifth harmonic component. Phase B contains third and seventh harmonic components with different amplitudes. Phase C analysis the performance analysis of both algorithms under multiple harmonic components. Figure 5.9 presents the results for three-phase harmonic groups measured under distorted voltage waveforms. The results show that the leakage in the neighboring bands is much higher for WPT as compared to IIR filter bank.

The harmonic groups measurement results are summarized in Table 5.1. For phase A, the results obtained using WPT is 0.0886 while for IIR it is 0.0869 pu. The actual value of third harmonic was 0.0869 pu. It can be seen that the IIR filter bank not only successfully measure the value of fifth harmonic component but also presents a lower leakage to the neighboring bands as compared to WPT. Similarly, for phase B, the harmonic contents available at third and seventh harmonic were 0.043 and 0.0869. The measured harmonic groups using WPT are 0.0505 and 0.0841 pu while IIR gives 0.0426 and 0.0850 pu.

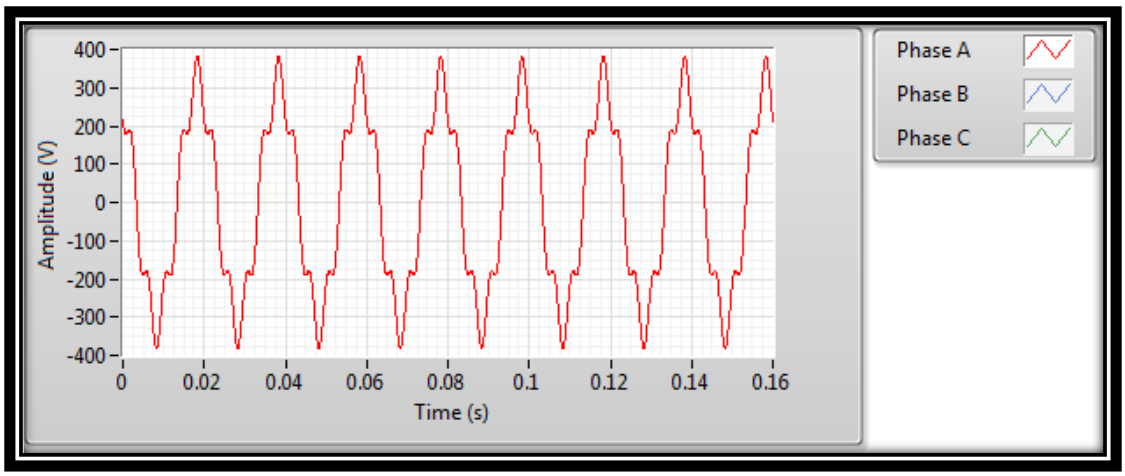

Figure 5.6 Distorted Voltage Supply of Phase A with Fifth Harmonic Component

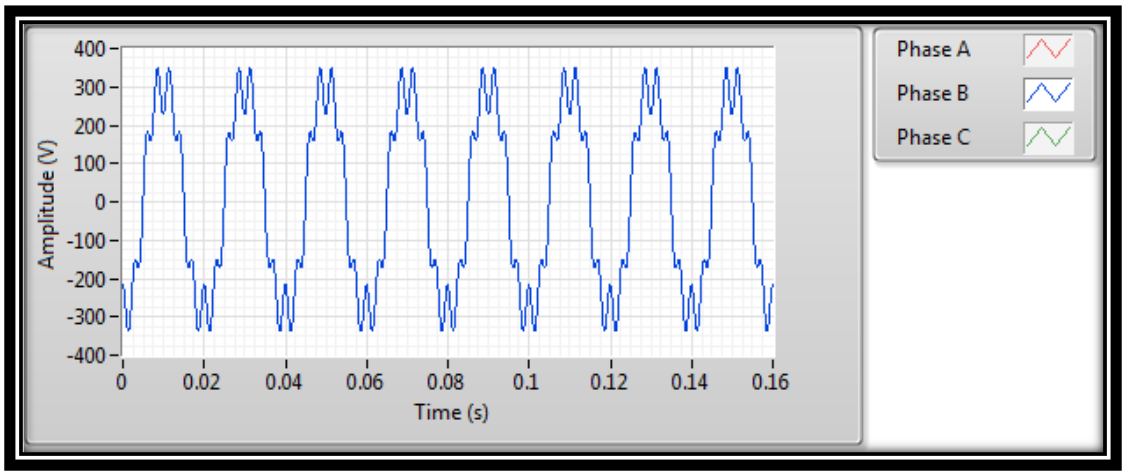

Figure 5.7 Distorted Voltage Supply of Phase B with Third and Seventh Harmonic

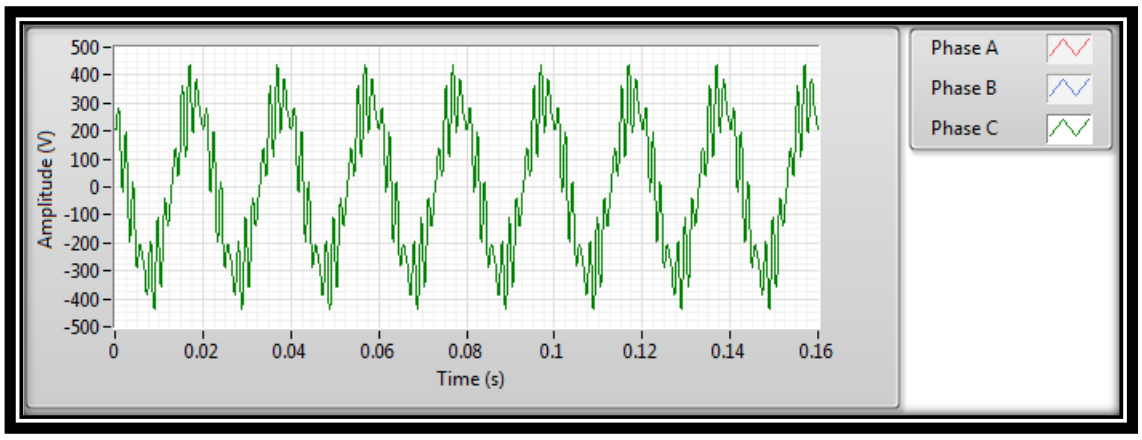

Figure 5.8 Distorted Voltage Supply of Phase C with Multiple Harmonic Components

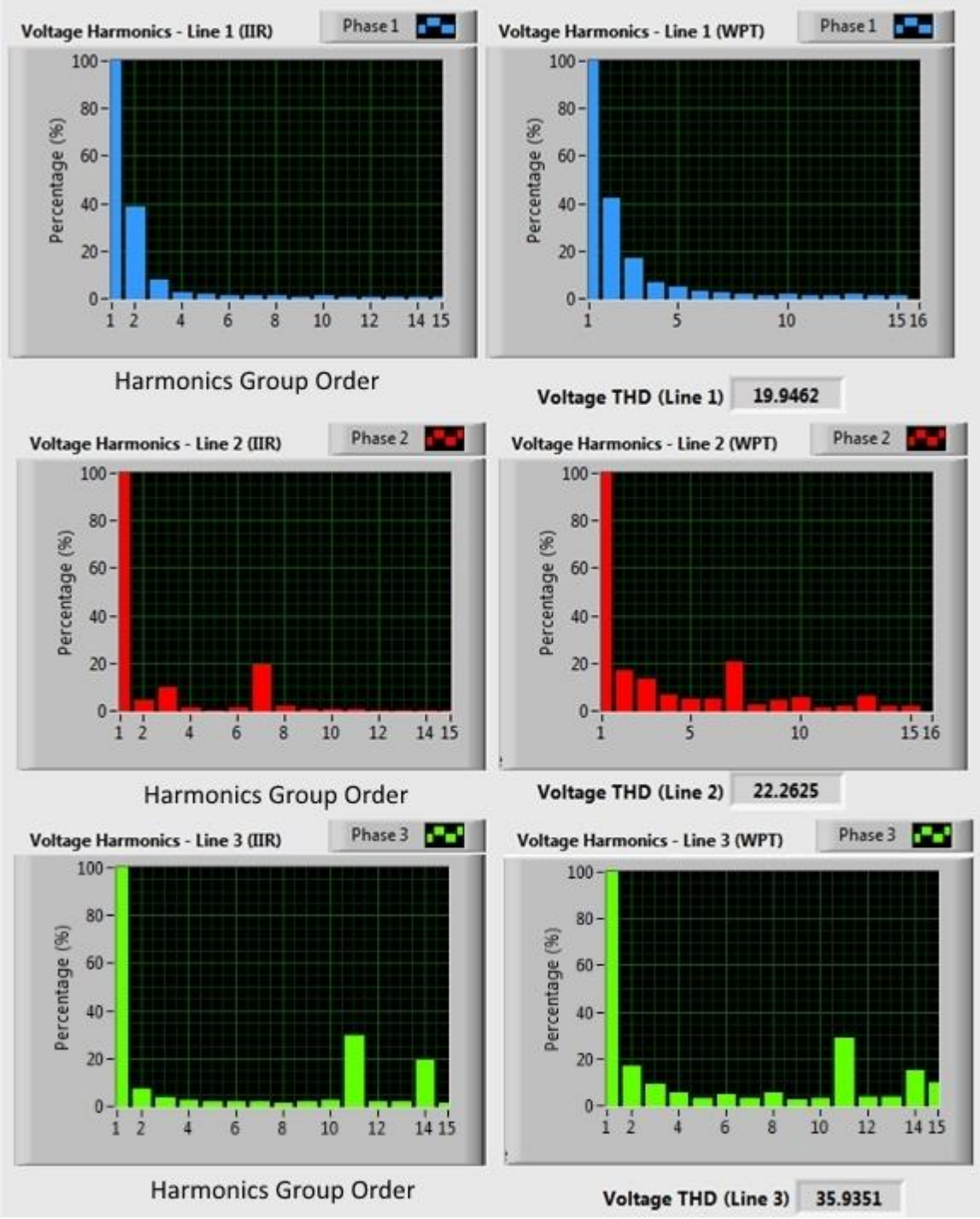

Figure 5.9 Comparative Analysis of WPT and IIR Filter for Three Phase Distorted Voltage Supply

The performance of both algorithms is tested under higher order 11^{th} and 14^{th} harmonics in phase C with amplitude of 0.1304 and 0.0869, respectively. It can be seen in Table 5.1, the measured harmonic groups using WPT are 0.1265 and 0.0651 pu while IIR gives 0.1285 and 0.0845 pu at 11^{th} and 14^{th} harmonic groups. A very high-energy leakage is observed using WPT at15^{th} harmonic group from neighboring band with 0.0425 pu.

Table 5.1 Real Time Comparative Analysis of Harmonic Groups Measurement using WPT and IIR for Distorted Voltage Supply

N	**Phase A**			**Phase B**			**Phase C**		
	Actual Value	**Prop. WPT**	**Prop. IIR**	**Actual Value**	**Prop. WPT**	**Prop. IIR**	**Actual Value**	**Prop. WPT**	**Prop. IIR**
1	1	1	1	1	1	1	1	1	1
2	0	0.0709	0.0287	0	0.0978	0.0178	0	0.0732	0.0309
3	0	0.0457	0.0130	***0.043***	***0.0505***	***0.0426***	0	0.0380	0.0154
4	0	0.0304	0.0100	0	0.0302	0.0042	0	0.0242	0.0107
5	***0.0869***	***0.0886***	***0.0869***	0	0.0203	0.0009	0	0.0136	0.0085
6	0	0.0192	0.0087	0	0.0140	0.0046	0	0.0217	0.0071
7	0	0.0116	0.0056	***0.0869***	***0.0841***	***0.0850***	0	0.0134	0.0065
8	0	0.0061	0.0046	0	0.0282	0.0069	0	0.0246	0.0061
9	0	0.0069	0.0039	0	0.0222	0.0033	0	0.0099	0.0067
10	0	0.0070	0.0035	0	0.0221	0.0022	0	0.0138	0.0102
11	0	0.0040	0.0031	0	0.0090	0.0016	***0.1304***	***0.1265***	***0.1285***
12	0	0.0043	0.0028	0	0.0079	0.0013	0	0.0145	0.0085
13	0	0.0061	0.0026	0	0.0251	0.0011	0	0.0150	0.0074
14	0	0.0045	0.0024	0	0.0079	0.0009	***0.0869***	***0.0651***	***0.0845***
15	0	0.0054	0.0022	0	0.0092	0.0007	0	**0.0425**	0.0051

The second test case consists of a distorted voltage waveform and the six-pulse diode rectifier load current. The distorted voltage signal is taken from the load bus in the test system consisting of a full wave six-pulse bridge rectifier at the load bus as shown in Figure 5.10. The frequencies and respective voltage amplitude of the harmonics of the test signal are listed in Table 5.2. The signal under analysis consists of fundamental component along with 5^{th}, 7^{th}, 11^{th} and 13^{th} harmonic components with different magnitudes. A little energy leakage in the neighboring harmonic bands is expected due to the imperfect frequency response of the filters.

Table 5.2 shows the harmonic groups ranges from one to fifteen obtained by applying the five level WP decomposition and IIR filter bank. The results obtained show a close resemblance to the actual harmonic contents present in the test signal. The actual rms values of 5^{th}, 7^{th}, 11^{th} and 13^{th} current harmonics are 0.09, 0.043, 0.03 and 0.033 pu. The measured rms values of the 5^{th}, 7^{th}, 11^{th} and 13^{th} current harmonics using WPT are 0.0803, 0.0371, 0.0291 and 0.0264 respectively, while the proposed IIR filter bank approach result are 0.0823, 0.0374, 0.0268 and 0.0298 respectively. It can be seen that the results of IIR are much closer to the actual harmonic content as compared to the WPT.

The current harmonics present in the phase B of a six-pulse diode rectifier is presented in Table 5.2. The distorted load current waveform is shown in Figure 5.11. The current signal contains the 3^{rd}, 5^{th} and 8^{th} harmonics with the value of 0.45, 0.09 and 0.27 pu respectively. The WPT based results shows a very high leakage on 8^{th} and 9^{th} harmonics as expected due to the poor response of mid tree filters. These harmonic groups lies on the edge frequency of 1^{st} stage of WPT filtering resulting in a very high leakage due to the imperfect filtering response and roll off factor of the filter. The successive filtering makes the situation worst

and results in a very high leakage. This problem can easily solved by avoiding the successive filtering. Apart from the middle frequency bands, it is also observed that the 2nd harmonic frequency has a high leakage due to the very large amplitude of the neighboring fundamental frequency. The proposed IIR results show a substantial improvement not only in the successful detection of harmonics but also a very low competitive leakage in the neighboring bands.

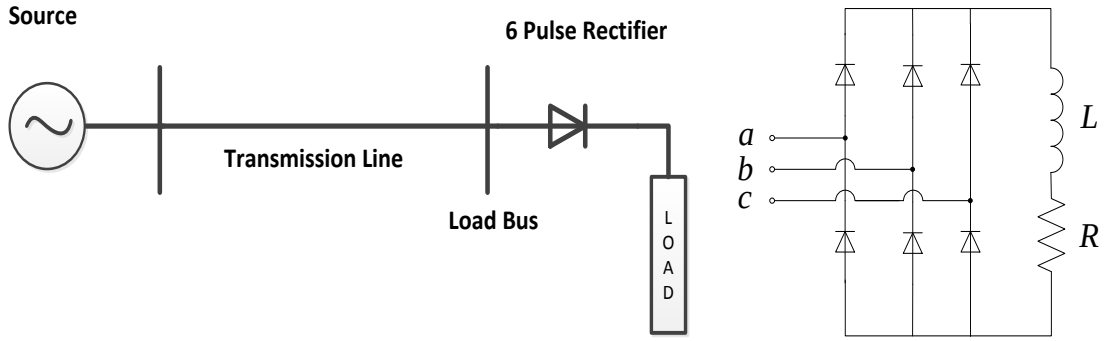

Figure 5.10 Six-Pulse Diode Rectifier Load

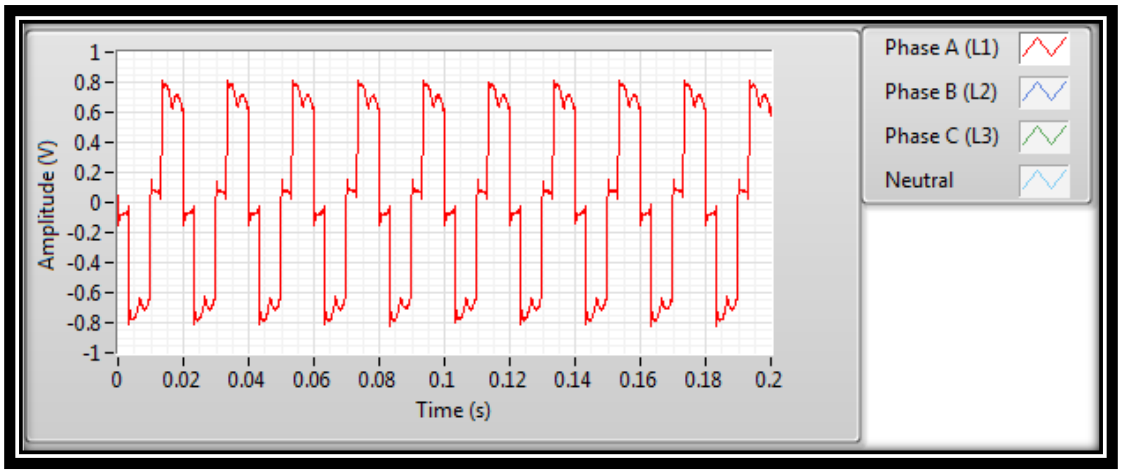

Figure 5.11 Load Current for Six-Pulse Diode Rectifier

Table 5.2 Experimental Results for Harmonic Groups Measurement

N	Distorted Voltage (Phase B)			Distorted Current (Phase B)	
	Actual Amplitude (pu)	**WPT (pu)**	**Prop. IIR (pu)**	**WPT (pu)**	**Prop. IIR (pu)**
1	***0.95***	***0.9444***	***0.9463***	***1***	***1***
2	0	0.0941	0..0735	0.1173	0.0845
3	0	0.0391	0.0374	0.4402	0.4571
4	0	0.0305	0.0255	0.0673	0.0313
5	***0.09***	***0.0803***	***0.0823***	0.0734	0.0898
6	0	0.0300	0.0210	0.0441	0.0073
7	***0.043***	***0.0371***	***0.0374***	0.0499	0.0126
8	0	0.0204	0.0146	0.1460	0.2701
9	0	0.0161	0.0130	0.1324	0.0239
10	0	0.0192	0.0114	0.0247	0.0142
11	***0.03***	***0.0291***	***0.0268***	0.0132	0.0112
12	0	0.0088	0.0139	0.0135	0.0097
13	***0.033***	***0.0264***	***0.0298***	0.0381	0.0085
14	0	0.0060	0.0088	0.0105	0.0077
15	0	0.0041	0.0094	0.0172	0.0070

CHAPTER 6

CLASSIFICATION OF POWER QUALITY DISTURBANCES

In this chapter, an efficient PQ disturbance classification technique is proposed using WT and optimized ANN. The WT based multi-resolution technique is applied for the analysis and feature extraction of PQ disturbances. An optimized ANN model is developed by taking the advantage of the global search ability of differential evolution (DE) algorithm to train the network.

6.1 Wavelets for PQ Analysis

Wavelet transform is an attractive technique for analyzing PQ waveform due to its ability to decompose a signal into multiple frequency bands. WT reveals the aspects of data that other analysis tools would miss, like trends, discontinuities, interruptions, and self-similarity. In addition, it has proven to be very strong and efficient technique for feature extraction from PQ disturbance data.

6.1.1 Detection and Localization

The distorted signal can be decomposed using WT into different resolution levels. Generally, any discontinuity or sudden change in the signal can be easily detected using first level wavelet decomposition. The detail coefficients at first decomposition levels are adequate to detect and localize the disturbance. However, the higher level decomposition is mostly used to extract the features that are helpful in the disturbance classification and

harmonic measurements.

6.1.2 Classification

PQ disturbances can be easily classified using the energy distribution across the multiple frequency bands. Application of Parseval's theorem can be used to obtain the energy of the distorted signal using the orthogonal wavelet coefficients. The energy or norm of the signal can be partitioned according to the following [110]:

$$\int |f(t)|^2 dt = \sum_{j \le j_0} \sum_{k} |D_j(k)|^2 \tag{6.1}$$

where, D_j represents the wavelet coefficients of the j^{th} decomposition level and k represents the wavelet coefficients at each decomposition level.

6.2 Optimized Artificial Neural Network Using Differential Evolution

6.2.1 Artificial Neural Network

Artificial neural network (ANN) is a computational model, which mimics the behavior of human brain. Extremely complex problems are usually dealt with ANN, which becomes one of the promising computation techniques in power system application because of its abilities of parallel computation and adaptiveness to external disturbances. This work uses the most commonly and widely used feed-forward multilayer perceptron (MLP) structure ANN to classify PQ disturbances. As shown in Figure 6.1, a typical neural network consists of three (input, hidden and output) layers, interconnected by modifiable weights represented by links between layers [111]–[113]. In Figure 6.1, w_{ij} represents the connecting weights between *i-th* and *j-th* nodes whereas w_{bk} represents the bias of *k-th* node. Input layer receives data and sends it to the hidden layer with the help of associated connection weights. After processing through hidden layer with the help of activation

function, the output layer provides the targeted data. The weights are initialized with pseudo-random values and are changed in a direction that will reduce the error through supervised learning method. However, in the beginning the error is high but through the learning process, the error becomes smaller. The algorithm terminates when error does not change for a pre-specified number of epochs or becomes smaller than some preset value. The search can be also terminated if it reaches the maximum number of epochs.

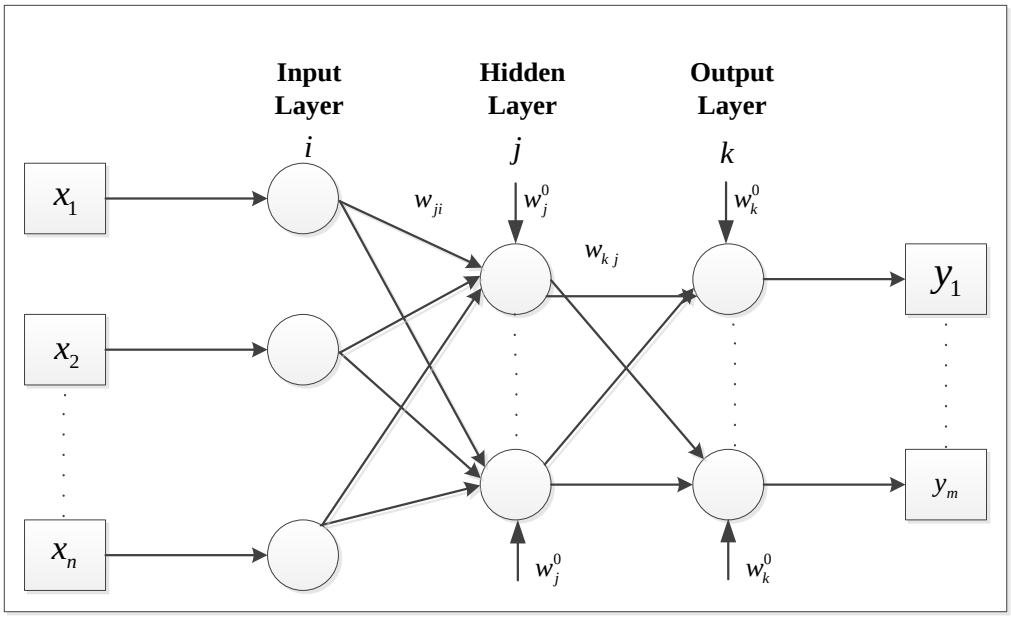

Figure 6.1 Generic Feed-forward MLP

6.2.2 ANN Weights Optimization using Differential Evolution Algorithm

R. Storn, K. Price [114] introduced one of the most promising population based optimization technique called differential evolution. Researchers prefer DE compared to other techniques [115], [116] because it is simple, robust and more diversified. In addition, it requires minimal number of control variables. DE is one of the well-suited techniques for solving non-differentiable, non-linear optimization problems. DE is a population based direct search algorithm, which comprises the following steps:

Step-1: Population initialization

The preliminary step for the implementation of DE is the generation of initial population. As there is no prior knowledge at the beginning about the global optimal solution, initial population is generated randomly within given boundary constraints using the following equation.

$$P_{ij} = x_{\min j} + rand * \left(x_{\max j} - x_{\min j} \right) \tag{6.2}$$

Where, $i = 1, 2, 3, \ldots, N_p$ and $j = 1, 2, 3, \ldots, D$. Here, N_p and D represent the size of population and dimension of the problem respectively, *rand* is a random number between [0, 1], P_{ij} represents the population and x_{min} and x_{max} represent the minimum and maximum values of the constraint parameters.

Step-2: Fitness test and storing the best solution

Fitness of all randomly generated individuals are evaluated and the best-fitted one is stored.

Step-3: Mutation

The mutation operation is considered as the primary step towards the generation of new solutions and to get mutant vector the following equation is used.

$$M_{ij} = P_{ij} + F_1 * \left(P_{rand1,j} - P_{rand2,j} \right) + F_2 * \left(P_{best,j} - P_{ij} \right) \tag{6.3}$$

Where, M represents the mutant vector, P_{best} is stored optimal solution, P_{rand1} and P_{rand2} are randomly selected solutions or vectors ($rand1 \neq rand2$) and F_1 and F_2 are mutation factor.

Step-4: Crossover

The crossover operation is applied in DE to further perturb the generated solution to get better diversity. If a randomly generated value between [0, 1] is greater than crossover rate, the new generation is selected from mutant vector otherwise from old solutions.

Step-5: Selection

Fitness of all individuals after mutation and crossover operations are evaluated. Based on fitness values and previously evaluated fitness for old generation a new set of solutions is selected for the next iteration.

Step-6: Termination Criteria

After producing new population following above mentioned steps, the algorithm updates the global optimum solution and simultaneously checks the stopping criterion. The algorithm terminates if the optimal solution does not change for a pre-specified number of iterations or the search reaches the maximum number of iterations.

6.2.3 Optimization Problem Formulation

The objective function of the problem is to minimize the mean squared error (MSE) of the ANN output which can be written as follows:

$$\textit{Minimize} \quad J \tag{6.4}$$

where,

$$J = MSE = \frac{1}{N}\sum_{i=1}^{N}\left\{Y(i) - Z(i)\right\}^2 \tag{6.5}$$

N is the number data points in target *(Y)* and output *(Z)* data set.

6.3 Proposed Algorithm

Generally, a signal *f* can be decomposed into approximation and detail components, as follows:

$$f = \sum_{k} a_{j_0 k} \varphi_{j_0 k} + \sum_{j \le j_0} \sum_{k} d_{jk} \psi_{jk} \tag{6.6}$$

where,

$$\psi_{jk}(t) = 2^{-j/2} \psi\left(2^{-j} t - k\right) \tag{6.7}$$

$$\varphi_{j_0 k}(t) = 2^{-j_0/2} \varphi\left(2^{-j_0} t - k\right) \tag{6.8}$$

$\psi(t)$ and $\varphi(t)$ represent the mother wavelet and the scaling function respectively.

$$d_{jk} = \int f(t) \psi_{jk}(t) dt \tag{6.9}$$

$$a_{j_0 k} = \int f(t) \varphi_{j_0 k}(t) dt \tag{6.10}$$

It is observed that coefficients corresponding to orthogonal signals are orthogonal sequences. Suppose *f*, $f^{\wedge}$ are orthogonal signals. i.e.

$$f \,.\, \tilde{f} = 0\,, \quad \left(\int f(t)\, \tilde{f}(t) dt = 0\right) \tag{6.11}$$

where

$$f = \sum_{j,k} d_{jk} \psi_{jk} \quad , \qquad \tilde{f} = \sum_{j',k'} \tilde{d}_{j'k'} \psi_{jk'} \tag{6.12}$$

$$0 = f \,, \tilde{f} = \sum_{j,k} d_{jk} \psi_{jk} \quad , \sum_{j',k'} \tilde{d}_{j'k'} \psi_{jk'} \tag{6.13}$$

$$\left\| d_{jk} \right\|_{\Delta_j} = \left(\sum_{k \in \Delta_j} {d_{jk}}^2 \right)^{\frac{1}{2}} \quad , \quad \left\| \tilde{d}_{jk} \right\|_{\Delta_j} = \left(\sum_{k \in \Delta_j} {\tilde{d}_{jk}}^2 \right)^{\frac{1}{2}} \tag{6.14}$$

- *f:* Pure signal.
- d_{jk}*:* Wavelet detail coefficients of the pure signal at the scale level *j*.
- $\tilde{d}_{jk}$*:* Wavelet detail coefficients of the disturbance signal at the scale level *j*.

Feature vector (F_v) for pure and disturbance signal is constructed using the energy of approximation and detail coefficients as:

$$F_v = [\left\| a_j \right\|, \left\| d_j \right\|, \left\| d_{j-1} \right\|, ..., \left\| d_{j-k} \right\|] \tag{6.15}$$

$$\tilde{F}_v = [\left\| \tilde{a}_j \right\|, \left\| \tilde{d}_j \right\|, \left\| \tilde{d}_{j-1} \right\|, ..., \left\| \tilde{d}_{j-k} \right\|] \tag{6.16}$$

where $k = j-1$.

The feature vector used for the classification of PQ disturbances is the measure of the deviation of disturbance signal feature to the pure signal features as:

$$\Delta F_v = F_v - \tilde{F}_v \tag{6.17}$$

The above feature vector ΔF_v is constructed using MATLAB wavelet toolbox. The obtained feature vector is passed to the next stage for ANN based PQ classification. The weights of ANN are optimized using DE as shown in proposed algorithm block diagram Figure 6.2. The distinctive feature vector used by optimized ANN for the classification of six different types of disturbances as shown in Figure 6.3. These disturbances are constructed using the parametric equations of different disturbances as shown in Table 6.1.

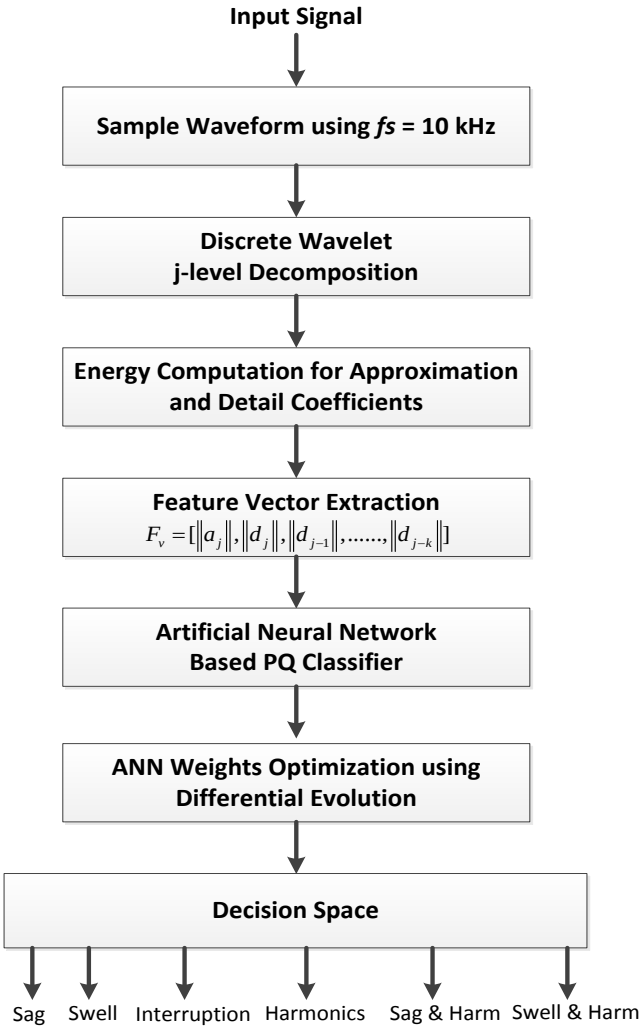

Figure 6.2 Block Diagram of PQ Disturbances Classification using the Proposed WT Based Optimized ANN

Table 6.1 Modelling of PQ Disturbances and Their Parameters Variations

Disturbance	Symbol	Modeling	Parameter
Sag	C1	$x(t) = A(1-\alpha(u(t-t_1)-u(t-t_2)))\sin(\omega t)$	$0.1<\alpha<0.9$, $T<t_2-t_1<11T$
Swell	C2	$x(t) = A(1+\alpha(u(t-t_1)-u(t-t_2)))\sin(\omega t)$	$0.1<\alpha<0.9$, $T<t_2-t_1<11T$
Harmonics	C3	$x(t) = A(\alpha_1 \sin(\omega t)) + \alpha_3 \sin(3\omega t)$ $+\alpha_5 \sin(5\omega t) + \alpha_7 \sin(7\omega t)$	$0.05<\alpha_1,\alpha_3,\alpha_5<0.15$, $\sum \alpha_i^2 = 1$
Interruption	C4	$x(t) = A(1-\alpha(u(t-t_1)-u(t-t_2)))\sin(\omega t)$	$0.9<\alpha<1$, $T<t_2-t_1<11T$
Sag and Harmonics	C5	$x(t) = A(1-\alpha(u(t-t_1)-u(t-t_2)))\alpha_1 \sin(\omega t)$ $\alpha_3 \sin(3\omega t) + \alpha_5 \sin(5\omega t) + \alpha_7 \sin(7\omega t)$	$0.1<\alpha<0.9$, $T<t_2-t_1<11T$ $0.05<\alpha_1,\alpha_3,\alpha_5<0.15$, $\sum \alpha_i^2 = 1$
Swell and Harmonics	C6	$x(t) = A(1+\alpha(u(t-t_1)-u(t-t_2)))\alpha_1 \sin(\omega t)$ $\alpha_3 \sin(3\omega t) + \alpha_5 \sin(5\omega t) + \alpha_7 \sin(7\omega t)$	$0.1<\alpha<0.9$, $T<t_2-t_1<11T$ $0.05<\alpha_1,\alpha_3,\alpha_5<0.15$, $\sum \alpha_i^2 = 1$

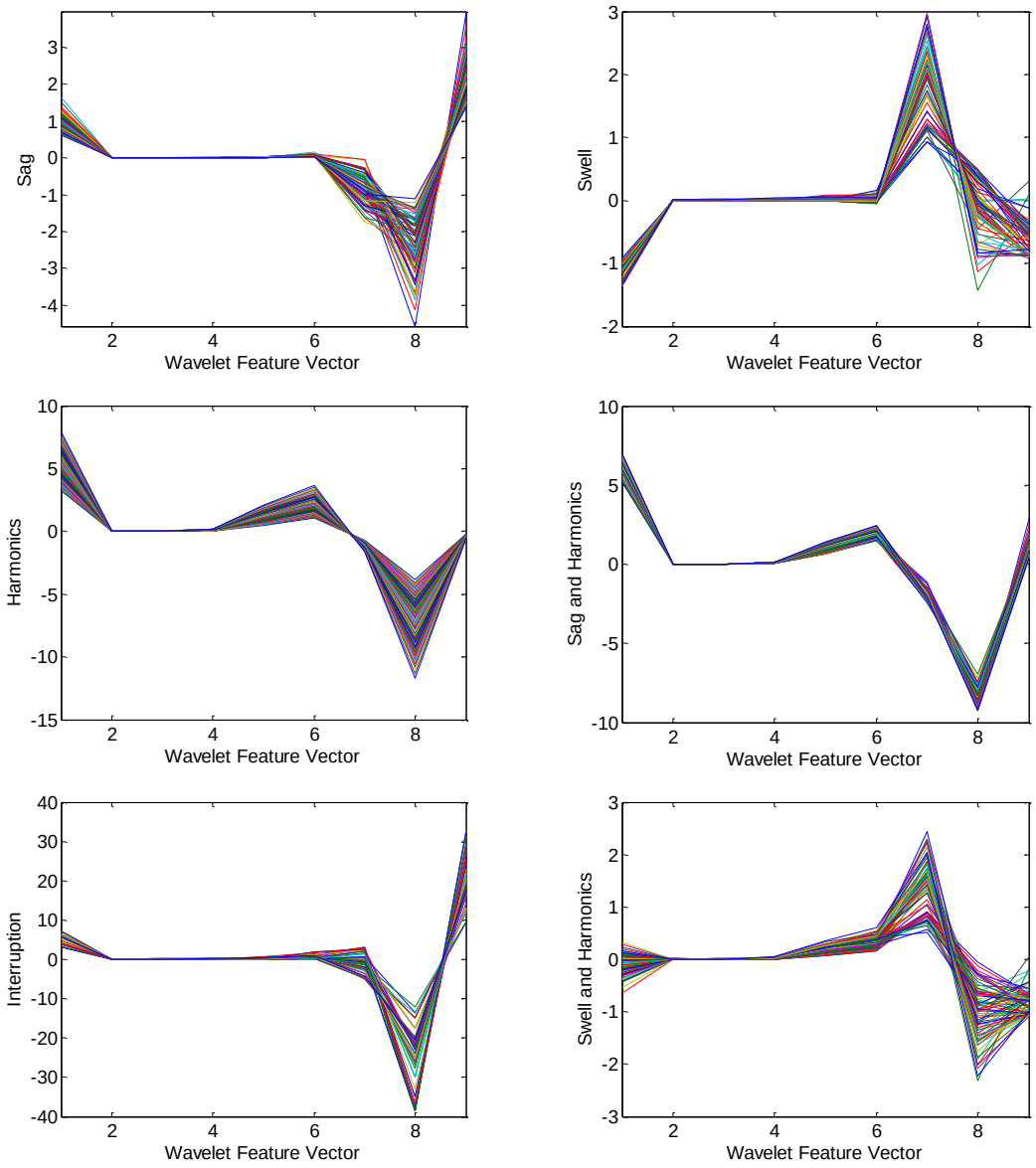

Figure 6.3 Distinctive Feature Vectors for Different PQ Disturbances

6.4 Simulation Results

Six different types of PQ disturbances are considered in order to examine the effectiveness of the proposed WT based method. These are voltage sag, voltage interruption, voltage swell, harmonics, and composite disturbances like voltage sag with harmonics and voltage swell with harmonics. The WT has been applied on the test signals that consist of 12 cycles, with 60Hz, 220V and sampling frequency of 10 kHz (166 sample/cycle).

The different types of power quality disturbances are generated using the parametric equations given in Table 6.1. For training and testing purposes of ANN, 200 samples for each of the six types of disturbance are generated using randomly distinctive disturbance magnitudes, time duration and different harmonics orders. A twelve level wavelet decomposition is proposed in [80] to classify the PQ disturbances, but it is observed that an eight level wavelet decomposition equivalent to the half fundamental frequency resolution is enough for PQ classification. Daubechies (db4) mother wavelet is used to obtain the eight level wavelet decomposition in this study. The feature vector consists of the energy content of the obtained approximation and detail coefficients using (6.15) and (6.16). A nine dimensional feature vector is constructed using the eight level detail and approximation coefficients. These two sets of feature vectors are used to train and test the proposed DE based neural network. The overall sample size used for ANN training and testing is 9×1200. The weights of the ANN are optimized using DE. Figure 6.4 presents the convergence characteristics of DE for the optimization of ANN weights with respect to the MSE defined in equation (6.5).

A 6×6 confusion matrix is obtained by the ANN and optimized ANN to classify the six different types of disturbances as shown in Table 6.2 and Table 6.3 respectively. The

diagonal elements of confusion matrix represent the successful detection while the off-diagonal elements represents the unsuccessful classification. Apart from the improvement in classification of individual disturbances, the overall accuracy of successfully classified PQ disturbances using optimized ANN is improved from 98.83% to 99.8%.

Table 6.2 Confusion Matrix for PQ classification using ANN

Symbol	C1	C2	C3	C4	C5	C6
C1	200	0	0	0	0	0
C2	0	197	0	0	0	3
C3	0	0	198	0	2	0
C4	5	0	0	195	0	0
C5	0	0	4	0	196	0
C6	0	0	0	0	0	200

Table 6.3 Confusion Matrix using Proposed Optimized ANN

Symbol	C1	C2	C3	C4	C5	C6
C1	200	0	0	0	0	0
C2	0	200	0	0	0	0
C3	2	0	198	0	0	0
C4	0	0	0	200	0	0
C5	0	0	0	0	200	0
C6	0	0	0	0	0	200

Neural networks are also built with different number of neurons to find the best possible neural network structure. In the supervised learning procedure to construct the network, 70% of data were used to train the network, 15% to test the network and rest 15% to validate the network. The performance of the network with respect to the different number

of neurons in the hidden layer is also investigated. MSE with different number of neurons is tabulated in Table 6.4, which shows that the network with nine hidden neurons gives the best performance with respect to the minimum MSE and overall accuracy. The comparison of the proposed algorithm in terms of overall accuracy with the literature [77]–[80] is presented in Table 6.5. The results demonstrate the high accuracy of successful disturbance classification using optimized ANN.

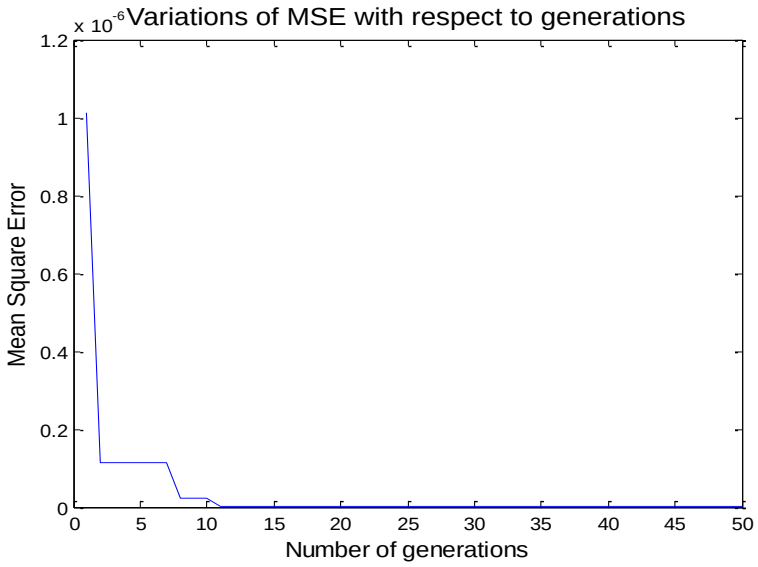

Figure 6.4 Variation of Objective Functions for an ANN With Nine Neurons

Table 6.4 MSE Errors with Optimized and General ANN

Number of Neurons	MSE		Accuracy in Classification (%)	
	General ANN	Optimized ANN	General ANN	Optimized ANN
2	4.16E-05	7.26e-12	98.3	99.6
6	1.63E-05	3.70e-12	98.8	99.8
8	1.43E-05	2.87e-12	99.5	99.8
9	1.31E-05	1.68e-12	99.6	100

Table 6.5 Performance Comparison of the Proposed Algorithm with the Literature

Symbol	Ref [77]	Ref [78]	Ref [79]	Ref [80]	Proposed %
C1	76.5	87	90	88	100
C2	97	100	100	96.5	100
C3	100	100	90	100	99
C4	90	80.5	100	85.5	100
C5	71.5	97	100	100	100
C6	98	100	100	100	100
Overall	88.83	94.08	96.66	95.00	99.83

6.5 Discussion

In this chapter, a novel approach for automatic classification of PQ disturbances using wavelet transform and optimized neural network is presented. The proposed approach utilizes a feature vector consisting of the energy content of detail and approximation coefficients of wavelet transform. This feature vector is fed to neural network based classifier for automatic classification of PQ disturbances. The weights of neural network are optimized using differential evolution algorithm. The optimized neural network results show the superiority of the proposed algorithm with respect to the improvement of accuracy in the classification of PQ disturbances.

CHAPTER 7

HARMONIC MITIGATION USING SHUNT ACTIVE POWER FILTER

This chapter presents the proposed harmonic mitigation techniques based on shunt active power filter. This chapter describes the modelling of SAPF, reference current generation algorithms, control strategies and parameter design for SAPF. Finally, simulation and experimental results are presented to validate the proposed strategies.

7.1 Modeling of SAPF

SAPF can be modeled as controlled current source, which injects the current in the power system to suppress the harmonics generated by the non-linear load [117]–[119]. This compensation current is calculated such that the source provides only the fundamental sinusoidal current. An installed SAPF is connected at point of common coupling as shown in Figure 7.1, where i_S represents the source current, while i_L and i_f are the distorted load current and compensation shunt active power filter current respectively.

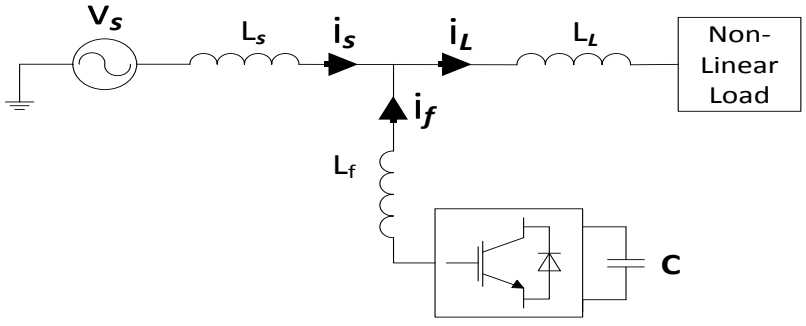

Figure 7.1 Single Line Diagram of Shunt Active Power Filter

The SAPF model is consisted of a three phase IGBT based switching devices, responsible to provide the harmonic compensation current i_f through the input inductor L_f as shown in Figure 7.2. The non-linear load is consisted of diode bridge rectifier with *RL* load on its dc side where i_L represents the distorted load current.

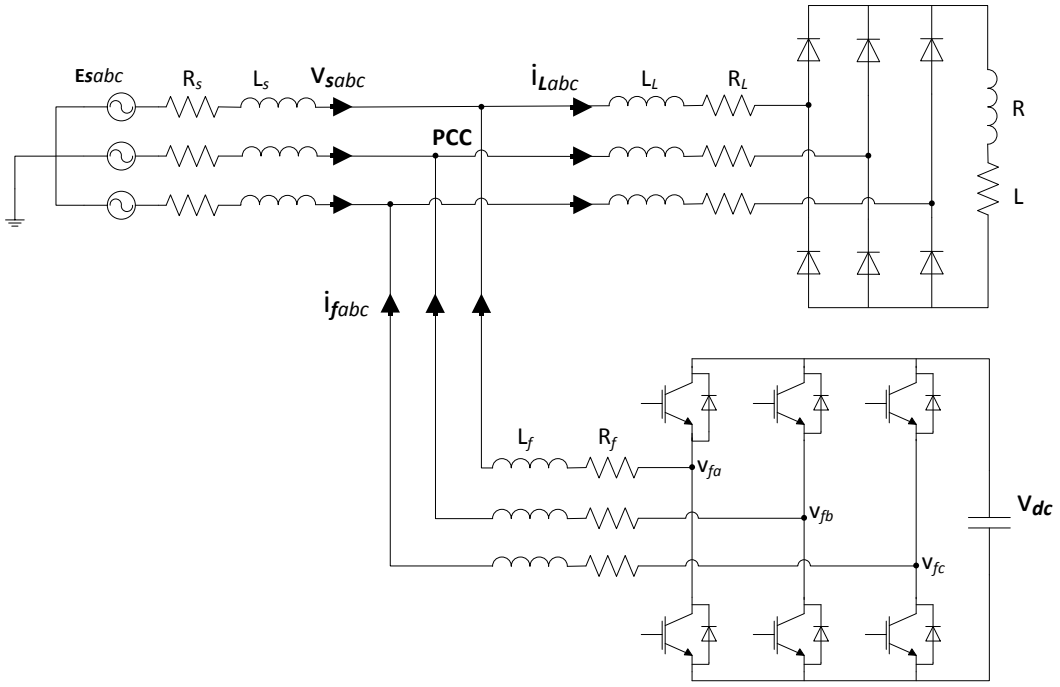

Figure 7.2 Topology Circuit for Three Phase Shunt Active Power Filter

where,

E_{sabc} : Three phase source voltage

i_{Labc} : Three phase load current

i_{fabc} : Three phase filter current

R_s and L_s : Source resistor and inductor

R_L and L_L : Load side resistor and inductor

R_f and L_f : Filter resistor and inductor

V_{dc} : DC side Capacitor Voltage

R and L : Resistive and Inductive Load

The three-phase source voltage source E_{sabc} is assumed to be a balanced source such that:

$$\begin{aligned} E_{sa}(\mathrm{t}) &= \mathrm{E}_{\mathrm{sm}}\sin(\omega \mathrm{t}) \\ E_{sb}(\mathrm{t}) &= \mathrm{E}_{\mathrm{sm}}\sin(\omega \mathrm{t}-\frac{2\pi}{3}) \\ E_{sc}(\mathrm{t}) &= \mathrm{E}_{\mathrm{sm}}\sin(\omega \mathrm{t}-\frac{4\pi}{3}) \end{aligned} \tag{7.1}$$

Where E_{sm} is the maximum source voltage and ω is the angular frequency. The voltage source is assumed to be a balanced source where the zero sequence can be neglected. The following assumptions are considered:

$$\begin{aligned} E_{sa}+E_{sb}+E_{sc} &= 0 \\ i_{sa}+i_{sb}+i_{sc} &= 0 \\ i_{La}+i_{Lb}+i_{Lc} &= 0 \\ i_{fa}+i_{fb}+i_{fc} &= 0 \end{aligned} \tag{7.2}$$

The SAPF is normally connected through a low pass RL filter at the PCC such that:

$$v_{sk} = v_{fk} - v_{Lfk} - v_{Rfk} \tag{7.3}$$

$$v_{sk} = v_{fk} - L_f \frac{di_{fk}}{dt} - R_f i_{fk} \tag{7.4}$$

Where $k = a, b, c$ represents the three phase system. Considering a balanced three phase system, the nonlinear current supplied by the inverter can be obtained by applying Kirchhoff laws as:

$$\begin{aligned} L_f \frac{di_{fa}}{dt} &= -R_f i_{fa} + v_{fa} - v_{sa} \\ L_f \frac{di_{fb}}{dt} &= -R_f i_{fb} + v_{fb} - v_{sb} \\ L_f \frac{di_{fc}}{dt} &= -R_f i_{fc} + v_{fc} - v_{sc} \end{aligned} \tag{7.5}$$

where i_{fa}, i_{fb} and i_{fc} are the three phase compensation current injected by the inverter.

The dc side capacitor equation can be written as:

$$C_{dc} \frac{dV_{dc}}{dt} = S_a i_{fa} + S_b i_{fb} + S_c i_{fc} \tag{7.6}$$

where C_{dc} is the capacitance of the dc side capacitor.

Above equations can be written in stationary reference frame using Concordia transform [120] as:

$$\begin{aligned} L_f \frac{di_{f\alpha}}{dt} &= -R_f i_{f\alpha} + v_{f\alpha} - v_{s\alpha} \\ L_f \frac{di_{f\beta}}{dt} &= -R_f i_{f\beta} + v_{f\beta} - v_{s\beta} \end{aligned} \tag{7.7}$$

$$C_{dc} \frac{dV_{dc}}{dt} = S_\alpha i_{f\alpha} + S_\beta i_{f\beta} \tag{7.8}$$

7.2 Reference Current Generation Algorithm for Shunt APF

Active power filters are designed to inject the nonlinear part of the load current in such a way that, the source should provide the purely sinusoidal current. The performance of active filter is highly dependent on the calculation of nonlinear load current. This nonlinear current also called as compensation current is calculated with the aid of reference current generation algorithms. These current extraction algorithms can be mainly divided into two main categories known as frequency domain current extraction algorithms [121]–[124] and time domain current extraction algorithms. The frequency domain extraction methods uses DFT and wavelet transform [125]–[128] to extract the compensation current. The major disadvantage of frequency domain methods are larger delays in transformation, filtering and inverse transformation, degraded performance during transients, large amount of processing delays and memory usage restrict their applicability in real time applications. On the other hand, the time domain methods are faster, accurate and require less processing delays and memory.

In this work, two different time domain current extraction algorithms have been implemented. Namely: instantaneous active and reactive power theory and synchronous reference frame theory have been utilized to obtain the compensation current for shunt active power filter.

7.2.1 Instantaneous Active and Reactive Power p–q Method

Most SAPFs have been designed using the instantaneous active and reactive power theory (p-q) proposed by Akagi [129]. The p-q theory is based on the computation of instantaneous powers defined in the time domain [130]–[132]. Clark Transformation (CT) [129] is used to transform the distorted currents and voltage signals from three phase frame

abc into bi-phase stationary frame *αβ*. The basic block diagram of instantaneous active and reactive power methodology is shown in Figure 7.3. The voltage and current signals are converted to stationary reference frame, fundamental power is extracted using low pass filter and finally the compensation current is converted back from stationary axis into three phases *abc*. The detailed methodology of instantaneous active and reactive power is given below:

The Clarke transformation for the three phase voltage and current signals is given by

$$\begin{bmatrix} v_\alpha \\ v_\beta \\ v_o \end{bmatrix} = \sqrt{\frac{2}{3}} \begin{bmatrix} 1 & -\frac{1}{2} & -\frac{1}{2} \\ 0 & \frac{\sqrt{3}}{2} & -\frac{\sqrt{3}}{2} \\ \frac{1}{\sqrt{2}} & \frac{1}{\sqrt{2}} & \frac{1}{\sqrt{2}} \end{bmatrix} \begin{bmatrix} v_a \\ v_b \\ v_c \end{bmatrix} \tag{7.9}$$

$$\begin{bmatrix} i_\alpha \\ i_\beta \\ i_o \end{bmatrix} = \sqrt{\frac{2}{3}} \begin{bmatrix} 1 & -\frac{1}{2} & -\frac{1}{2} \\ 0 & \frac{\sqrt{3}}{2} & -\frac{\sqrt{3}}{2} \\ \frac{1}{\sqrt{2}} & \frac{1}{\sqrt{2}} & \frac{1}{\sqrt{2}} \end{bmatrix} \begin{bmatrix} i_a \\ i_b \\ i_c \end{bmatrix} \tag{7.10}$$

The time domain instantaneous active and reactive power *p(t)* and *q(t)* in three phase system *abc* and stationary frame *αβ* is given as:

$$p(\mathrm{t}) = v_a i_{la} + v_b i_{lb} + v_c i_{lc} \tag{7.11}$$

$$p(\mathrm{t}) = v_\alpha i_{l\alpha} + v_\beta i_{l\beta} \tag{7.12}$$

$$q(\mathrm{t}) = -\frac{1}{\sqrt{3}}(v_\alpha i_{l\beta} - v_\beta i_{l\alpha}) \tag{7.13}$$

The above equations can be written in matrix form as

$$\begin{bmatrix} p \\ q \end{bmatrix} = \begin{bmatrix} v_\alpha & v_\beta \\ -v_\beta & v_\alpha \end{bmatrix} \begin{bmatrix} i_{l\alpha} \\ i_{l\beta} \end{bmatrix} \tag{7.14}$$

The instantaneous active and reactive powers p and q in (7.14) contain ac and dc power components. In order to obtain the purely sinusoidal source current, the compensation current should be calculated from AC power. The cutoff frequency of the low pass filter should be the same as the fundamental component frequency. The compensation current using the filtered power can be calculated as:

$$\begin{bmatrix} i^*_\alpha \\ i^*_\beta \end{bmatrix} = \frac{1}{v_\alpha^2 + v_\beta^2} \begin{bmatrix} v_\alpha & -v_\beta \\ v_\beta & v_\alpha \end{bmatrix} \begin{bmatrix} \tilde{p} \\ q \end{bmatrix} \tag{7.15}$$

where $\hat{p}$ represents the fundamental active power obtained after passing through the low pass filter as shown in Figure 7.4. The three phase compensation current is obtained from $\alpha\beta$ using inverse clark transformation as:

$$\begin{bmatrix} i^*_a \\ i^*_b \\ i^*_c \end{bmatrix} = \sqrt{\frac{2}{3}} \begin{bmatrix} 1 & 0 \\ -\frac{1}{2} & \frac{\sqrt{3}}{2} \\ -\frac{1}{2} & -\frac{\sqrt{3}}{2} \end{bmatrix} \begin{bmatrix} i^*_\alpha \\ i^*_\beta \end{bmatrix} \tag{7.16}$$

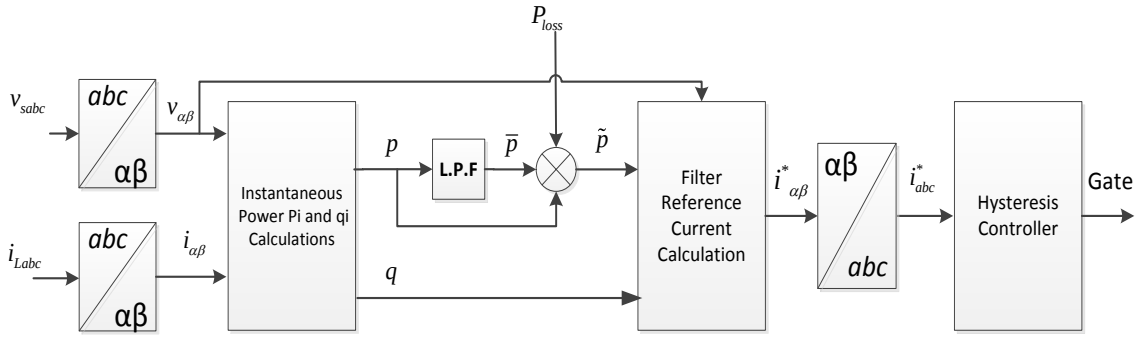

Figure 7.3 Block Diagram of Instantaneous Active and Reactive Power Theory for SAPF

Figure 7.4 Feed Forward Low Pass Filter

7.2.2 Synchronous Reference Frame d-q Method

Synchronous reference frame also known as instantaneous current method that transforms the three phase voltage and currents to the synchronous frame [132]–[135]. In this method, three phase quantities are transformed to the direct and quadrature axis. A phase locked loop (PLL) circuit is used to lock the phase of distorted mains voltage [136]–[140]. The block diagram of the synchronous reference frame based compensation current extraction method is shown in Figure 7.5. The three phase load current i_{Labc} is transformed into the synchronous frame load current i_{Ldq} using equation (7.17) as:

$$\begin{bmatrix} i_{ld} \\ i_{lq} \\ i_{lo} \end{bmatrix} = \sqrt{\frac{2}{3}} \begin{bmatrix} \cos\theta & \cos(\theta - \frac{2\pi}{3}) & \cos(\theta + \frac{2\pi}{3}) \\ -\sin\theta & -\sin(\theta - \frac{2\pi}{3}) & -\sin(\theta + \frac{2\pi}{3}) \\ \frac{1}{\sqrt{2}} & \frac{1}{\sqrt{2}} & \frac{1}{\sqrt{2}} \end{bmatrix} \begin{bmatrix} i_{la} \\ i_{lb} \\ i_{lc} \end{bmatrix} \quad (7.17)$$

where, θ represents the angular position of synchronous reference obtained using the phase locked loop. The angular position θ is a linear function of fundamental frequency. It is locked via the synchronous speed of the three phase grid voltage v_{sabc}.

In order to obtain the purely sinusoidal source current, the compensation current should be calculated from AC components of the direct and quadrature axis current i_{dq}. The decomposition of load current into fundamental and harmonics part can be written as:

$$\begin{aligned} i_{ld} &= \bar{i}_{ld} + \tilde{i}_{ld} \\ i_{lq} &= \bar{i}_{lq} + \tilde{i}_{lq} \end{aligned} \quad (7.18)$$

where, $\overline{i_{ld}}$ and $\widetilde{i_{ld}}$ are the fundamental and harmonic components of the load current i_{ld}. The AC components can be obtained via the aid of a feed forward low pass filter topology as shown in Figure 7.4. The compensation current is calculated as from the synchronous current:

$$\begin{bmatrix} \tilde{i}_{la} \\ \tilde{i}_{lb} \\ \tilde{i}_{lc} \end{bmatrix} = \sqrt{\frac{2}{3}} \begin{bmatrix} \cos\theta & -\sin\theta \\ \cos(\theta - \frac{2\pi}{3}) & -\sin(\theta - \frac{2\pi}{3}) \\ \cos(\theta + \frac{2\pi}{3}) & \sin(\theta + \frac{2\pi}{3}) \end{bmatrix} \begin{bmatrix} \tilde{i}_{ld} \\ \tilde{i}_{lq} \end{bmatrix} \quad (7.19)$$

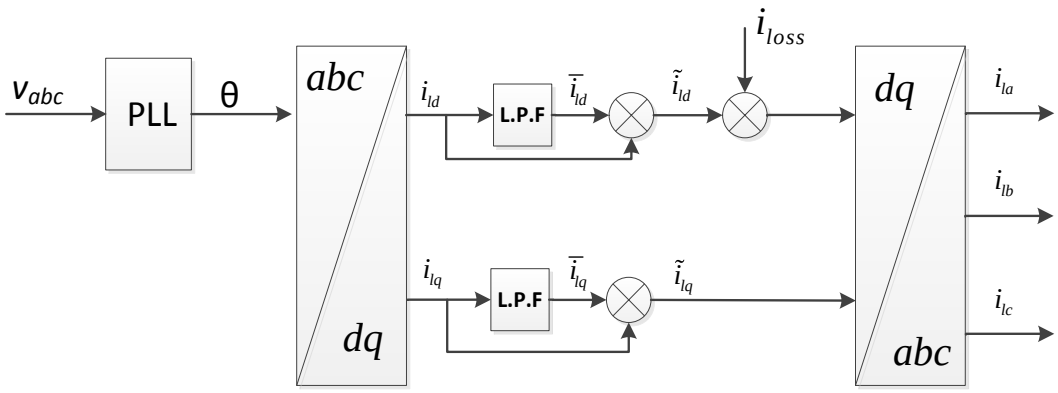

Figure 7.5 Synchronous Reference Frame Based Compensation Current Extraction for SAPF

7.3 Control Methods of VSI

The current control strategies play a vital role to generate the switching signals for fast and accurate response of inverters such as SAPF. The current controller is used to generate the switching patterns for SAPF.

7.3.1 Hysteresis Control Method

The hysteresis current control method for shunt active power filters can be used to generate the switching pattern of the inverter. Hysteresis current control method is the most commonly used control method due to its simple structure for implementation, fast and robust response, and computationally light as it does not required any separate controller or a modulator [141]–[146].

Hysteresis current controller operates the voltage source inverter by comparing the actual current with the reference current as shown in Figure 7.6. If the error between the actual current and the reference current value is larger than the predefined hysteresis band (Upper

or lower band) a switching pulse is generated immediately to open or close a specific inverter gate [147]. The SAPF compensation currents are regulated to be in good agreement with the reference current.

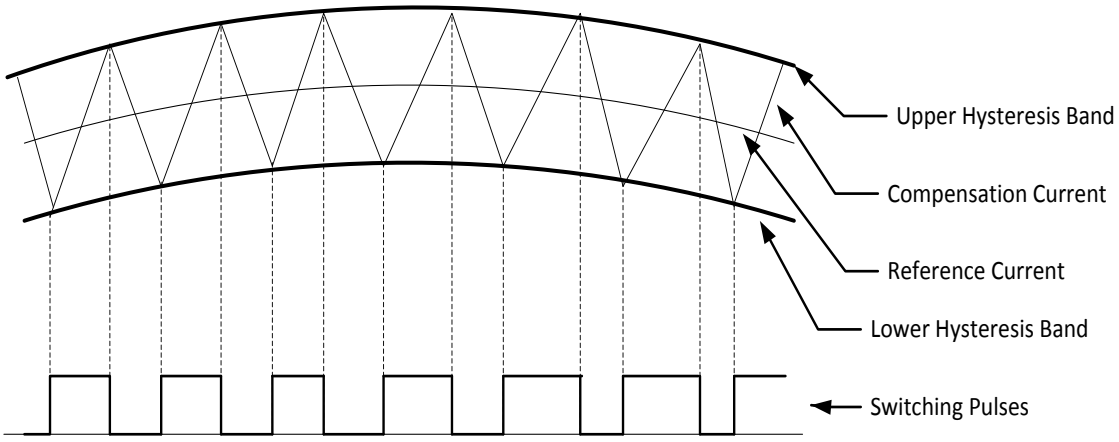

Figure 7.6 Hysteresis Current Controller

The switching pulses for SAPF three phases are generated as follows:

- If $Ica^* - Ica > HB$, the switching gate $g1$ is OFF while $g4$ is ON.
- If $Ica^* - Ica < HB$, the switching gate $g1$ is ON while $g4$ is OFF.

Where HB is the hysteresis band, Ica^* is the compensation current while Ica is the reference current for the phase a of SAPF. The switching pulses for remaining phases b and c can be generated in a similar way by comparing the corresponding reference and measured current with the hysteresis band.

7.4 DC Bus Voltage Regulation

The voltage source inverter based SAPF utilizes a DC-bus capacitor C_{dc} as a source to supply the reactive power and compensation current at high switching frequency. Under steady state conditions, the DC link capacitor is charged and discharged during the source

voltage period in order to provide the required compensation current. The peak harmonic and reactive loads are the primary factors that determine the value of DC link capacitor. The voltage across the DC link capacitor is kept high enough as compared to the peak source voltage in order to inject the required non-linear compensation current at PCC [148].

The block diagram of adopted DC bus voltage control through PI controller is shown in Figure 7.7 [149]. The error between the measured DC bus voltage and reference voltage can be calculated as:

$$\tilde{v}_{dc} = v_{dc}^{*} - v_{dc} \tag{7.20}$$

To regulate the voltage across dc link, the error signal $\widetilde{v_{dc}}$ is passed through a PI controller as:

$$u_{dc} = k_1 \tilde{v}_{dc} + k_2 \int \tilde{v}_{dc} dt \tag{7.21}$$

The transfer function of the PI controller is given as:

$$G(\mathrm{s}) = \frac{U_{dc}(\mathrm{s})}{\tilde{V}_{dc}(\mathrm{s})} = k_1 \frac{s + \frac{k_2}{k_1}}{s} \tag{7.22}$$

The closed loop transfer function is given by:

$$\frac{V_{dc}(\mathrm{s})}{V_{dc}^{*}(\mathrm{s})} = 2\zeta\omega_n \frac{s + \frac{\omega_n}{2\zeta}}{s^2 + 2\zeta\omega_n s + \omega_n^2} \tag{7.23}$$

where, the gain of the PI controller are:

$$k_1 = 2\zeta\omega_n C_{dc} \quad , \quad k_2 = \omega_n^2 C_{dc}$$

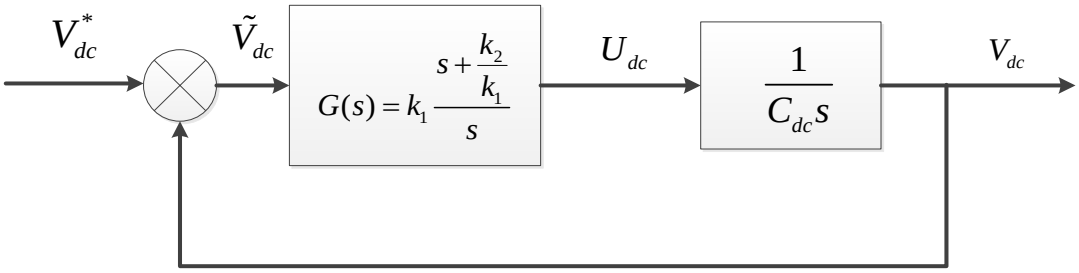

Figure 7.7 DC Bus Voltage Control Loop

7.5 SAPF Parameter Design

The selection of SAPF parameters like DC link capacitor and AC link reactor values have a greater impact on the performance of SAPF.

7.5.1 The DC Link Capacitor

The dc bus capacitor voltage value is limited by the actual capacitor size and the power ratings of the inverter. The following relation is used to design the dc bus voltage across the dc link capacitor [150]:

$$V_c \geq \frac{V_{s\max}}{(1 - f_s(T_{\min} + T_d)} \tag{7.24}$$

where, V_c and V_{smax} are the voltages across the capacitor and maximum source voltage, f_s is the switching frequency of the IGBTs while T_{min} and T_d are the minimum on time and dead time respectively.

$$V_c = \frac{(V_s - Li_L)i_L}{CV_c} \tag{7.25}$$

The energy stored across the capacitor can be calculated as:

$$\Delta W = \frac{1}{2}C(V_c^2 - V_o^2) = \int_0^t V_s i_L dt - \frac{1}{2}Li_L^2 \quad (7.26)$$

where, V_o is the initial voltage across the capacitor.

$$\Delta W = \frac{1}{2}C(V_c^2 - V_o^2) \approx C.\Delta V_c.V_o \quad (7.27)$$

The maximum allowable voltage variation across the capacitor is $\Delta V_c = \varepsilon V_o$

$$C \approx \frac{\Delta W}{\Delta V_c.V_o} = \frac{\Delta W}{\varepsilon.V_o^2} \quad (7.28)$$

7.5.2 The AC Link Reactor

The SAPF is connected with the distribution network at the PCC through an interfacing inductor. The values of the interacting inductor have a high impact on the system performance as a larger inductor value might result in small switching ripples but the dynamic response of the system is degraded. Similarly, a smaller inductor value results in a better utilization of dc voltage but the controller design becomes complex.

In this work, a maximum current criterion is considered to design the AC link reactor. The SAPF will provide the maximum current required by the nonlinear purely inductive load. The interfacing inductor value can be calculated as follows [151]:

$$L_{\min} = \frac{\Delta V_{\min}}{\omega I_{max}} \quad (7.29)$$

where, ω represents the source voltage angular frequency, I_{max} is the maximum current to be provided by the SAPF and ΔV_{min} is the difference between the source voltage and the fundamental inverter voltage.

7.6 Simulation Results

This section presents the simulation results of SAPF to mitigate the harmonics generated by non-linear loads. The simulation of the proposed control strategies of SAPF are carried out using MATLAB/SIMULINK software. The performance of the SAPF is verified using two different set of loads. These are static and dynamic RL load. The response of the system to a sudden change in the load is observed. The simulated load is highly non-linear in both test cases, so the load draws a highly enriched harmonic current from the grid. The system parameters used for the simulation are presented in Table 7.1

Table 7.1 System Parameter for Simulation

System Parameter	Value
Supply Voltage (V_s)	110 V
Supply Frequency (f)	50 Hz
DC Link Capacitance and Voltage (C, V_{dc})	2200 μF, 700V
Load Impedance (R_L, L_L)	10Ω, 2 mH
Filter Inductance	3.5 mH
p - q Controller (K_p, K_i)	20, 30
d - q Controller (K_p, K_i)	0.7 , 1

7.6.1 Case I: Static Three Phase Diode Rectifier RL Load

In this case, a static RL load is connected on the DC side of the rectifier. The rectifier injects the harmonics in the system. The performance of both controllers, instantaneous power controller and synchronous reference frame controller is analyzed under the same test conditions. The simulation results presents a detailed analysis of the system including

three phase source voltage, three phase source current, load and active filter current, dc link voltage and THDs of source and load current.

Figure 7.8 and Figure 7.9 present the system response for instantaneous power pq controller and synchronous reference frame *d* - *q* controller for a 100 ms window. The SAPF starts its operation at 20 ms and injects the nonlinear current required by the load.

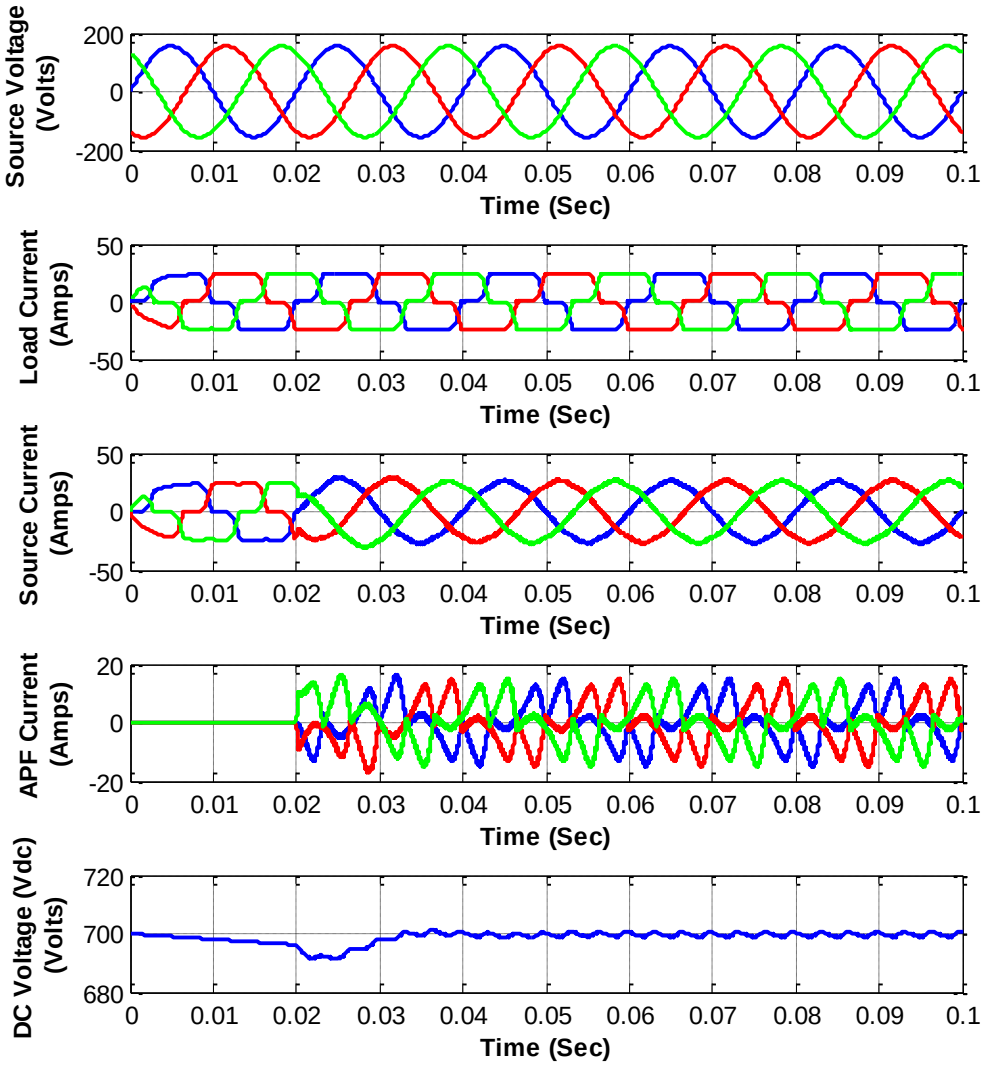

Figure 7.8 System Performance under Static Load and *p* - *q* Controller

The detailed analysis of Figure 7.8 and Figure 7.9 reveals that the voltage recovery on the dc link in *p* - *q* controller takes approximately 12 ms while in case of *d* - *q* controller DC link voltage recovers within 3 ms, much faster as compared to the *p* - *q* controller. Apart from that the current THD in case of *p* - *q* controller is 2.89% while in case of d - *q* controller it is 2.38%. The load current THD was 20.97% without the SAPF as shown in Figure 7.10.

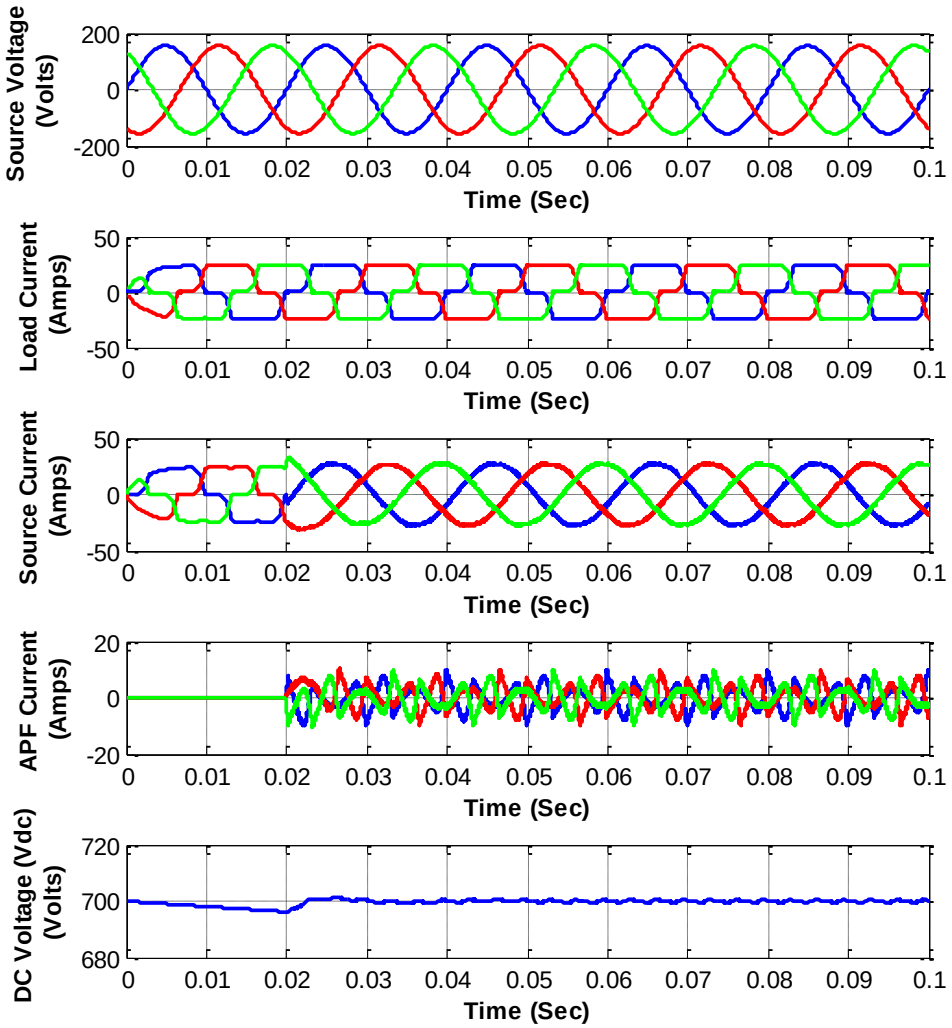

Figure 7.9 System Performance under Static Load and *d* - *q* Controller

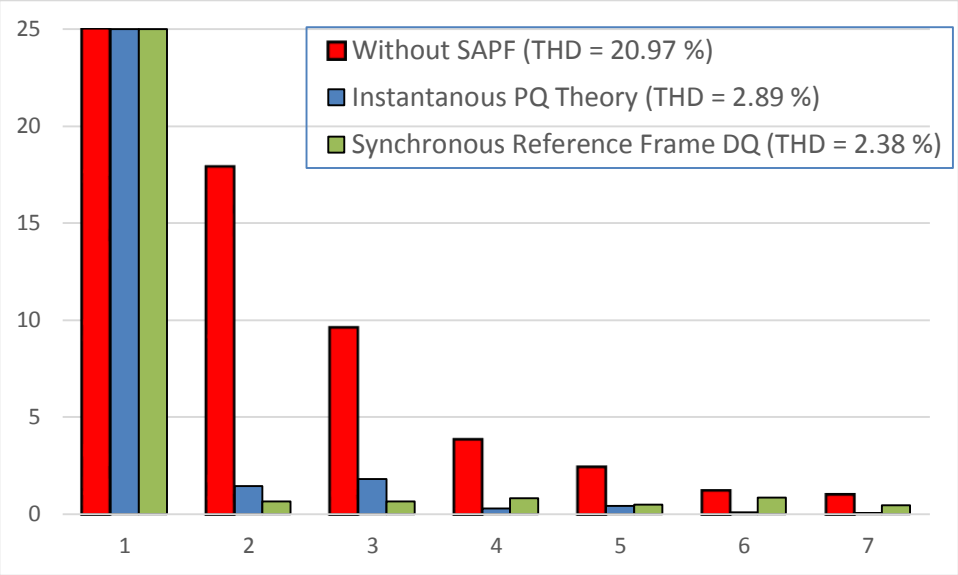

Figure 7.10 Harmonic Spectra for Source Current under Static RL Load

7.6.2 Case II: Variable Three Phase Diode Rectifier RL Load

In this test case, a variable load is connected to the grid through a three phase rectifier. This variable load is used to test the dynamic performance of the SAPF.

The initial load connected to the system was 20 Amps and the load current is doubled to 40 Amps at the 50ms. Figure 7.11 and Figure 7.12 presents the performance analysis of the *p* - *q* and *d* - *q* based SAPF respectively. Both controller adapt the new reference current quite accurately. The dc link voltage of *p* - *q* controller recovers to its reference value within one cycle of load current, while the dc link voltage recovers within half cycle of load current in case of *d* - *q* controller. Therefore, the dynamic response of *d* - *q* controller is much faster as compared to the *p* - *q* controller. The source current THD without SAPF was recorded as 26.14% while the source current THD was reduced to 3.15% for *p* - *q* controller and 1.82% for *d* - *q* controller as shown in Figure 7.13. Thus, the simulation results reveal that the dynamic response of *d* - *q* controller is much faster and accurate as

compared to the p - q controller. The SAPF follow the change in the load current and quickly adapt the new reference current, when the connected load changes.

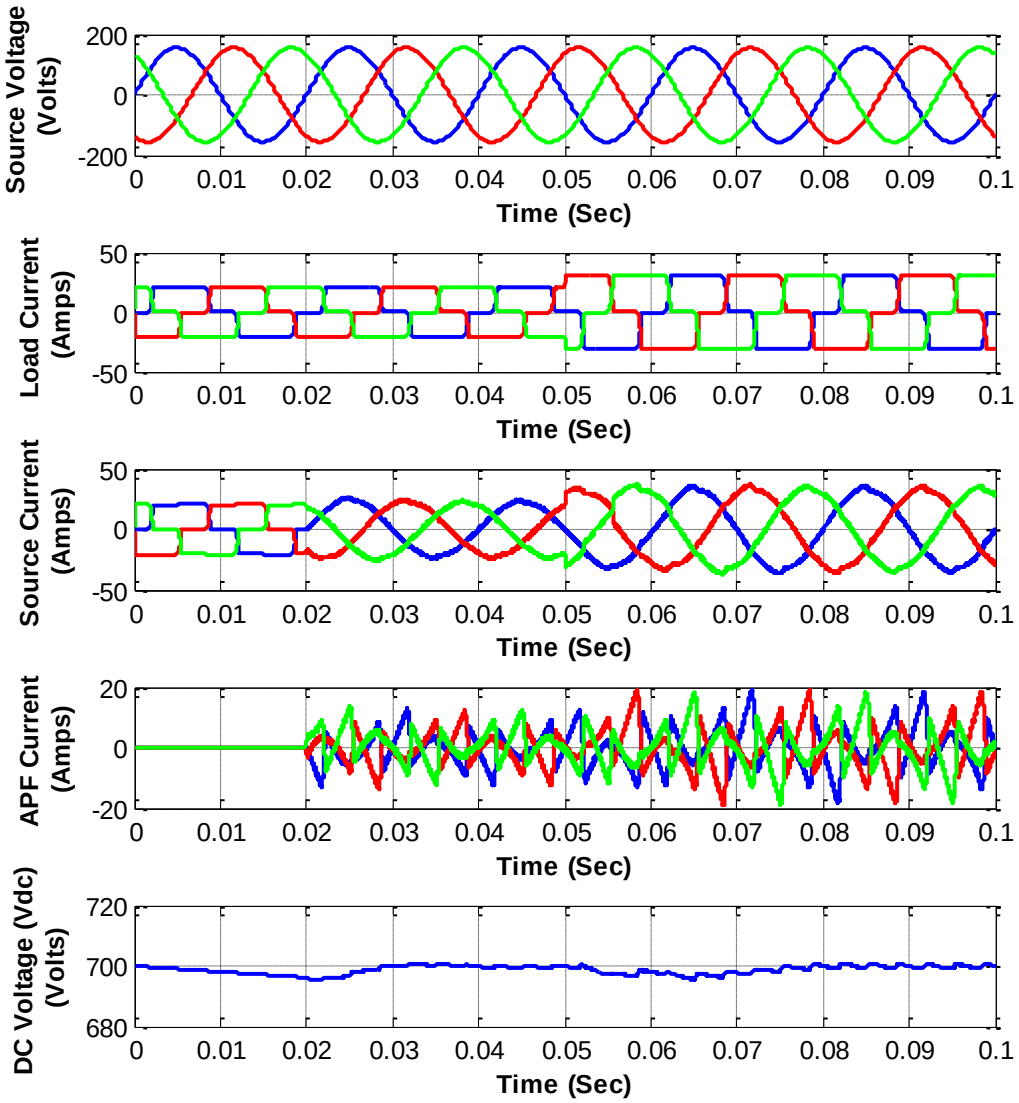

Figure 7.11 Performance Analysis of p - q Controller under Dynamic Load Change

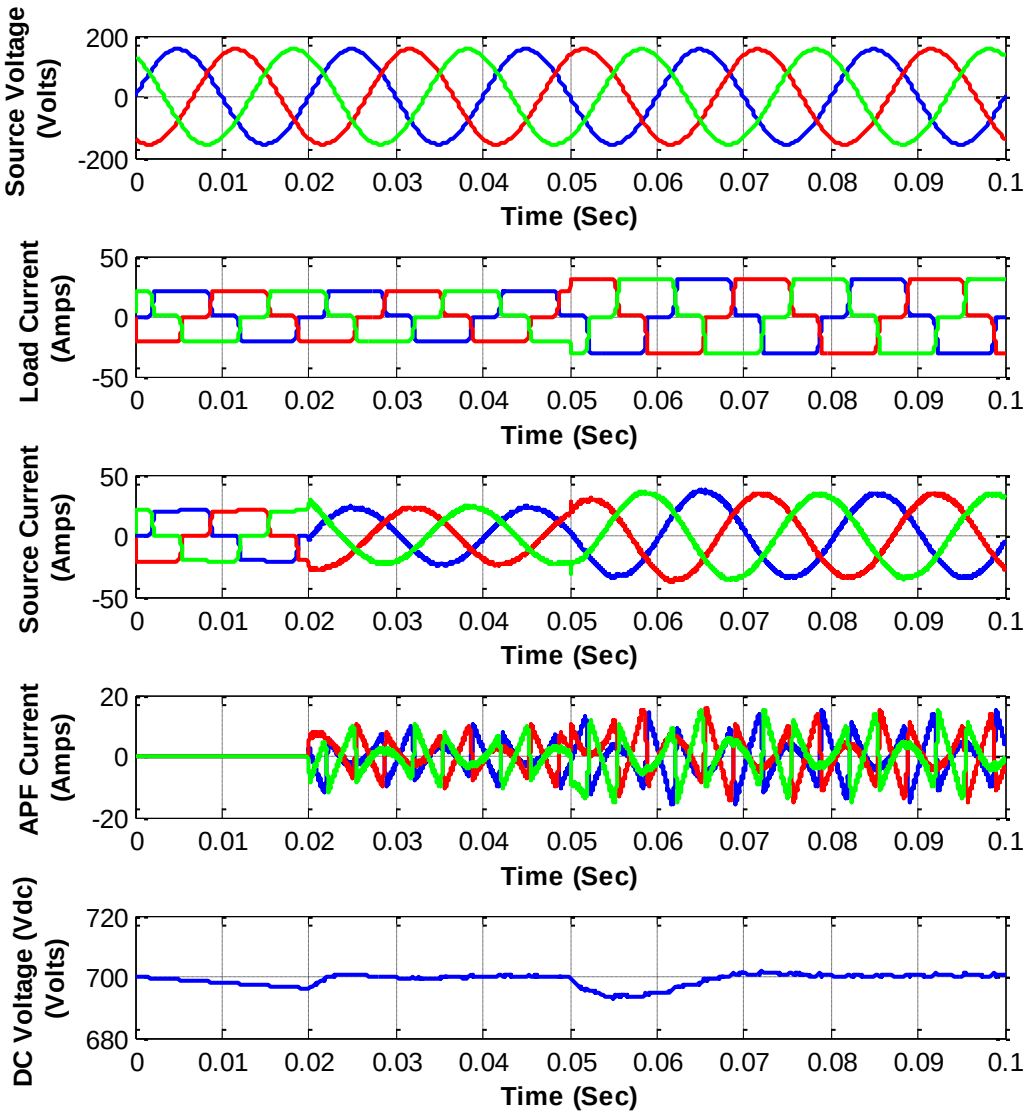

Figure 7.12 Performance Analysis of *d* - *q* Controller under Dynamic Load Change

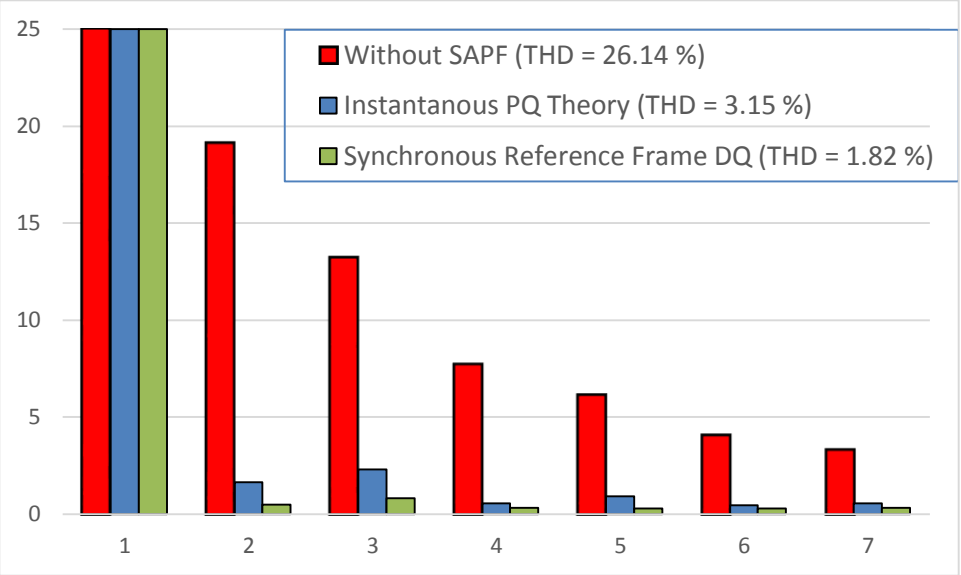

Figure 7.13 Harmonic Spectra for Source Current under Sudden Load Change

7.7 Real-Time Digital Simulator (RTDS) with Hardware in the Loop Simulation

Nowadays, modern power system needs very fast, flexible and scalable real time simulators. RTDS hardware discussed in Appendix C is based on the parallel processing architecture specifically designed to solve the transient simulation algorithm. RSCAD is the software package used to access the hardware resources of RTDS. RSCAD provide the draft and run time files for designing and testing the power systems respectively.

RTDS is equipped with Giga-Transceiver Analog Input/output (GTA I/O) cards. The GTA I/O cards have 12 Inputs/outputs used to interface RTDS with external devices either regular (~ 50 μsec) or small time step (< 2 μsec) in case of power electronic devices simulations. In this work, a simplified power system model is developed in RTDS using three phase source, rectifier and inverter. The small time step simulation is used for fast switching of the inverter. The controller for SAPF is implemented in dSPACE DS1103.

The RTDS and dSPACE are interfaced together to exchange the signals for SAPF hardware in the loop implementation as shown in Figure 7.14. A workstation is used to monitor, control and record the current and voltage waveforms. The Giga Transceiver Workstation Interface Card (GTWIF) card is responsible for the communication with the RSCAD to start and stop the simulation. The RTDS processor card GPC is used to solve the power/control systems components equations. The interface between RTDS and dSPACE controller is built to exchange the voltage and current signals using analog and digital cards as shown in Figure 7.15. dSPACE uses DS-817 and DS-814 to communicate with the workstation where Matlab/Simulink is installed.

The block diagram of the basic active filter model built in RTDS is shown in Figure 7.16. The SAPF model consists of the source model along with the three phase diode rectifier and inverter modules. The source and load signals are transmitted using small time step simulation (< 2 μses) to achieve the fast IGBT switching required by the inverter circuit. The RTDS GTA I/O card sends and receives the analog voltage, current and reset signals to dSPACE. A single-phase breaker on the dc side of the rectifier is used to study the transient response of the SAPF using load scheduling.

7.8 Hardware in the Loop Results

The hardware in the loop RTDS implantation is developed with the aim of meeting the transient simulation needs. Figure 7.17 and Figure 7.18 present the performance analysis of SAPF under static and variable nonlinear load respectively. Each figure is divided into five groups namely: (a) source voltages (b) source currents (c) load currents (d) SAPF currents (e) dc link voltage. Figure 7.17 presents the results for static RL nonlinear load. The nonlinear load extracts the sinusoidal current from the source and the nonlinear current

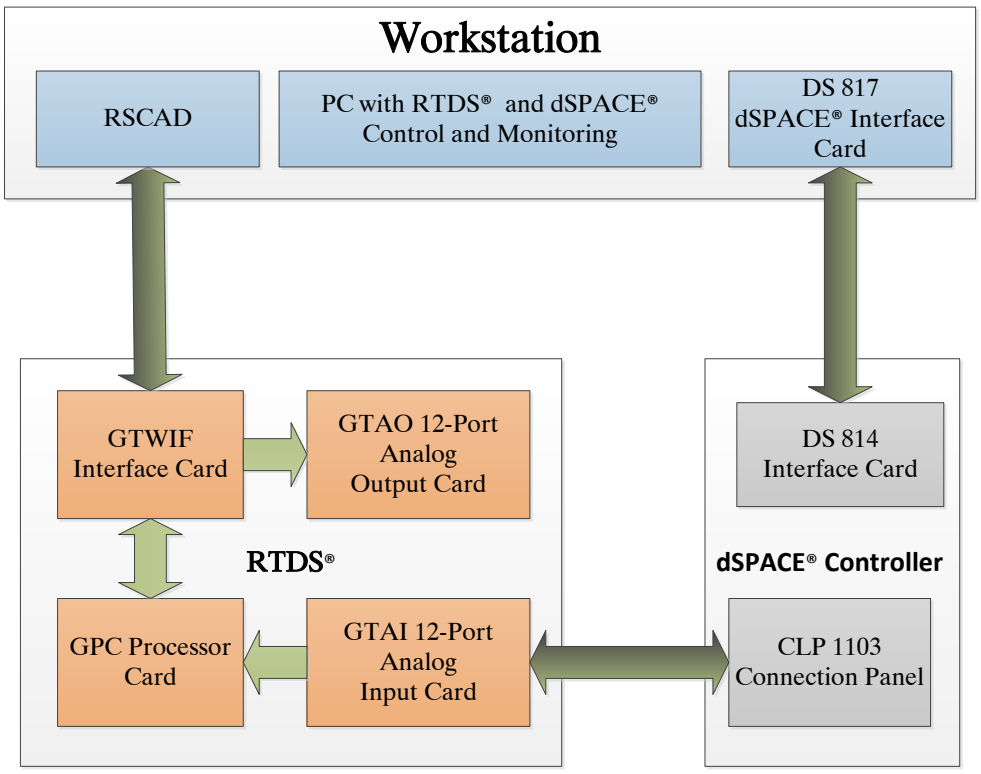

Figure 7.14 RTDS and dSPACE Interfacing for Hardware in the Loop Implementation of SAPF

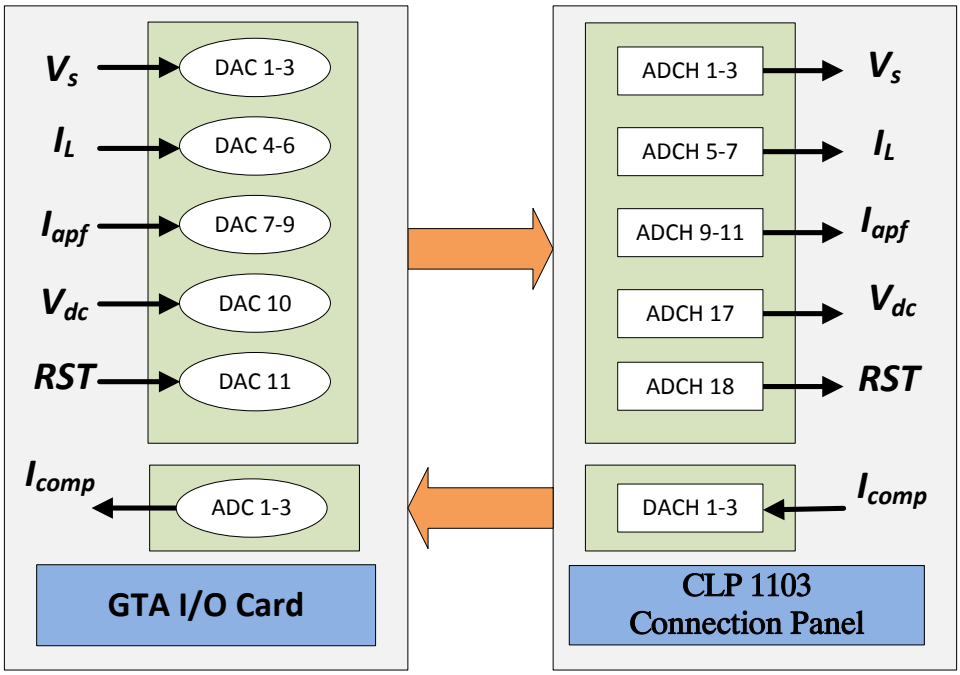

Figure 7.15 Signal Routing between RTDS and dSPACE

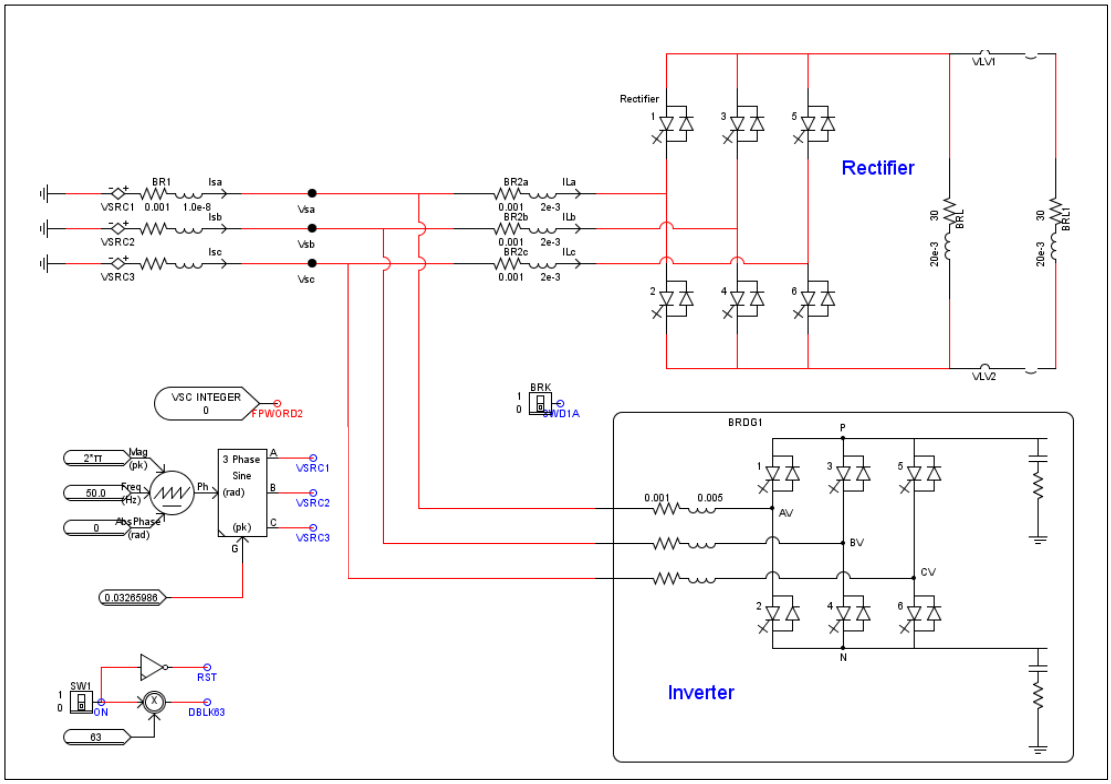

Figure 7.16 Power System Model Built in RTDS

is provided by SAPF. The PI controller tracks the reference voltage 700V quite accurately across dc link. The dynamic analysis of the SAPF is studied under the variable load conditions. A load scheduling mechanism is implemented in RTDS which doubles the load demand from the 200ms to 700ms and returns back to the normal loading conditions afterwards. It can be seen from the Figure 7.18 that the dc link reacts to the change of load conditions quite accurately and provides the real power difference between the load and supply during transitions. The dc link voltage recovers to its reference value within 1 cycle of voltage supply. Figure 7.19 and Figure 7.20 present the source current spectra before and after compensation. It can be seen that, the harmonics level is significantly reduced after compensation as THD of source current drops from 20.6% to 4.07% after compensation.

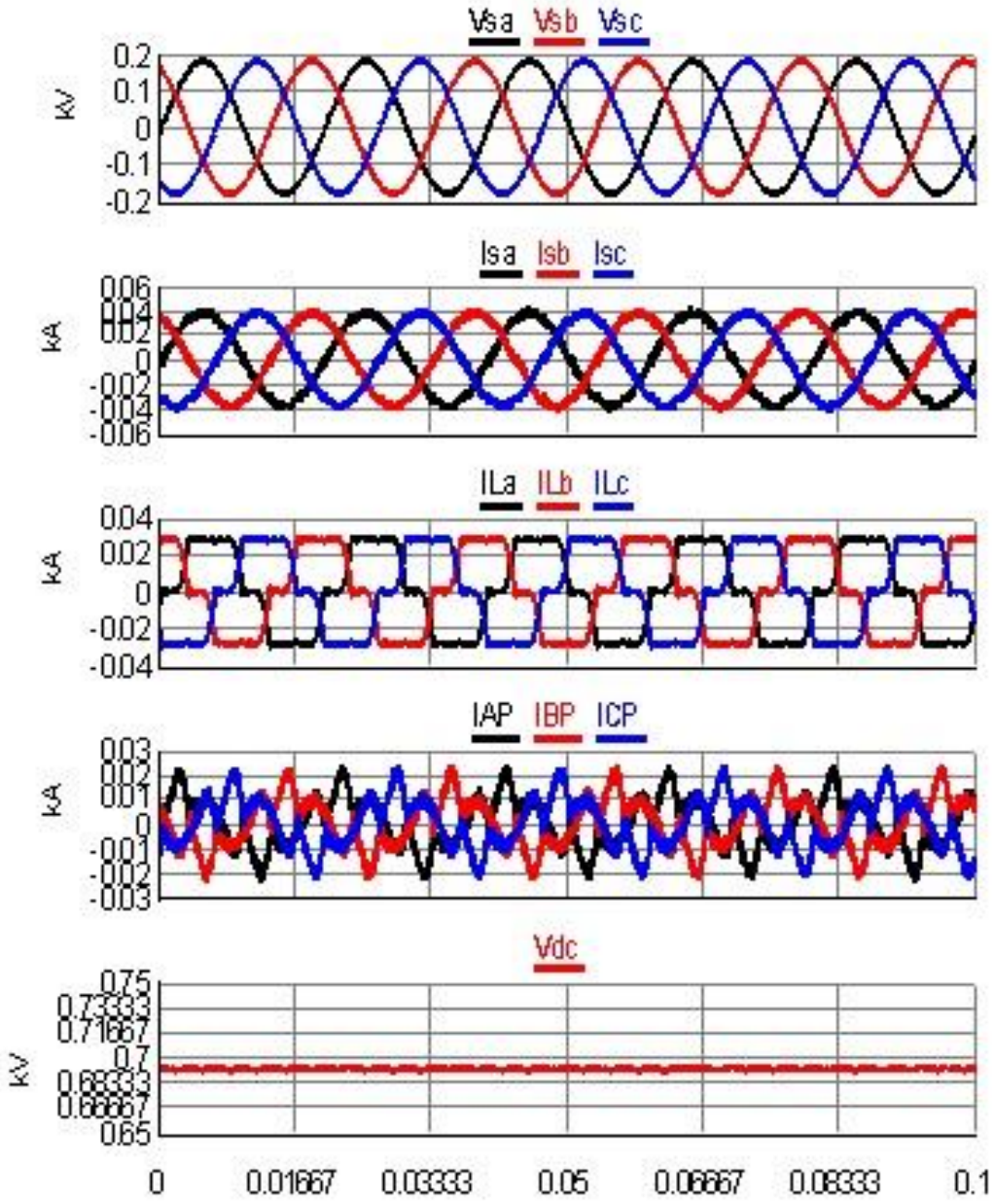

Figure 7.17 Performance Analysis of RTDS based SAPF under Static Load (a) Source Voltage (b) Source Current (c) Load Current (d) SAPF Current (e) dc Link Voltage

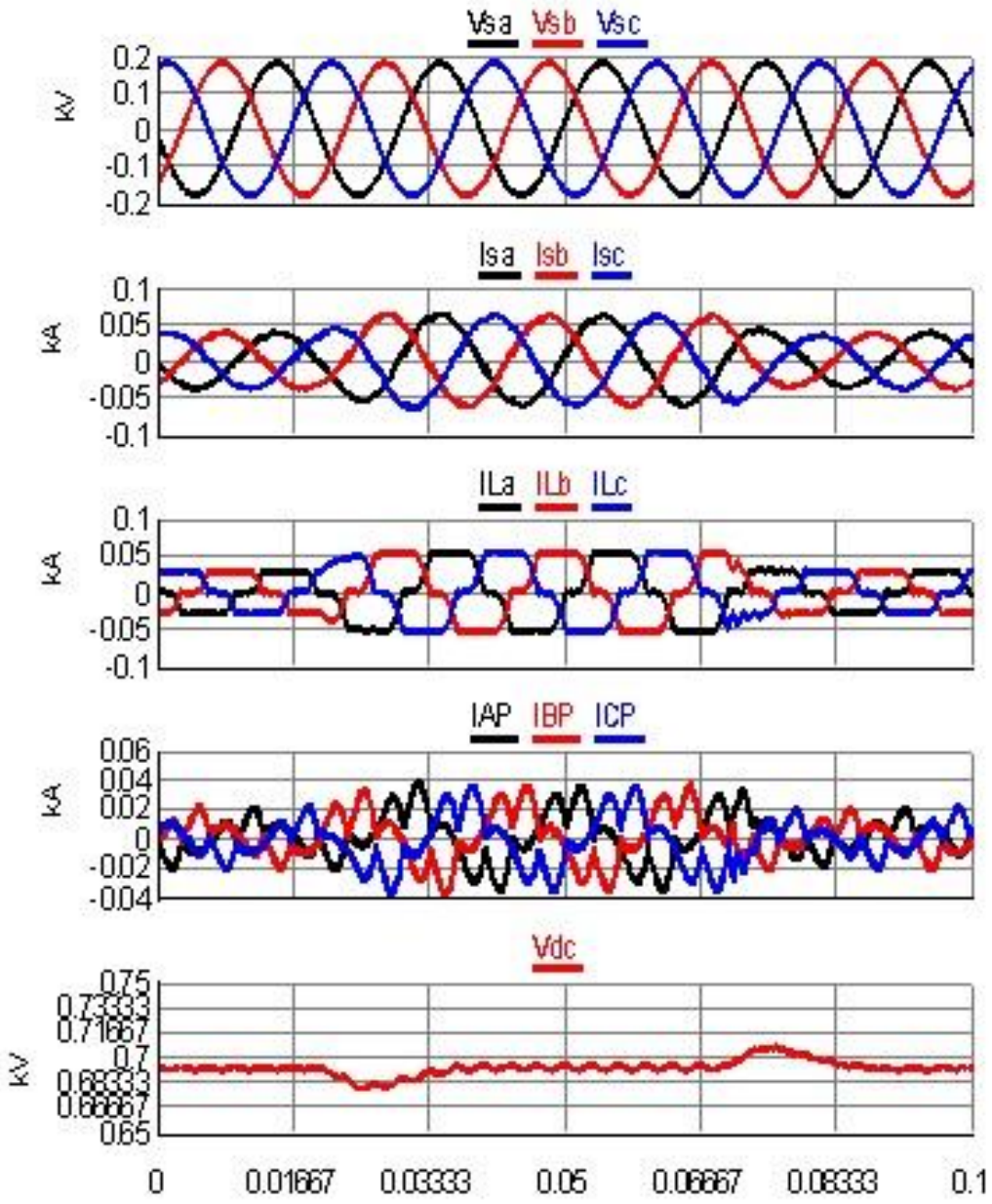

Figure 7.18 Performance Analysis of RTDS based SAPF under Variable Load (a) Source Voltage (b) Source Current (c) Load Current (d) SAPF Current (e) dc Link Voltage

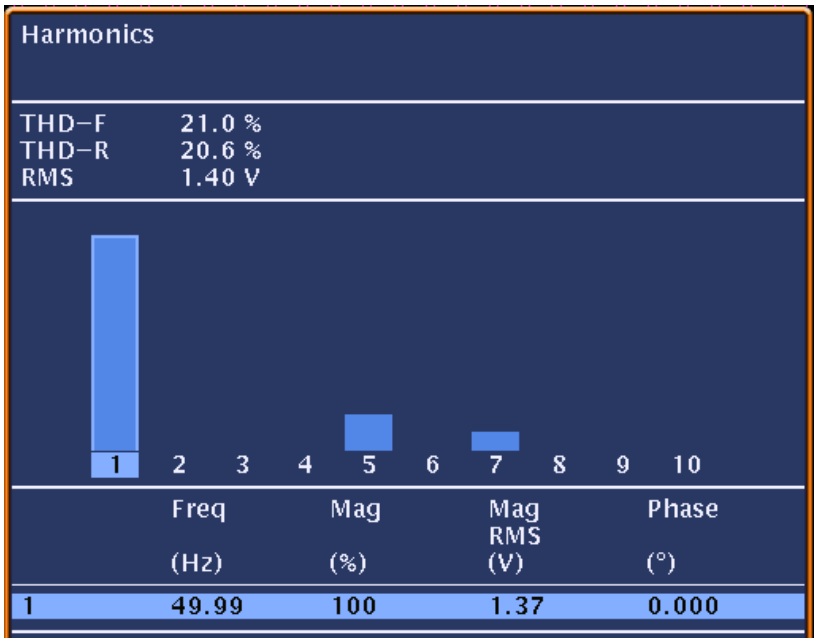

Figure 7.19 Source Current Spectra without SAPF

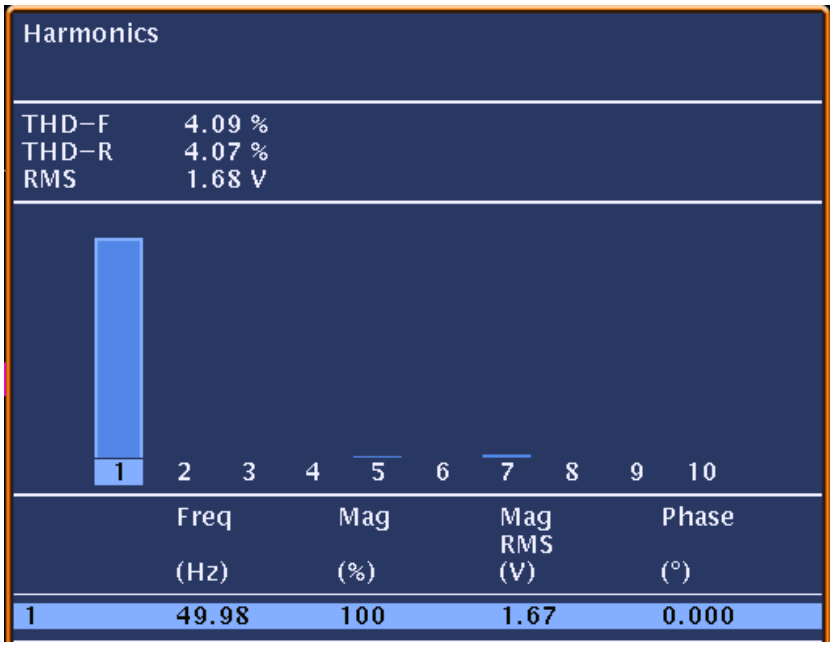

Figure 7.20 Source Current Spectra using SAPF

CHAPTER 8

EXPERIMENTAL IMPLEMENTATION OF SHUNT ACTIVE POWER FILTER

This chapter investigates the performance analysis of shunt active power filter by means of experimental setup. A laboratory scale prototype is developed using digital controller, voltage and current sensors, controllable source and load modules and real time inverter module. The control strategy of SAPF to generate the required harmonic current is implemented in digital controller board dSPACE. This chapter explains in detail the preparation of the experimental setup, implementation of the control strategies and the analysis of the obtained results.

8.1 Experimental Setup

The performance of the SAPF is evaluated experimentally. A comparison between the *p - q* and *d - q* based reference current extraction methods are discussed in detail based on the analysis of the experimental results.

A hardware laboratory scale prototype is developed using controllable source, loads and real time inverter modules to mitigate the harmonics generated by the nonlinear load current. The details of the experimental setup built to investigate the performance of SAPF are shown in Figure 8.1 and Figure 8.2. The three-phase source voltage is generated using programmable AC source. The static loads are implemented using controllable loads, while the non-linear load is implemented using RL load on the dc side of the rectifier. The *p - q*

and *d* - *q* based reference current tracking controllers are implemented in dSPACE controller. The three-phase source voltage and dc link voltage are measured using voltage transducers. The phase currents of load and shunt active power filter are measured by current transducers. Tektronix mixed domain oscilloscope MDO4000B is used to display and record the experimental results like source, load and SAPF currents and three phase source voltage etc. A detailed description of all the equipment used in the experimental setup is given in the next section.

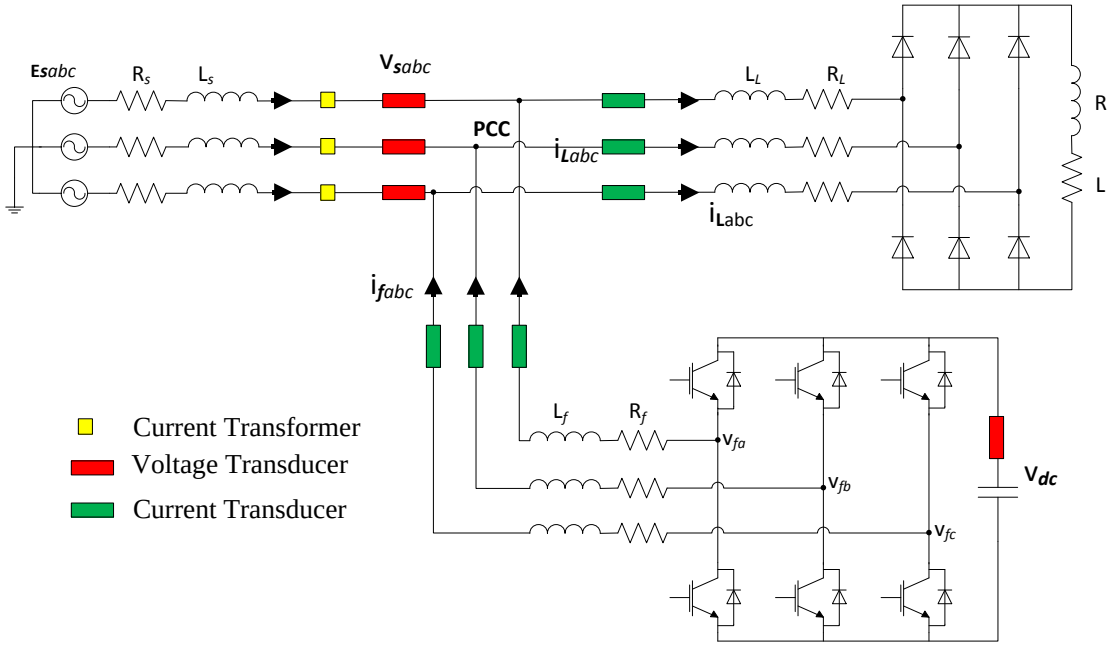

Figure 8.1 Block Diagram of Experimental Setup

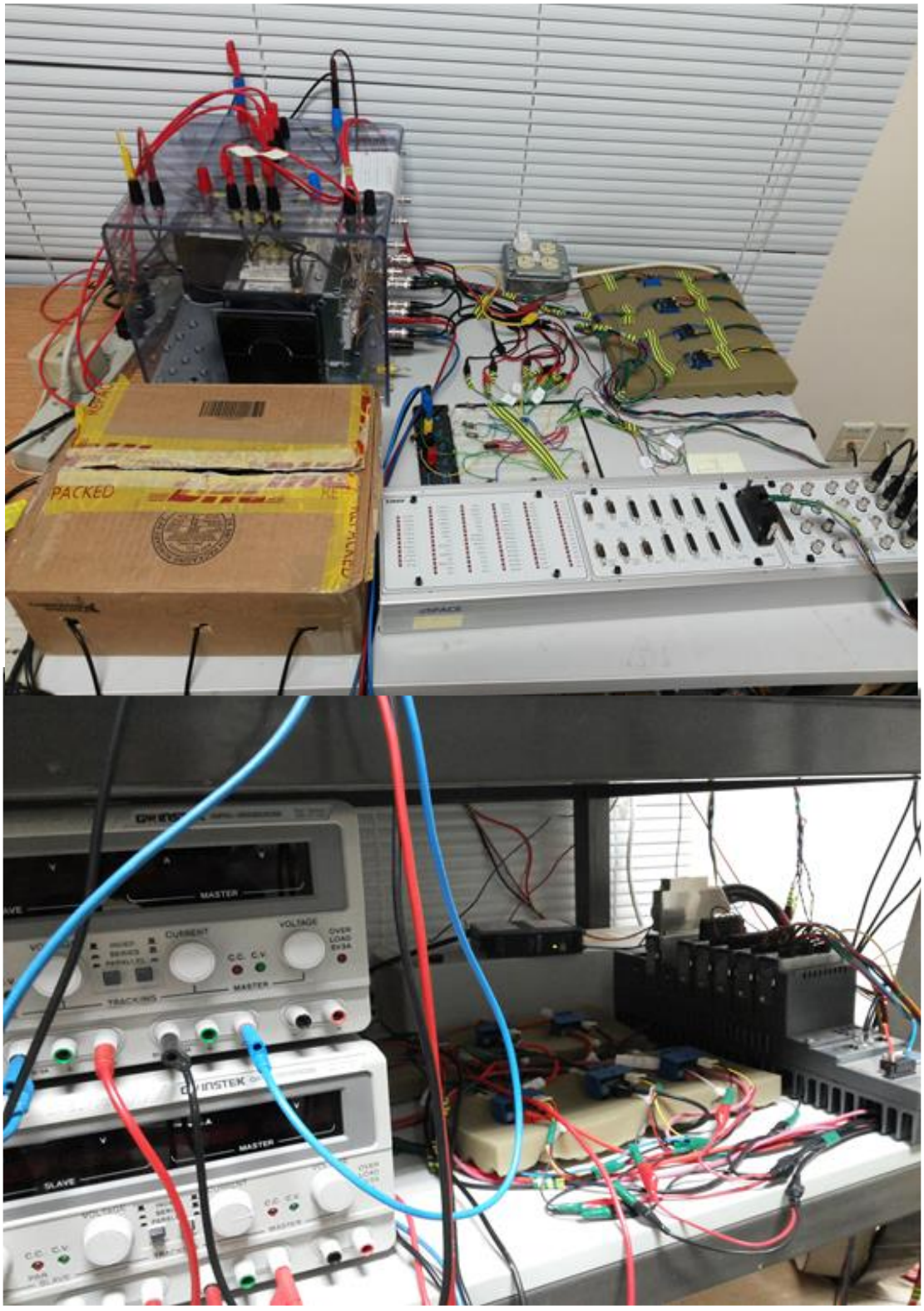

Figure 8.2 Experimental Setup for SAPF

8.1.1 Voltage Transducers

Voltage transducers are used to reduce the level of the voltage signals, which can be fed to the controller for a possible control action. The dSPACE controller, used in this work has input output range up to ±10V while the actual voltage ratings are much higher. So, voltage and transducers are used to make the input voltage waveform compatible with the permissible controller I/O range.

LEM LV 25P/SP5 sensor is used as a voltage transducer for the real time measurement of voltage signal. It can measure DC, AC and pulsed voltage signals from 10 to 1500 V using the Hall effect. The basic block diagram of the current transducer is shown in the Figure 8.3. The terminals *HT*+ and *HT*- represent the signal phase connection terminals of supply voltage. The user specified resistor *R* is used as an input resistors to limit the input current less than 10mA at the primary side. The current conversion ratio of the LV 25-P/SP5 is 2500 : 1000. The resistor R_M is used as a measurement resistor. The value of R_M should be carefully selected so that the output voltage will remain the range less than ± 10V. The voltage terminal $\pm V_c$ represents the terminal of the supplied dc voltage of ±15V. An example is illustrated below to explain the functionality of voltage transducer.

Suppose V_s = 230 V

Input Resistor = R = 47000 Ω

Measurement Resistor = 500 Ω

$$\text{Primary Currnet} = I_p = \frac{V_s}{R} = \frac{230V}{47,000} = 4.8936\,mA$$

$$I_s = 2.5\ x\ I_p = 12.2340\ mA$$

$$Output\ Voltage = V_M = I_s \, x \, R_M$$
$$= 12.2340 \ x \ 0.5$$
$$= 6.11 Volts$$

It can be seen that for a supply voltage of 230V, the transducer output voltage is 6.11 volts, which is far less than 10 Volts. Therefore, the transducer output can be fed to the dSPACE controller.

In this work, input resistor of 47 kΩ is used for the three-phase voltage measurement while 94 kΩ is used for the dc bus side with a 500Ω as a measurement resistor.

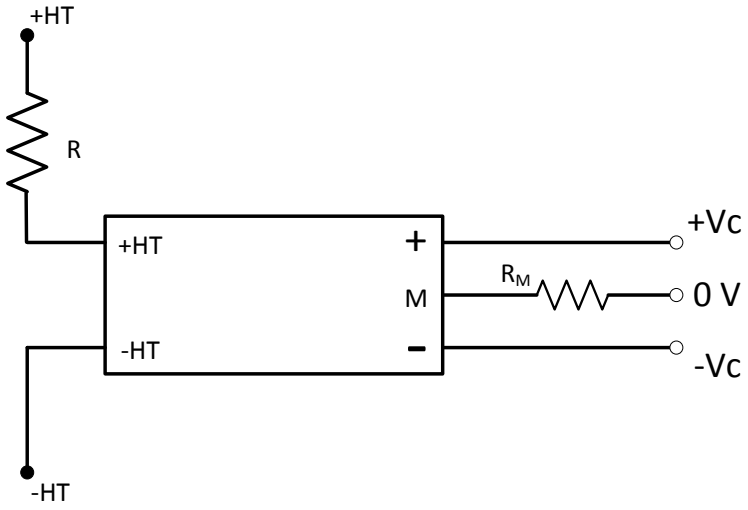

Figure 8.3 Circuit Diagram of Voltage Transducer

8.1.2 Current Transducers

Current transducers are utilized to transform the high rated current signals into the low valued voltage signals in the distribution system, which can be fed to the controller for a possible control action.

HAS 50-s sensor is used as a current transducer for the real time measurement of source load and active power filter current. It is a closed loop sensor, which can measure DC, AC

and pulsed current signals up to 50A using the Hall Effect. A single-phase wire is passed through the sensor to induce the current in the sensor coil. The output of this sensor is an AC voltage signal, which can be easily used in any industrial controller like dSPACE. The basic block diagram of the current transducer is shown in the Figure 8.4, where I_p represents the measured current. The voltage terminal $\pm V_c$ represents the terminal of the supplied DC voltage of ±15V. The resistor R_M is used as a measurement resistor. The value of R_M should be carefully selected so that the output voltage will remain the range less than ± 10V.

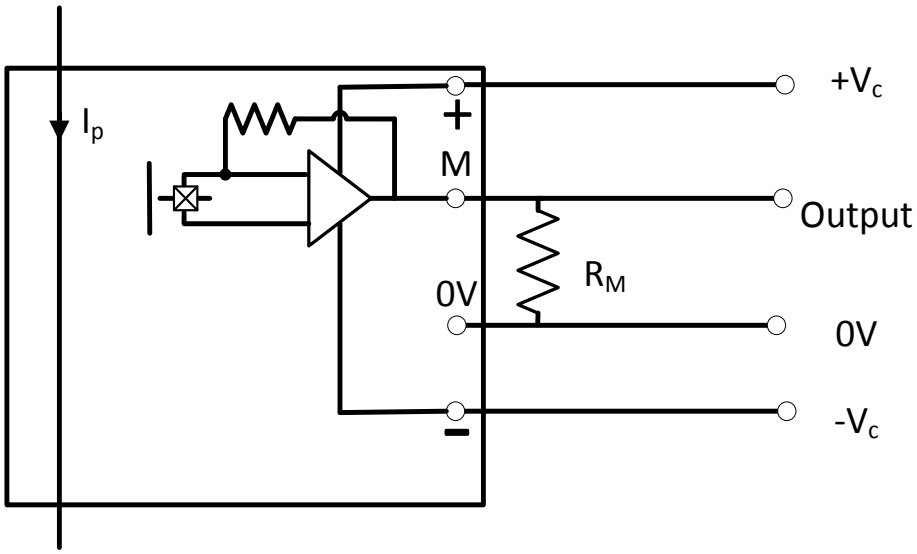

Figure 8.4 Circuit Diagram of Current Transducer

8.1.3 dSPACE Controller

dSPACE is an industrial controller mainly used for the application development and prototyping. In this study, DS-1103 is used for the real time controller implementation of SAPF as shown in Figure 8.5. The instantaneous power *p* - *q* and synchronous reference current *d* - *q* controllers are designed in Matlab/Simulink environment with the aid of RTI and RTW tools provided by the dSPACE. The dSPACE DS-1103 controller has two major

parts: expansion box and connection panel. The connection panel contains 20 analog to digital input channel (ADCH) and 8 digital to analog output channels (DACH).

The three-phase source voltage and dc bus voltage waveforms are fed to the dSPACE controller using DACH 1-4 obtained from the voltage transducers. The real time current waveforms consisting of three phase load current and three phase SAPF current are input to the dSPACE controller using DACH 5-7 and DACH 9-11 respectively. The instantaneous power p - q and synchronous reference current d - q controllers are implemented using 50 μsec sampling time. The gate pulses are obtained from the dSPACE using high speed digital DS1103BIT_OUT block of master PCC.

Figure 8.5 dSPACE Controller

8.1.4 Amplifier Design

The digital output of the dSPACE controller is in the range of ±10V, while the gate pulses input required by the real time inverters are ±15V. Therefore, a double gain amplifier is designed using the hex inverter TTL logic integrated circuit SN7416. The schematic diagram of the hex inverter circuit is shown in Figure 8.6. This TTL hex inverter has a minimum breakdown voltage of 15 volts. A 15 volts DC supply is provided at the Vcc terminal. The output level can be adjusted using pull up resistors. This TTL hex inverter can sink maximum current up to 30mA.

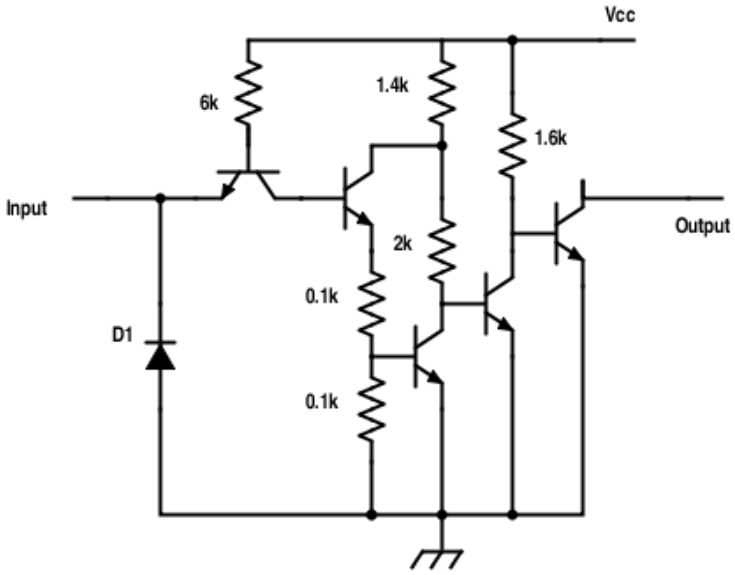

Figure 8.6 Schematic Diagram of SN7416 TTL hex Inverter

8.1.5 Inverter and Diode Rectifier

SEMITEACH – IGBT inverter and rectifier module is used for real time voltage source inverter implementation. This module has three major functions including single and three-phase voltage source inverter, buck or boost converter and brake chopper. An isolated uncontrolled rectifier is also a part of this system. The basic block diagram of this module

is shown in Figure 8.7, where a pair of 2200μF DC capacitor is also installed for energy storage purpose. The rectifier input is 230/ 400V while the output may vary up to 600V DC. The input output range of inverter can also varied up to 400V AC and 600V DC with 30A as a maximum current.

In this study, the voltage source inverter and three phase diode rectifier are used. The voltage source inverter is used to inject the nonlinear harmonic current required by the load attached to the dc side of the diode rectifier. The gate pulses are provided to the inverter generated by the dSAPCE controller using amplifier. A DC voltage source of 15 volts is applied to the gate driven circuit of the inverter. The dc bus capacitor are used to store the energy and provide the required nonlinear current while maintaining the certain reference value.

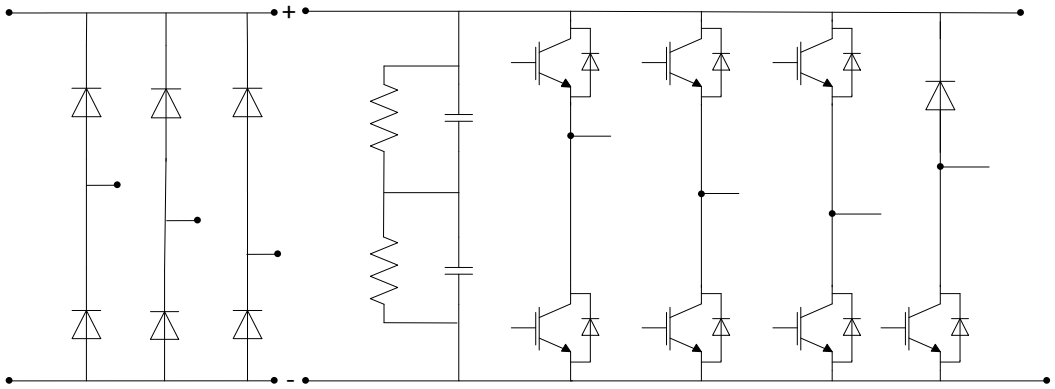

Figure 8.7 Blocks Diagram of Inverter and Rectifier

8.2 Experimental Results

This section presents the experimental results of SAPF to mitigate the harmonics generated by non-linear loads. The implementation of the instantaneous power and synchronous

reference frame control strategies of SAPF are carried out using real time hardware prototype. The performance of the SAPF is verified under balanced and unbalanced source voltage. The response of the system to the source voltage and the nonlinear load current is observed. The load is highly non-linear in both test cases, so the load draws a highly enriched harmonic current from the grid.

The experimental results comprises of the performance analysis of two control strategies under balanced and unbalanced source voltage. The obtained results are compared in terms of THD.

8.2.1 Case I: Performance Analysis under Balanced Source Voltage

In this case, a resistive load is connected on the dc side of the diode rectifier. The rectifier load injects the harmonics in the power systems. The performance of both controllers, instantaneous power controller and synchronous reference frame controller is analyzed under the same test conditions. The experimental results present a detailed analysis of the system including three phase source voltage, source current, load current and active filter current, individual harmonics level before and after compensation and finally THDs of source and load current.

Figure 8.8 presents the three phase balanced source voltage. Figure 8.9 contains three current waveforms including source current, load current and shunt active power filter current respectively. It can be seen that the load current is highly nonlinear, while the source current becomes sinusoidal after compensation. The SAPF current presented in Figure 8.9 is calculated using instantaneous power theory. The results of the experiments are recorded using Tektronix mixed domain oscilloscope MDO4000B.

A comparative analysis for the measurement of load current harmonics using IIR filter bank and WPT based approach presented in chapter 3 and chapter 4 is shown in Figure 8.10. The results comprise of the measurement of first fifteen three-phase harmonic groups using IIR filter bank and WPT. The results show that, the odd harmonics are present in the load current introduced by the diode rectifier. It can be seen that WPT based results shows a higher leakage in the neighboring bands as compared to the IIR filter bank approach. The measurement of harmonic spectra for source current after compensation is presented in Figure 8.11 using IIR filter bank and WPT. The results confirm that the harmonics previously present in the source current are efficiently eliminated or suppressed with the application of SAPF.

Figure 8.12 and Figure 8.13 presents the individual harmonics levels present in the source current before and after the harmonic compensation using SAPF. The results shows that, the THD of source current before SAPF was 28%, which is substantially reduced up to 6%.

The application of synchronous reference frame d - q controller is studied under the balanced source voltage conditions. Figure 8.14 presents the three current waveforms obtained using d - q controller. It contains the source current, load current and shunt active power filter current. It can be seen that the load current is purely nonlinear, while the source current becomes sinusoidal after compensation. The individual harmonic contents are presented in Figure 8.15. It can be seen that, the harmonics levels are significantly reduced with the application of d - q controller. The THD of source current after compensation is 5.29%, which is even improved as compared to the p - q controller.

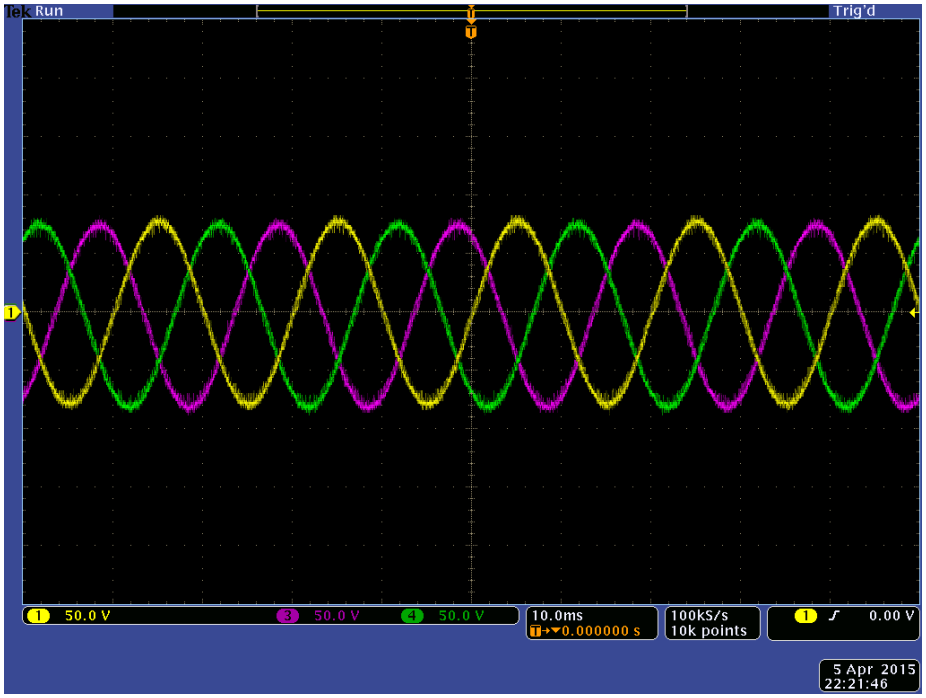

Figure 8.8 Three Phase Balanced Source Voltage

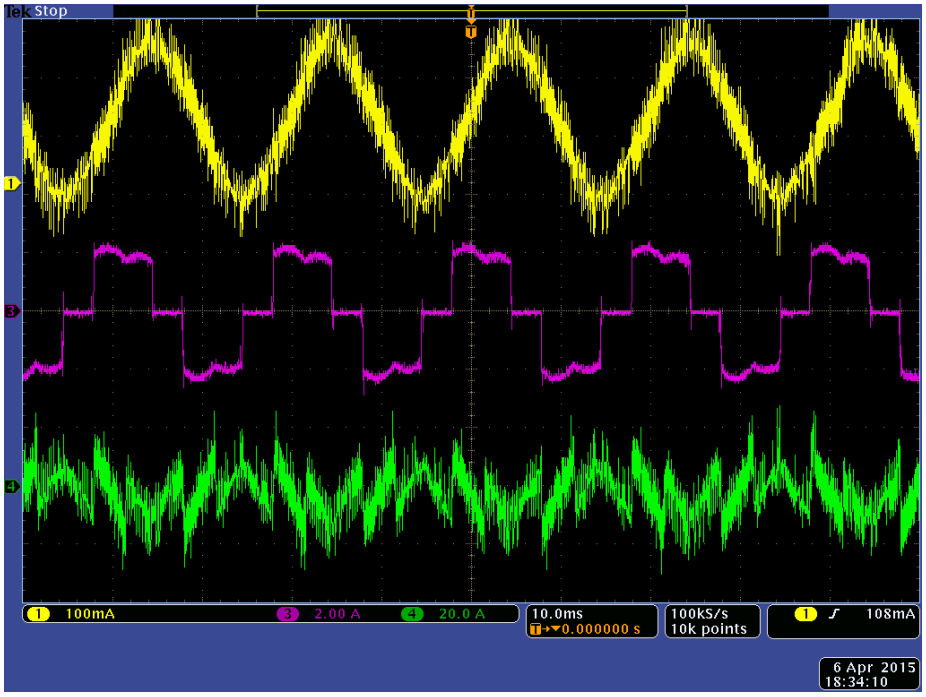

Figure 8.9 Currents Waveforms under Balanced Voltage and *p* - *q* Controller (a) Source Current (b) Load Current (c) Active Filter Current

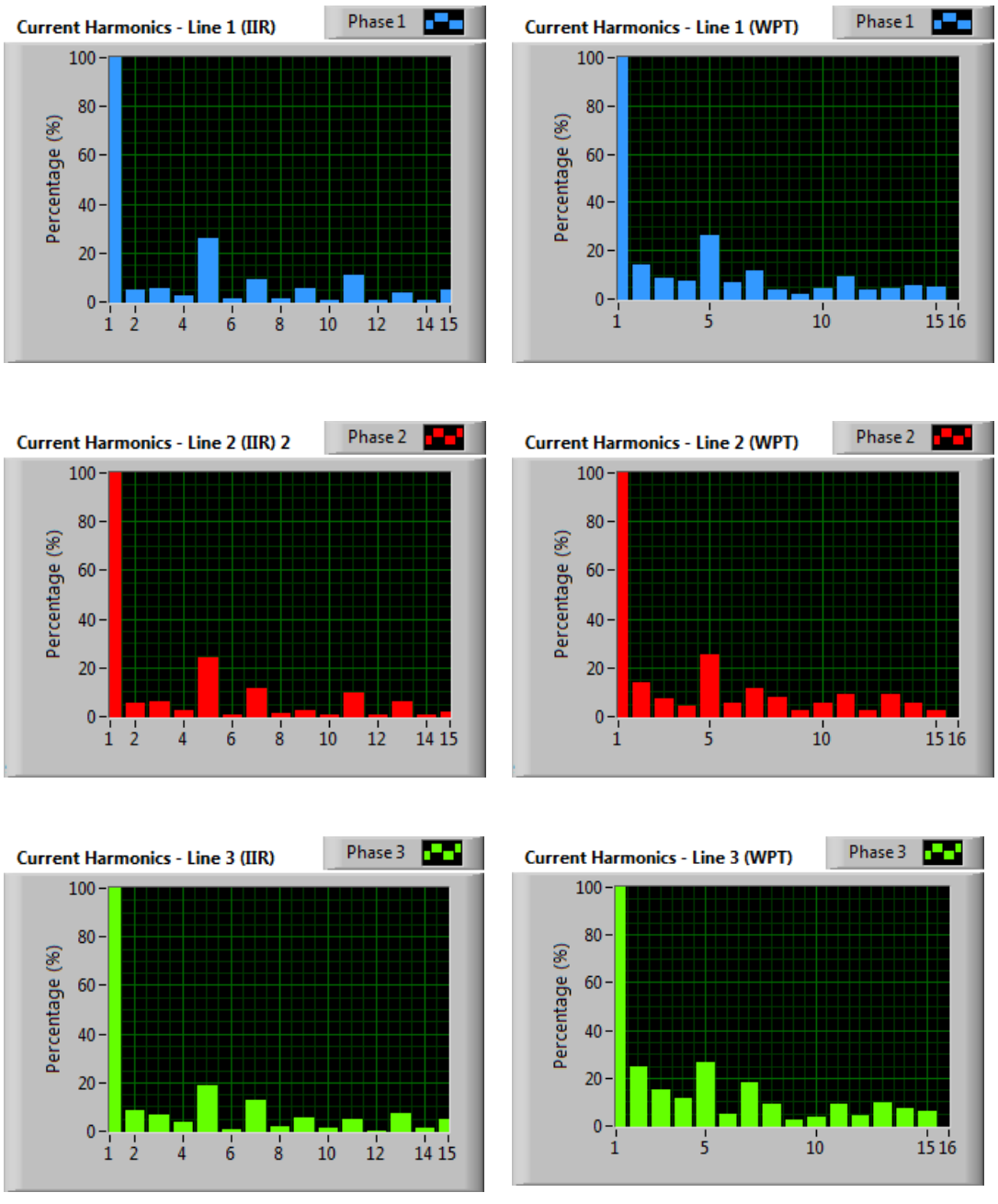

Figure 8.10 Harmonic Spectra of Load Current using IIR Filter Bank and WPT

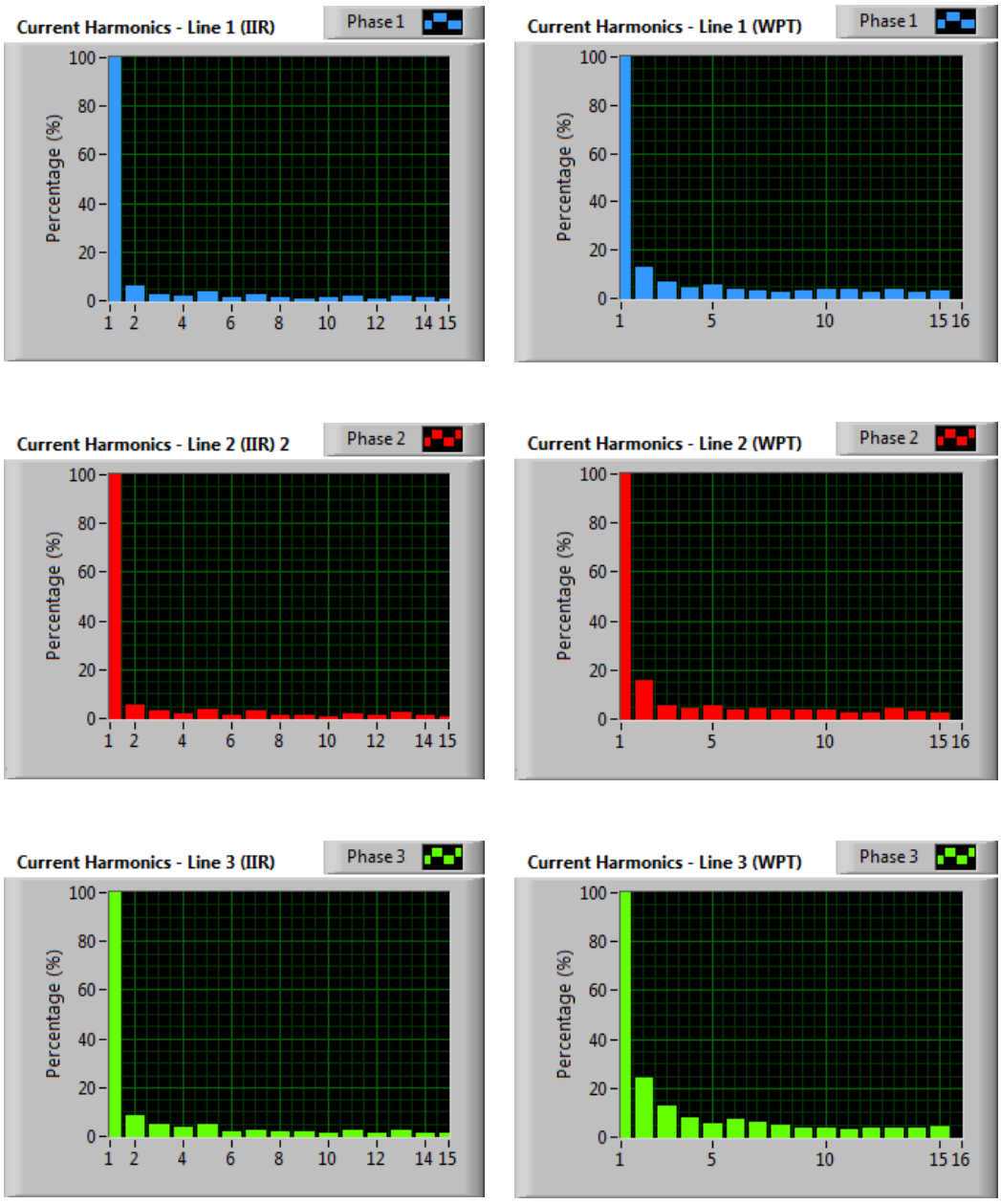

Figure 8.11 Harmonic Spectra of Source Current after Compensation using IIR Filter Bank and WPT

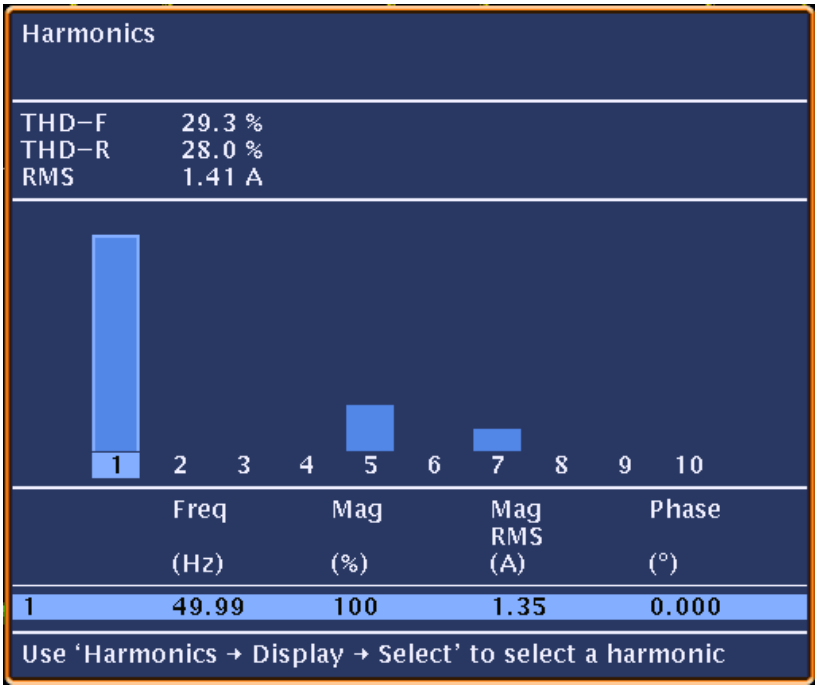

Figure 8.12 Source Current Spectra before Compensation

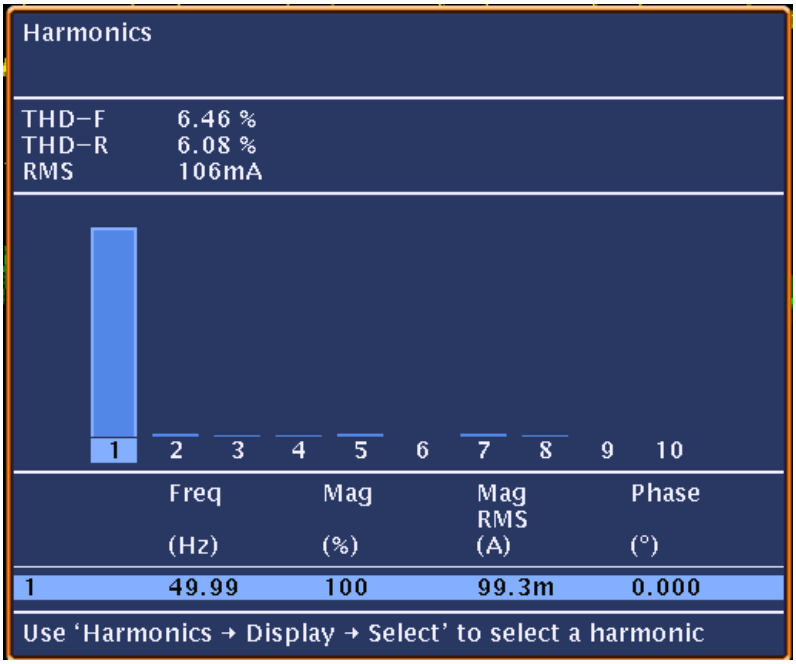

Figure 8.13 Current Spectra under Balanced Source Voltage and *p* - *q* Controller Compensation

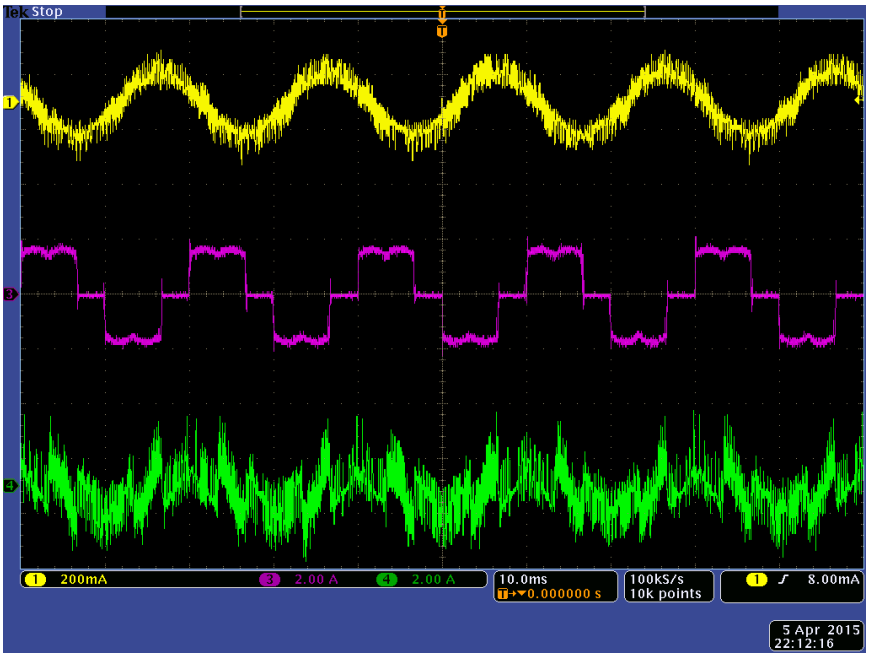

Figure 8.14 Currents Waveforms under Balanced Voltage and *d* - *q* Controller (a) Source Current (b) Load Current (c) Active Filter Current

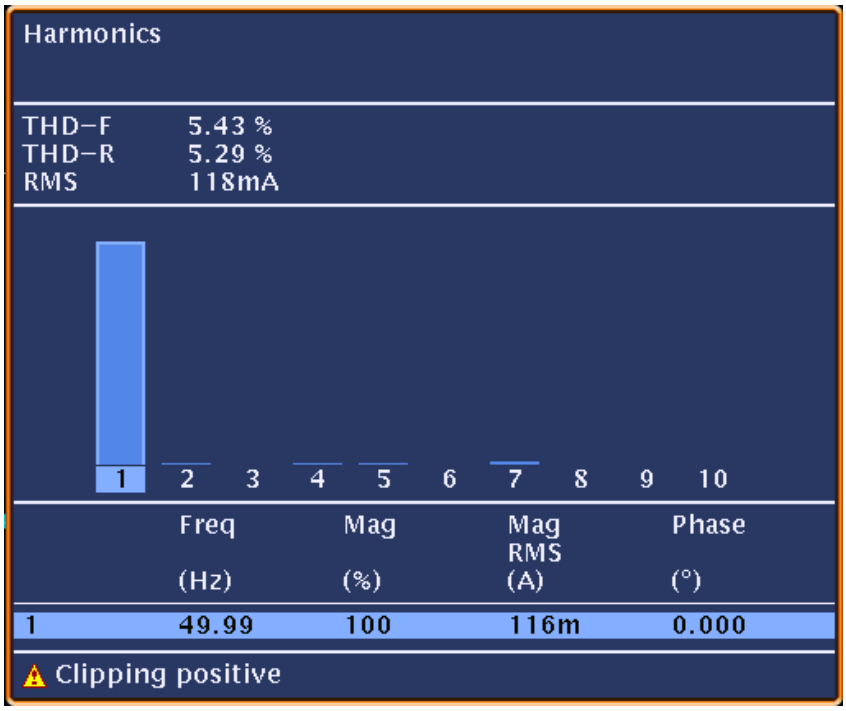

Figure 8.15 Source Current Spectral using *d* - *q* Controller Compensation

8.2.2 Case II: Performance Analysis under Unbalanced Source Voltage

In this section, the performance of both controllers, instantaneous power controller and synchronous reference frame controller is analyzed under the unbalanced source voltage conditions.

Figure 8.16 presents the three phase unbalanced source voltage. The three phases have same frequency but their rms voltage differ up to 20%. Figure 8.17 presents the three current waveforms of load current, source current and shunt active power filter current. It can be seen that the load current is highly nonlinear, while the source current becomes sinusoidal after compensation. The SAPF currents are obtained using instantaneous power theory. The THD of source current before and after compensation is presented in Figure 8.18 and Figure 8.19 respectively. It can be seen that very large fifth and seventh harmonics are present in the load current. The source current spectrum after compensation shows a significant reduction in these harmonics. The source current THD before and after compensation was recorded as 33.9% and 7.73% respectively.

The performance of the synchronous reference frame based SAPF strategy under unbalanced source voltage conditions is presented in Figure 8.20. It contains the source current, load current and filter current injected by the SAPF. It can be seen that the source provides the sinusoidal current while the nonlinear current is provided to the load by SAPF. The THD of the source current after compensation is recorded as 5.94%. The results show that the synchronous reference frame based d - q controller is capable enough to compensate the harmonics even in highly unbalanced voltage conditions.

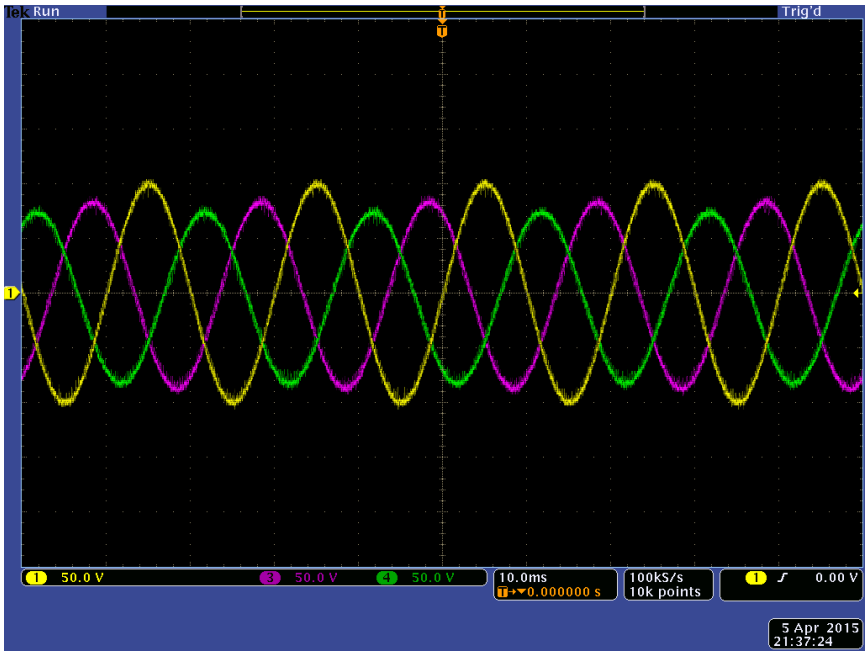

Figure 8.16 Unbalanced Three Phase Source Voltage

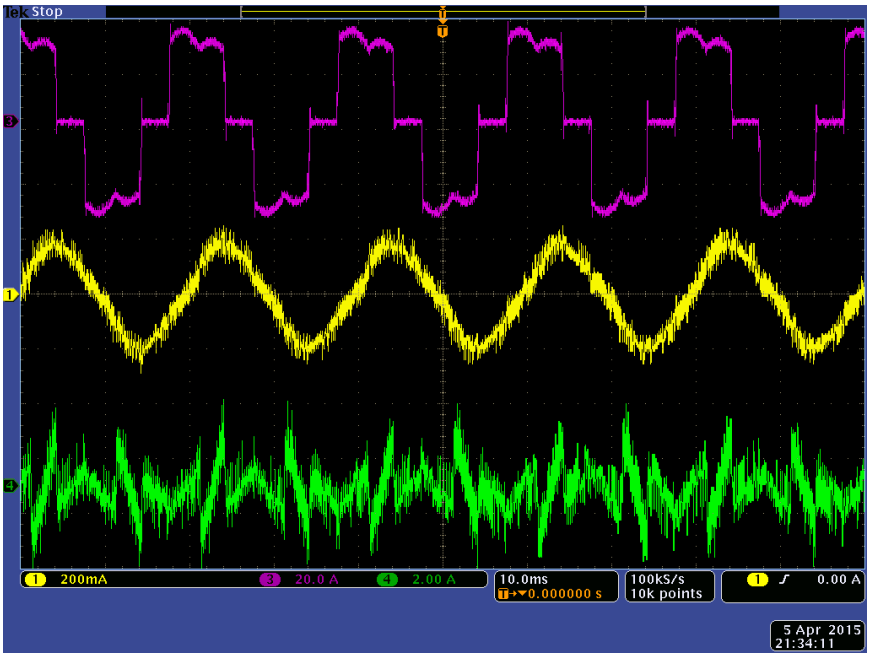

Figure 8.17 Currents Waveforms under Unbalanced Voltage and *d* - *q* Controller (a) Load Current (b) Source Current (c) Active Filter Current

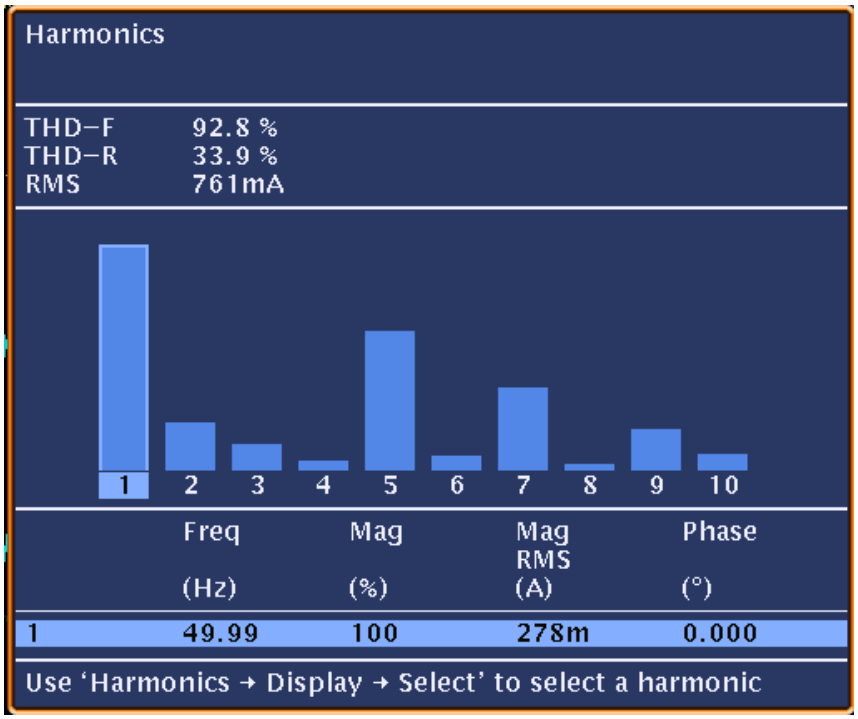

Figure 8.18 Source Current Spectra without SAPF under Unbalanced Source Voltage

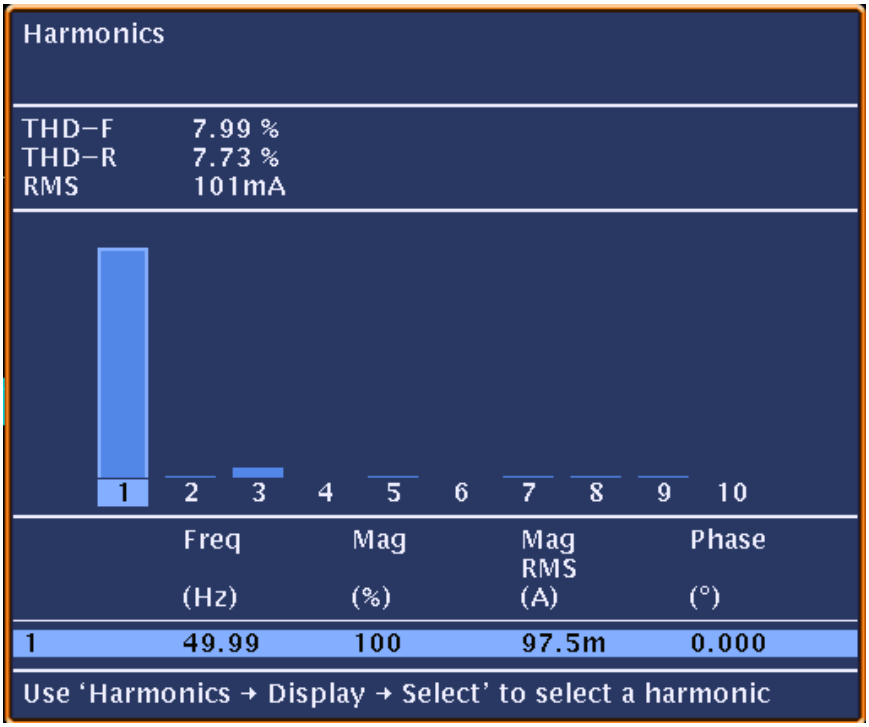

Figure 8.19 Current Spectra under Unbalanced Source Voltage and *p* - *q* Controller Compensation

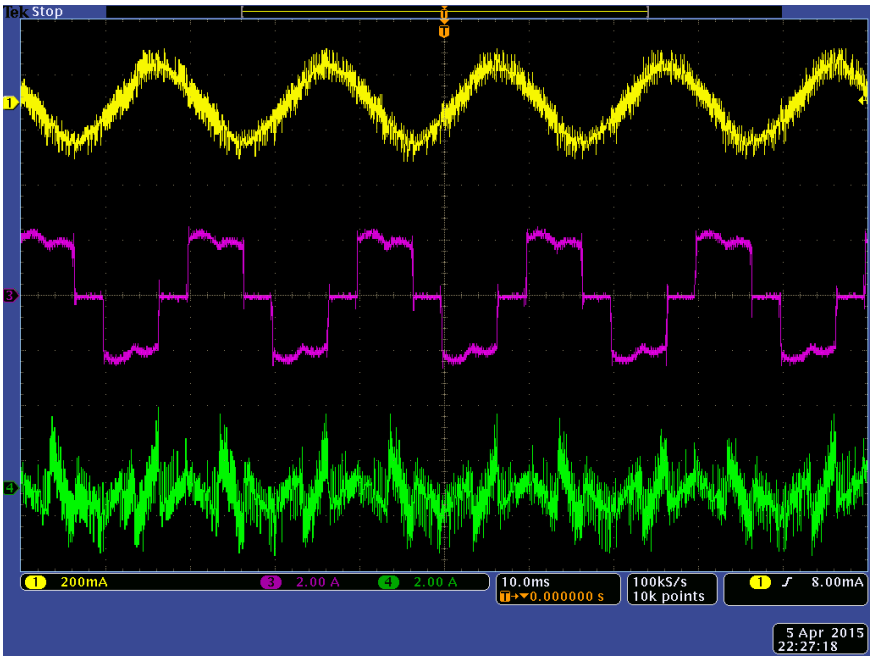

Figure 8.20 Currents Waveforms under Unbalanced Voltage and *d* - *q* Controller

(a) Source Current (b) Load Current (c) Active Filter Current

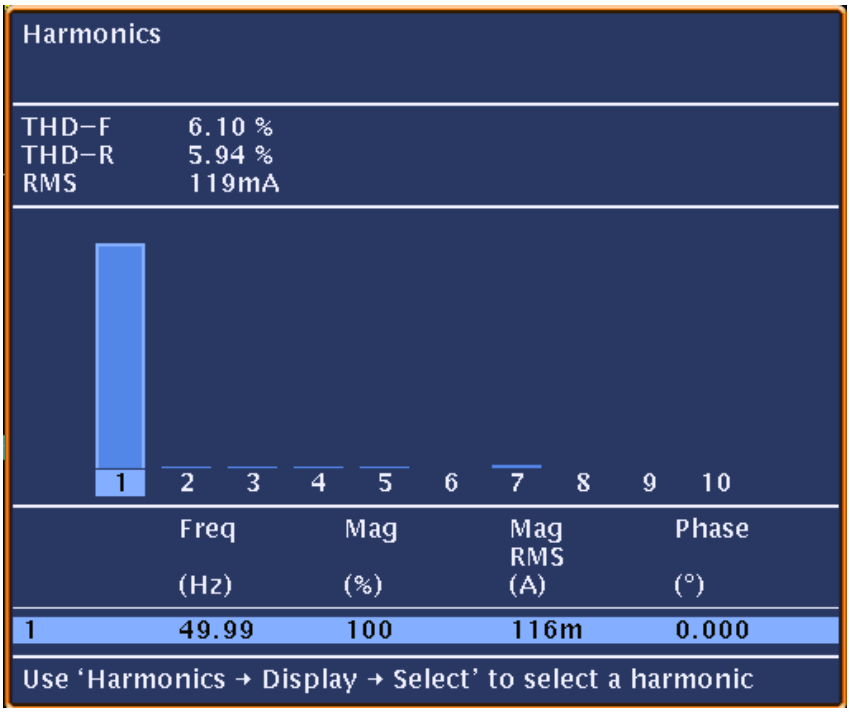

Figure 8.21 Current Spectra under Unbalanced Source Voltage and *p* - *q* Controller

Compensation

8.3 Discussion

In this chapter, the experimental implementation of SAPF is discussed in detail. This chapter describes the construction and working principle of SAPF using voltage and current sensors, dSPACE controller, amplifier and inverter and other related equipment. The performance of the SAPF is tested using instantaneous power p - q theory and synchronous reference frame d - q theory based controllers. Finally, the experimental results are presented under balanced and unbalanced source voltage conditions. The experimental results comprise of the source voltage, current waveforms including source current, load current and active filter current. The individual and grouped harmonic spectra is also presented for detailed analysis. A comparative analysis in terms of THD of source current is presented for the performance analysis of p - q and d - q controller under balanced and unbalanced voltage conditions. It can be seen that the performance of $d - q$ is much better than the p - q controller in terms of THD and dc link voltage recovery.

CHAPTER 9

CONCLUSION AND FUTURE WORK

9.1 Conclusion

The purpose of this thesis was to develop a real time harmonic detection and mitigation system. The system would collect voltage and current waveforms from various location in distribution system. These waveforms were processed to find the various power quality parameters like voltage, current, frequency, power, power factor crest factor, total harmonic distortion etc.

In this thesis, a comprehensive literature review has been established. Two novel methods have been developed and implemented for online monitoring and measurement of harmonics and interharmonics distortion. A laboratory scale prototype has been developed for online monitoring, detection and measurement of harmonics and interharmonics.

Furthermore, two control strategies for shunt active power filters have been designed and implemented to mitigate the harmonics. A laboratory scale prototype has been developed to mitigate the harmonics in power system.

The main conclusion of this thesis can be drawn as:

- A comprehensive literature review has been accomplished for real time monitoring, measurement and mitigation of harmonics and interharmonics in voltage and current signals.

- A new method based on wavelet packet transform for harmonics and interharmonics group distortion measurement according to the IEC standard 61000-4-7 has been developed and implemented in real time environment.
- A novel technique based on infinite impulse response filter bank has been proposed and developed for the purpose of accurate measurement of harmonics and interharmonics in power distribution networks.
- The simulation results of the proposed methods demonstrate the effectiveness and suitability of these methods for monitoring and measurement of harmonics in power systems.
- A novel power quality disturbance classifier has been designed and implemented using wavelet transform and optimized artificial neural networks to classify the power quality disturbances.
- Two control strategies based on instantaneous power theory and synchronous reference frame for harmonic mitigation has been developed using shunt active power filter.
- The proposed harmonic mitigation strategies has been implemented for hardware in loop testing using real time digital simulator (RTDS) and industrial controller dSPACE.
- The proposed monitoring, measurement and mitigation techniques for harmonics and interharmonics have been implemented in laboratory scale prototype using LabVIEW software, cRIO, real time processors, data acquisition cards, real time inverter, dSPACE controller and a simplified model for the distribution network with its associated bulk loads.

- The obtained results have been compared with the published literature and a substantial improvement has been observed.
- A good agreement has been observed between the experimental results and the simulation results for monitoring, measurement and mitigation of harmonics and interharmonics.

9.2 Future Work

For a future work, the following points can be considered as extension to the work done in this thesis.

- In this thesis, WPT and IIR filter banks are studied for the measurement of harmonics and interharmonics distortion. A combine strategy using IIR quadrature mirror filter can be implemented with the aid of WPT. This may lead to an improved performance and reduction in computational complexity.
- The proposed research implements the harmonic measurement and mitigation strategies using SAPF. The proposed work can be extended to improve the power factor and reduce the harmonic THD simultaneously. This may lead to the development of a multi-objective optimization strategy. A tradeoff analysis between power factor improvement and THD reductions is an interesting study.
- The performance analysis of p - q and d - q based reference current extraction is studied in this thesis. A new control strategy using neural network and fuzzy optimization can be developed which might result in good performance under unbalanced and distorted source voltage conditions.

- A novel power quality event classification strategy is proposed using optimized artificial neural network. The experimental verification of the proposed strategy along with their underlying causes is an interesting research point.

References

[1] A. Kusko and M. Thompson, *Power Quality in Electrical Systems*. McGraw Hill Professional, 2007.

[2] S. Chattopadhyay, M. Mitra, and S. Sengupta, *Electric Power Quality*. Springer Science & Business Media, 2011.

[3] B. Singh, A. Chandra, and K. Al-Haddad, *Power Quality: Problems and Mitigation Techniques*. John Wiley & Sons, 2015.

[4] "IEEE Recommended Practice and Requirements for Harmonic Control in Electric Power Systems." pp. 1–29, 2014.

[5] "Electromagnetic Compatibility (EMC)—Part 4–7: Testing and Measurement Techniques—General Guide on Harmonics and Interharmonics Measurements and Instrumentation, for Power Supply Systems and Equipment Connected Thereto," *IEC 61000-4-7*, 2002.

[6] J. Barros and R. I. Diego, "A new method for measurement of harmonic groups in power systems using wavelet analysis in the IEC standard framework," *Electr. Power Syst. Res.*, vol. 76, no. 4, pp. 200–208, Jan. 2006.

[7] H. C. Lin, "Power Harmonics and Interharmonics Measurement Using Recursive Group-Harmonic Power Minimizing Algorithm," *IEEE Trans. Ind. Electron.*, vol. 59, no. 2, pp. 1184–1193, Feb. 2012.

[8] T. Keppler, N. R. Watson, and J. Arrillaga, "Theoretical assessment of light flicker caused by sub- and interharmonic frequencies," *IEEE Trans. Power Deliv.*, vol. 18, no. 1, pp. 329–333, Jan. 2003.

[9] T. Tayjasanant, W. Wang, C. Li, and W. Xu, "Interharmonic-Flicker Curves," *IEEE Trans. Power Deliv.*, vol. 20, no. 2, pp. 1017–1024, Apr. 2005.

[10] J. Arrillaga, *Power System Harmonic Analysis*. John Wiley & Sons, 1997.

[11] G. J. Wakileh, *Power Systems Harmonics: Fundamentals, Analysis and Filter Design*. Springer Science & Business Media, 2001.

[12] IEC/TR-61000-2-1, *Electromagnetic compatibility (EMC) - Part 2: Environment - Section 1: Description of the environment - Electromagnetic environment for low-frequency conducted disturbances and signalling in public power supply systems*, First Edit. 1990.

[13] E. W. Gunther, “Interharmonics in power systems,” in *2001 Power Engineering Society Summer Meeting. Conference Proceedings (Cat. No.01CH37262)*, 2001, vol. 2, pp. 813–817.

[14] H. Qian, R. Zhao, and T. Chen, “Interharmonics Analysis Based on Interpolating Windowed FFT Algorithm,” *IEEE Trans. Power Deliv.*, vol. 22, no. 2, pp. 1064–1069, Apr. 2007.

[15] Quanming Zhang, Huijin Liu, Hongkun Chen, Qionglin Li, and Zhenhuan Zhang, “A Precise and Adaptive Algorithm for Interharmonics Measurement Based on Iterative DFT,” *IEEE Trans. Power Deliv.*, vol. 23, no. 4, pp. 1728–1735, Oct. 2008.

[16] J. Barros, “Simultaneous measurement of harmonics, interharmonics and flicker in a power system for power quality analysis,” in *Fifth International Conference on Power System Management and Control*, 2002, vol. 2002, pp. 100–105.

[17] E. J. Powers, W. M. Grady, and A. Arapostathis, “Detection of Flicker Caused by Interharmonics,” *IEEE Trans. Instrum. Meas.*, vol. 58, no. 1, pp. 152–160, Jan. 2009.

[18] J. H. B. Deane and D. C. Hamill, “Instability, subharmonics, and chaos in power electronic systems,” *IEEE Trans. Power Electron.*, vol. 5, no. 3, pp. 260–268, Jul. 1990.

[19] K. T. Chau, J. H. Chen, C. C. Chan, and D. T. W. Chan, “Modeling of subharmonics and chaos in DC motor drives,” in *Proceedings of the IECON’97 23rd International Conference on Industrial Electronics, Control, and Instrumentation (Cat. No.97CH36066)*, 1997, vol. 2, pp. 523–528.

[20] R. K. Jardan, P. Stumpf, P. Bartal, Z. Varga, and I. Nagy, “A Novel Approach in Studying the Effects of Subharmonics on Ultrahigh-Speed AC Motor Drives,” *IEEE Trans. Ind. Electron.*, vol. 58, no. 4, pp. 1274–1281, Apr. 2011.

[21] M. Pepliński and P. Gnaciński, “Induction cage machine supplied with voltage containing subharmonics and interharmonics,” *IET Electr. Power Appl.*, vol. 8, no. 8, pp. 287–295, Sep. 2014.

[22] H. C. Lin, “Power Harmonics and Interharmonics Measurement Using Recursive Group-Harmonic Power Minimizing Algorithm,” *IEEE Trans. Ind. Electron.*, vol. 59, no. 2, pp. 1184–1193, Feb. 2012.

[23] F. J. Harris, “On the use of windows for harmonic analysis with the discrete Fourier transform,” *Proc. IEEE*, vol. 66, no. 1, pp. 51–83, 1978.

[24] O. M. Solomon, “The use of DFT windows in signal-to-noise ratio and harmonic distortion computations,” *IEEE Trans. Instrum. Meas.*, vol. 43, no. 2, pp. 194–199, Apr. 1994.

[25] D. J. Nyarko and K. a. Strsmsmoe, “A modified DFT for improved accuracy in harmonic measurements of periodic waveforms,” *Proc. 1996 Can. Conf. Electr. Comput. Eng.*, vol. 2, no. 2, pp. 708–711, 1996.

[26] J. Xi and J. F. Chicharo, “A time-domain interpolation approach for DFT harmonic analysis,” *Signal Processing*, vol. 58, no. 2, pp. 181–192, Apr. 1997.

[27] H. Wen, J. Zhang, Z. Meng, S. Guo, F. Li, and Y. Yang, “Harmonic Estimation Using Symmetrical Interpolation FFT Based on Triangular Self-Convolution Window,” *IEEE Trans. Ind. Informatics*, vol. 11, no. 1, pp. 16–26, Feb. 2015.

[28] G. Andria, M. Savino, and A. Trotta, “Windows and interpolation algorithms to improve electrical measurement accuracy,” *IEEE Trans. Instrum. Meas.*, vol. 38, no. 4, pp. 856–863, 1989.

[29] H. Qian, R. Zhao, and T. Chen, “Interharmonics Analysis Based on Interpolating Windowed FFT Algorithm,” *IEEE Trans. Power Deliv.*, vol. 22, no. 2, pp. 1064–1069, Apr. 2007.

[30] S. Lu, “Application of DFT filter bank to power frequency harmonic measurement,” vol. 152, no. 1, pp. 1–5, 2005.

[31] M. A. Platas-Garza and J. A. de la O Serna, “Dynamic Harmonic Analysis Through Taylor–Fourier Transform,” *IEEE Trans. Instrum. Meas.*, vol. 60, no. 3, pp. 804–813, Mar. 2011.

[32] M. D. Kusljevic and J. J. Tomic, “Multiple-Resonator-Based Power System Taylor-Fourier Harmonic Analysis,” *IEEE Trans. Instrum. Meas.*, vol. 64, no. 2, pp. 554–563, Feb. 2015.

[33] Q. Zhang, H. Liu, H. Chen, Q. Li, and Z. Zhang, “A Precise and Adaptive Algorithm for Interharmonics Measurement Based on Iterative DFT,” *IEEE Trans. Power Deliv.*, vol. 23, no. 4, pp. 1728–1735, Oct. 2008.

[34] H. C. Lin, G. Huang, and L. Y. Liu, “Non-stationary Harmonic Tracking using Piecewise-overlapped Group-harmonic Algorithm,” vol. 1, no. 2, pp. 3542–3547, 2013.

[35] F. Hlawatsch and G. F. Boudreaux-Bartels, “Linear and quadratic time-frequency signal representations,” *IEEE Signal Process. Mag.*, vol. 9, no. 2, pp. 21–67, Apr. 1992.

[36] S. Tomazic and S. Znidar, "A fast recursive STFT algorithm," in *Proceedings of 8th Mediterranean Electrotechnical Conference on Industrial Applications in Power Systems, Computer Science and Telecommunications (MELECON 96)*, 1996, vol. 2, pp. 1025–1028.

[37] C. K. Chui, *Wavelet analysis and its applications*. Academic Press, 1992.

[38] C. K. Chui, *Wavelets: A Tutorial in Theory and Applications*. Academic Press, 2012.

[39] T. Mathworks, *Wavelet tool box- user's guide*. 2012.

[40] G. Strang T. Nguyen, *Wavelet and Filter Banks*. Wellesley-Cambridge Press, 1996.

[41] P.Kailasapathi and D. Sivakumar, "Methods to Analyze Power Quality Disturbances," *Eur. J. Sci. Res.*, pp. 6–16, 2010.

[42] T. Keaochantranond and C. Boonseng, "Harmonics and interharmonics estimation using wavelet transform," *IEEE/PES Transm. Distrib. Conf. Exhib.*, vol. 2, no. 3, pp. 775–779, 2002.

[43] O. Mohammed, N. Abed, and S. Liu, "Characterization of transformer harmonic behavior using finite element analysis and discrete wavelet transforms," *Proc. 2007 IEEE SoutheastCon*, no. 2, pp. 354–357, 2007.

[44] C. Jaipradidtham and S. Pasomkusolsil, "Harmonic Analysis of Electromagnetic Transients in 500 kV Single Circuit Transmission System Using Discrete Wavelet Transform," in *2008 Joint International Conference on Power System Technology and IEEE Power India Conference*, 2008, pp. 1–4.

[45] S. Nath, P. Sinha, and S. K. Goswami, "A wavelet based novel method for the detection of harmonic sources in power systems," *Int. J. Electr. Power Energy Syst.*, vol. 40, no. 1, pp. 54–61, Sep. 2012.

[46] V. L. Pham and K. P. Wong, "Wavelet-transform-based algorithm for harmonic analysis of power system waveforms," *IEE Proc. - Gener. Transm. Distrib.*, vol. 146, no. 3, p. 249, 1999.

[47] E. Y. Hamid and Z. Kawasaki, "Wavelet packet transform for RMS values and power measurements," *IEEE Power Eng. Rev*, vol. 21, no. 9, pp. 49–51, 2001.

[48] T. Tarasiuk, "Hybrid Wavelet-Fourier Spectrum Analysis," *IEEE Trans. Power Deliv.*, vol. 19, no. 3, pp. 957–964, Jul. 2004.

[49] F. Vatansever and a. Ozdemir, "A new approach for measuring RMS value and phase angle of fundamental harmonic based on Wavelet Packet Transform," *Electr. Power Syst. Res.*, vol. 78, no. 1, pp. 74–79, Jan. 2008.

[50] J. Barros, S. Member, and R. I. Diego, “Analysis of Harmonics in Power Systems Using the Wavelet-Packet Transform,” vol. 57, no. 1, pp. 63–69, 2008.

[51] R. I. Diego and J. Barros, “Global method for time–frequency analysis of harmonic distortion in power systems using the wavelet packet transform,” *Electr. Power Syst. Res.*, vol. 79, no. 8, pp. 1226–1239, Aug. 2009.

[52] H. A. A. Reza Eslami, “A New Method for Measurement of Harmonic Groups Using Wavelet-Packet-Transform,” *J. Am. Sci.*, vol. 8, no. 2, pp. 546 – 550, 2012.

[53] A. A. Girgis, “Identification and tracking of harmonic sources in a power system using a Kalman filter,” *IEEE Trans. Power Deliv.*, vol. 11, no. 3, pp. 1659–1665, Jul. 1996.

[54] A. A. Girgis, “Identification and tracking of harmonic sources in a power system using a Kalman filter,” *IEEE Trans. Power Deliv.*, vol. 11, no. 3, pp. 1659–1665, Jul. 1996.

[55] K. K. C. Yu, N. R. Watson, and J. Arrillaga, “An Adaptive Kalman Filter for Dynamic Harmonic State Estimation and Harmonic Injection Tracking,” *IEEE Trans. Power Deliv.*, vol. 20, no. 2, pp. 1577–1584, Apr. 2005.

[56] H. Hajimolahoseini, M. R. Taban, and H. R. Abutalebi, “Improvement of Extended Kalman Filter frequency tracker for nonstationary harmonic signals,” *2008 Int. Symp. Telecommun.*, no. 2, pp. 592–597, Aug. 2008.

[57] H. Hajimolahoseini, M. R. Taban, and H. Soltanian-Zadeh, “Extended Kalman Filter frequency tracker for nonstationary harmonic signals,” *Measurement*, vol. 45, no. 1, pp. 126–132, Jan. 2012.

[58] T. Lobos, T. Kozina, and H.-J. Koglin, “Power system harmonics estimation using linear least squares method and SVD,” in *IMTC/99. Proceedings of the 16th IEEE Instrumentation and Measurement Technology Conference (Cat. No.99CH36309)*, 1999, vol. 2, pp. 789–794.

[59] G. G. Richards and H. Yang, “Distribution system harmonic worst case design using a genetic algorithm,” *IEEE Trans. Power Deliv.*, vol. 8, no. 3, pp. 1484–1491, Jul. 1993.

[60] B. Ozpineci, L. M. Tolbert, and J. N. Chiasson, “Harmonic optimization of multilevel converters using genetic algorithms,” in *2004 IEEE 35th Annual Power Electronics Specialists Conference (IEEE Cat. No.04CH37551)*, 2004, vol. 5, pp. 3911–3916.

[61] M. Sabahi, a. R. M. Iranaq, K. M. Bahrami, K. M. Bahrami, and M. B. B. Sharifian, "Harmonics elimination in a multilevel inverter with unequal DC sources using genetic algorithm," *2011 Int. Conf. Electr. Mach. Syst.*, pp. 1–5, Aug. 2011.

[62] H. Chen and Y. Sun, "Harmonic Suppression of Grid-Connected Distributed Generation Using Multi-Objective Genetic Algorithm," in *2009 Asia-Pacific Power and Energy Engineering Conference*, 2009, pp. 1–4.

[63] S. S. Rao and N. Shailaja, "Improving Voltage Regulation and Harmonic Elimination using Genetic Algorithm in PWM Choppers," in *INTELEC 05 - Twenty-Seventh International Telecommunications Conference*, 2005, pp. 449–454.

[64] V. S. Kumar, P. S. Kannan, K. Kalaiselvi, and D. Kavitha, "Optimal Estimation of Harmonics in Power System using Intelligent Computing Techniques," in *2007 International Joint Conference on Neural Networks*, 2007, pp. 142–147.

[65] M. Bettayeb and U. Qidwai, "A hybrid least squares-GA-based algorithm for harmonic estimation," *IEEE Trans. Power Deliv.*, vol. 18, no. 2, pp. 377–382, Apr. 2003.

[66] Z. Lu, T. Y. Ji, W. H. Tang, and Q. H. Wu, "Optimal Harmonic Estimation Using A Particle Swarm Optimizer," *IEEE Trans. Power Deliv.*, vol. 23, no. 2, pp. 1166–1174, Apr. 2008.

[67] P. K. Ray and B. Subudhi, "BFO optimized RLS algorithm for power system harmonics estimation," *Appl. Soft Comput.*, vol. 12, no. 8, pp. 1965–1977, Aug. 2012.

[68] W. . Kazibwe and M. H. Sendaula, *Electric Power Quality Control Techniques*. New York: Van Nostrand Reinhold, 1993.

[69] M. A. S. Masoum, S. Jamali, and N. Ghaffarzadeh, "Detection and classification of power quality disturbances using discrete wavelet transform and wavelet networks," *IET Sci. Meas. Technol.*, vol. 4, no. 4, pp. 193–205, Jul. 2010.

[70] J. R. M. Jr, I. N. Gondim, J. F. B. Jr, C. E. Tavares, and A. J. P. R. Junior, "Practical Aspects of Performance Tests on Power Quality Analyzers," in *ICREPQ'12 - International Conference on Renewable Energies and Power Quality*, 2012.

[71] M. Albu and G. T. Heydt, "On the use of rms values in power quality assessment," *IEEE Trans. Power Deliv.*, vol. 18, no. 4, pp. 1586–1587, Oct. 2003.

[72] F. R. Zaro, M. A. Abido, S. Ameenuddin, and I. M. Elamin, "Characterization of short-duration voltage events," in *2012 IEEE International Conference on Power and Energy (PECon)*, 2012, pp. 650–654.

[73] S. Santoso, W. M. Grady, E. J. Powers, J. Lamoree, and S. C. Bhatt, "Characterization of distribution power quality events with Fourier and wavelet transforms," *IEEE Trans. Power Deliv.*, vol. 15, no. 1, pp. 247–254, 2000.

[74] Y. H. Gu and M. H. J. Bollen, "Time-frequency and time-scale domain analysis of voltage disturbances," *IEEE Trans. Power Deliv.*, vol. 15, no. 4, pp. 1279–1284, 2000.

[75] J. Chung, E. J. . Powers;, and W. McGrady, "Power quality assessment via the Teager energy operator," *Proc. IEEE PES Summer Meet.*, 2000.

[76] O. Poisson, P. Rioual, and M. Meunier, "Detection and measurement of power quality disturbances using wavelet transform," *IEEE Trans. Power Deliv.*, vol. 15, no. 3, pp. 1039–1044, Jul. 2000.

[77] T. K. Abdel-Galil, M. Kamel, A. M. Youssef, E. F. El-Saadany, and M. M. A. Salama, "Power Quality Disturbance Classification Using the Inductive Inference Approach," *IEEE Trans. Power Deliv.*, vol. 19, no. 4, pp. 1812–1818, Oct. 2004.

[78] H. He and J. A. Starzyk, "A Self-Organizing Learning Array System for Power Quality Classification Based on Wavelet Transform," *IEEE Trans. Power Deliv.*, vol. 21, no. 1, pp. 286–295, Jan. 2006.

[79] P. K. Dash, M. Nayak, M. R. Senapati, and I. W. C. Lee, "Mining for similarities in time series data using wavelet-based feature vectors and neural networks," *Eng. Appl. Artif. Intell.*, vol. 20, no. 2, pp. 185–201, Mar. 2007.

[80] M. Uyar, S. Yildirim, and M. T. Gencoglu, "An effective wavelet-based feature extraction method for classification of power quality disturbance signals," *Electr. Power Syst. Res.*, vol. 78, no. 10, pp. 1747–1755, Oct. 2008.

[81] G. W. Chang, S. Y. Chu, and H. L. Wang, "A new approach for placement of single-tuned passive harmonic filters in a power system," in *IEEE Power Engineering Society Summer Meeting*, 2002, vol. 2, pp. 814–817.

[82] Chih-Ju Chou, Chih-Wen Liu, June-Yown Lee, and Kune-Da Lee, "Optimal planning of large passive-harmonic-filters set at high voltage level," *IEEE Trans. Power Syst.*, vol. 15, no. 1, pp. 433–441, 2000.

[83] S. Jamali, M. A. S. Masoum, and S. A. Mousavi, "Influence of controller high pass filter on the performance of shunt hybrid power filter." pp. 1–6, 2008.

[84] G. Mishra and S. Gopalakrishna, "Design of passive high pass filter for shunt active power filter application," in *2013 International Conference on Circuits, Power and Computing Technologies (ICCPCT)*, 2013, pp. 17–21.

[85] J. C. Das, “Passive Filters—Potentialities and Limitations,” *IEEE Trans. Ind. Appl.*, vol. 40, no. 1, pp. 232–241, Jan. 2004.

[86] S. Gupta and P. Gupta, “Harmonics Mitigation Using Active Power Filter,” *Int. J. Adv. Comput. Res.*, vol. 3, no. 2, pp. 116–120, 2013.

[87] L. A. Moran, I. Pastorini, J. Dixon, and R. Wallace, “A fault protection scheme for series active power filters,” *IEEE Trans. Power Electron.*, vol. 14, no. 5, pp. 928–938, 1999.

[88] C. B. Jacobina, A. C. Oliveira, N. Rocha, R. R. Matias, W. R. N. Santos, and M. B. R. Correa, “Three-Phase Series Active Power Filter Without Isolation Transformer and Active DC Source,” in *2009 Twenty-Fourth Annual IEEE Applied Power Electronics Conference and Exposition*, 2009, pp. 1596–1601.

[89] H.-L. Jou, “New single-phase active power filter,” *IEE Proc. - Electr. Power Appl.*, vol. 141, no. 3, p. 129, 1994.

[90] M. I. Masoud, “Five-phase uncontrolled line commutated rectifier: AC side compensation using shunt active power filter,” in *2015 IEEE 8th GCC Conference & Exhibition*, 2015, pp. 1–6.

[91] P. Kanjiya, V. Khadkikar, and H. H. Zeineldin, “Optimal Control of Shunt Active Power Filter to Meet IEEE Std. 519 Current Harmonic Constraints Under Nonideal Supply Condition,” *IEEE Trans. Ind. Electron.*, vol. 62, no. 2, pp. 724–734, Feb. 2015.

[92] A. Ghosh, A. Joshi, and M. K. Mishra, “A new algorithm for active shunt filters using instantaneous reactive power theory,” *IEEE Power Eng. Rev.*, vol. 20, no. 12, pp. 56–58, 2000.

[93] M. Machmoum and N. Bruyant, “DSP based control of shunt active power filters for global or selective harmonics compensation,” in *Ninth International Conference on Harmonics and Quality of Power. Proceedings (Cat. No.00EX441)*, 2000, vol. 2, pp. 661–666.

[94] M. Sonnenschein and V. Staudt, “Evaluation of a shunt active filter using frequency identification,” in *8th International Conference on Harmonics and Quality of Power. Proceedings (Cat. No.98EX227)*, 1998, vol. 2, pp. 617–622.

[95] E. F. Couto, J. S. Martins, and J. L. Afonso, “Simulation Results of a Shunt Active Power Filter with Control Based on p-q Theory,” in *International Conference on Renewable Energies and Power Quality, ICREPQ’03*, 2003, pp. 1–6.

[96] R. Patel and A. K. Panda, “Real time implementation of PI and fuzzy logic controller based 3-phase 4-wire interleaved buck active power filter for mitigation of

harmonics with id–iq control strategy," *Int. J. Electr. Power Energy Syst.*, vol. 59, pp. 66–78, Jul. 2014.

[97] S. K. Bath and S. Kumra, "Simulation and Measurement of Power Waveform Distortions using LabVIEW," in *2008 IEEE International Power Modulators and High-Voltage Conference*, 2008, pp. 427–434.

[98] M. V. Chilukuri, "Remote power quality monitoring and analysis system using LabVIEW software," in *2009 IEEE Intrumentation and Measurement Technology Conference*, 2009, pp. 279–283.

[99] Y. Yang, X. Wang, and C. Chen, "Real-time power quality monitoring and analysis platform of rural power network based on virtual instrument," in *2009 9th International Conference on Electronic Measurement & Instruments*, 2009, pp. 1–630–1–635.

[100] J. Chen and T. Tang, "Power quality analysis based on LABVIEW for current power generation system," in *International Symposium on Power Electronics Power Electronics, Electrical Drives, Automation and Motion*, 2012, pp. 865–870.

[101] V. K. Suganthi, L. Madhuridevi, and K. Sindhuja, "Development of software tool for classroom teaching of power quality using LabVIEW," in *2014 International Conference on Advances in Electrical Engineering (ICAEE)*, 2014, pp. 1–6.

[102] Chunyan Zang, Yuanfang Wen, and Hao Wu, "The application of the virtual instrument technology in high voltage measuring system," in *IEEE/PES Transmission and Distribution Conference and Exhibition*, 2002, vol. 3, pp. 2300–2304.

[103] S. G. Mallat, "A theory for multiresolution signal decomposition: the wavelet representation," *IEEE Trans. Pattern Anal. Mach. Intell.*, vol. 11, no. 7, pp. 674–693, Jul. 1989.

[104] L. Tan and J. Jiang, "Novel adaptive IIR filter for frequency estimation and tracking [DSP Tips&Tricks," *IEEE Signal Process. Mag.*, vol. 26, no. 6, pp. 186–189, Nov. 2009.

[105] M. Karimi-Ghartemani, M. Mojiri, and A. R. Bakhshai, "A technique for extracting time-varying harmonics based on an adaptive notch filter," in *Proceedings of 2005 IEEE Conference on Control Applications, 2005. CCA 2005.*, 2005, pp. 624–628.

[106] Xiaobo Tan and Hang Zhang, "A novel adaptive IIR notch filter for frequency estimation and tracking," in *2010 3rd International Conference on Computer Science and Information Technology*, 2010, vol. 5, pp. 259–263.

[107] X. Guan, X. Chen, and G. Wu, “Implementation of harmonic IIR notch filter with the TMS320C55x,” in *2010 3rd International Congress on Image and Signal Processing*, 2010, vol. 7, pp. 3195–3199.

[108] A. L. Szczupak and L. W. P. Biscainho, “Adaptive IIR Notch Filters for tracking of quasi-harmonic signals.” pp. 2119–2123, 2012.

[109] M. Tarek, S. Mekhilef, and N. A. Rahim, “Application of adaptive notch filter for harmonics currents estimation.” pp. 1236–1240, 2007.

[110] W. G. Morsi and M. E. El-hawary, “components measurements for harmonics and inter-harmonics distortion based on Wavelet Packet transform ; Part I : Mathematical formulation Mesures des composants de puissance dans le domaine temporel et fréquentiel pour les distorsions harmoniques et inte,” vol. 35, no. 1, pp. 1–7, 2010.

[111] J. A. Anderson and E. Rosenfeld, *Talking Nets: An Oral History of Neural Networks*. MIT Press, 2000.

[112] D. Hunter, H. Yu, M. S. Pukish, III, J. Kolbusz, and B. M. Wilamowski, “Selection of Proper Neural Network Sizes and Architectures—A Comparative Study,” *IEEE Trans. Ind. Informatics*, vol. 8, no. 2, pp. 228–240, May 2012.

[113] S. Maiti, V. Verma, C. Chakraborty, and Y. Hori, “An Adaptive Speed Sensorless Induction Motor Drive With Artificial Neural Network for Stability Enhancement,” *IEEE Trans. Ind. Informatics*, vol. 8, no. 4, pp. 757–766, Nov. 2012.

[114] R. Storn and K. Price, “Minimizing the real functions of the ICEC’96 contest by differential evolution,” in *Proceedings of IEEE International Conference on Evolutionary Computation*, 1996, pp. 842–844.

[115] A. H. Syed and M. A. Abido, “Differential Evolution based intelligent control for speed regulation of a PMDC motor,” in *21st Mediterranean Conference on Control and Automation*, 2013, pp. 1451–1456.

[116] F. S. AL-Ismail, M. A. Hassan, and M. A. Abido, “RTDS Implementation of STATCOM-Based Power System Stabilizers,” *Can. J. Electr. Comput. Eng.*, vol. 37, no. 1, pp. 48–56, 2014.

[117] F. Barrero, S. Martinez, F. Yeves, and P. M. Martinez, “Active power filters for line conditioning: a critical evaluation,” *IEEE Trans. Power Deliv.*, vol. 15, no. 1, pp. 319–325, 2000.

[118] E. E. EL-Kholy, A. EL-Sabbe, A. El-Hefnawy, and H. M. Mharous, “Three-phase active power filter based on current controlled voltage source inverter,” *Int. J. Electr. Power Energy Syst.*, vol. 28, no. 8, pp. 537–547, Oct. 2006.

[119] N. Mesbahi, A. Ouari, D. Ould Abdeslam, T. Djamah, and A. Omeiri, "Direct power control of shunt active filter using high selectivity filter (HSF) under distorted or unbalanced conditions," *Electr. Power Syst. Res.*, vol. 108, pp. 113–123, Mar. 2014.

[120] M. KMAIL, "INVESTIGATION OF SHUNT ACTIVE POWER FILTER FOR POWER QUALITY IMPROVMENT," NEAR EAST, 2012.

[121] A. Abellan, J. M. Benavent, G. Garcera, and D. Cerver, "Fixed frequency current controller applied to shunt active filters with UPF control in four-wire power systems," in *IEEE 2002 28th Annual Conference of the Industrial Electronics Society. IECON 02*, 2002, vol. 1, pp. 780–785.

[122] Z. F. Hussien, N. Atan, and I. Z. Abidin, "Shunt active power filter for harmonic compensation of nonlinear loads," in *Proceedings. National Power Engineering Conference, 2003. PECon 2003.*, 2003, pp. 117–120.

[123] P. Agarwal and H. O. Gupta, "Modeling of frequency domain control of shunt active power filter using MATLAB Simulink and Power System Blockset," in *2005 International Conference on Electrical Machines and Systems*, 2005, vol. 2, pp. 1124–1129 Vol. 2.

[124] S. H. Fathi, M. Pishvaei, and G. B. Gharehpetian, "A Frequency Domain Method for Instantaneous Determination of Reference Current in Shunt Active Filter," in *TENCON 2006 - 2006 IEEE Region 10 Conference*, 2006, pp. 1–4.

[125] Hui Liu, Guohai Liu, and Yue Shen, "A Novel Harmonics Detection Method Based on Wavelet Algorithm for Active Power Filter," in *2006 6th World Congress on Intelligent Control and Automation*, 2006, vol. 2, pp. 7617–7621.

[126] M. Forghani and S. Afsharnia, "Online Wavelet Transform-Based Control Strategy for UPQC Control System," *IEEE Trans. Power Deliv.*, vol. 22, no. 1, pp. 481–491, Jan. 2007.

[127] T.-S. Lee, K.-S. Tzeng, and C.-J. Chang, "A repetitive control approach for three-phase shunt active power filters with real-time wavelet transform," in *2009 International Conference on Power Electronics and Drive Systems (PEDS)*, 2009, pp. 376–380.

[128] S. Y. Kamble, S. N. Mate, and M. M. Waware, "Online wavelet based control algorithm for Shunt Active Power Filter operation," in *2013 IEEE International Conference on Control Applications (CCA)*, 2013, pp. 1153–1158.

[129] H. Akagi, Y. Kanazawa, and A. Nabae, "Instantaneous Reactive Power Compensators Comprising Switching Devices without Energy Storage Components," *IEEE Trans. Ind. Appl.*, vol. IA-20, no. 3, pp. 625–630, May 1984.

[130] T. Noguchi, H. Tomiki, S. Kondo, and I. Takahashi, "Direct power control of PWM converter without power-source voltage sensors," *IEEE Trans. Ind. Appl.*, vol. 34, no. 3, pp. 473–479, 1998.

[131] M. C. Benhabib and S. Saadate, "New control approach for four-wire active power filter based on the use of synchronous reference frame," *Electr. Power Syst. Res.*, vol. 73, no. 3, pp. 353–362, Mar. 2005.

[132] V. Soares, P. Verdelho, and G. D. Marques, "An instantaneous active and reactive current component method for active filters," *IEEE Trans. Power Electron.*, vol. 15, no. 4, pp. 660–669, Jul. 2000.

[133] V. Khadkikar, M. Singh, A. Chandra, and B. Singh, "Implementation of single-phase synchronous d-q reference frame controller for shunt active filter under distorted voltage condition," in *2010 Joint International Conference on Power Electronics, Drives and Energy Systems & 2010 Power India*, 2010, pp. 1–6.

[134] A. Pigazo, Ví. M. Moreno, and E. J. EstÉbanez, "A Recursive Park Transformation to Improve the Performance of Synchronous Reference Frame Controllers in Shunt Active Power Filters," *IEEE Trans. Power Electron.*, vol. 24, no. 9, pp. 2065–2075, Sep. 2009.

[135] M. Kesler and E. Ozdemir, "Synchronous-Reference-Frame-Based Control Method for UPQC Under Unbalanced and Distorted Load Conditions," *IEEE Trans. Ind. Electron.*, vol. 58, no. 9, pp. 3967–3975, Sep. 2011.

[136] L. G. Barbosa Rolim, D. Rodrigues da CostaJr., and M. Aredes, "Analysis and Software Implementation of a Robust Synchronizing PLL Circuit Based on the pq Theory," *IEEE Trans. Ind. Electron.*, vol. 53, no. 6, pp. 1919–1926, Dec. 2006.

[137] Zeliang Shu, Yuhua Guo, and Jisan Lian, "Steady-State and Dynamic Study of Active Power Filter With Efficient FPGA-Based Control Algorithm," *IEEE Trans. Ind. Electron.*, vol. 55, no. 4, pp. 1527–1536, Apr. 2008.

[138] E. Lavopa, P. Zanchetta, M. Sumner, and F. Cupertino, "Real-Time Estimation of Fundamental Frequency and Harmonics for Active Shunt Power Filters in Aircraft Electrical Systems," *IEEE Trans. Ind. Electron.*, vol. 56, no. 8, pp. 2875–2884, Aug. 2009.

[139] Y. Han, L. Xu, M. M. Khan, G. Yao, L.-D. Zhou, and C. Chen, "A novel synchronization scheme for grid-connected converters by using adaptive linear optimal filter based PLL (ALOF–PLL)," *Simul. Model. Pract. Theory*, vol. 17, no. 7, pp. 1299–1345, Aug. 2009.

[140] R. K. Patjoshi and K. K. Mahapatra, “Performance analysis of shunt active power filter using PLL based control algorithms under distorted supply condition,” in *2013 Students Conference on Engineering and Systems (SCES)*, 2013, pp. 1–6.

[141] M. Kale and E. Ozdemir, “A novel adaptive hysteresis band current controller for shunt active power filter,” in *Proceedings of 2003 IEEE Conference on Control Applications, 2003. CCA 2003.*, 2003, vol. 2, pp. 1118–1123.

[142] G. Panda, S. K. Dash, and N. Sahoo, “Comparative performance analysis of Shunt Active power filter and Hybrid Active Power Filter using FPGA-based hysteresis current controller,” in *2012 IEEE 5th India International Conference on Power Electronics (IICPE)*, 2012, pp. 1–6.

[143] A. K. Panda, M. Suresh, and Y. Suresh, “Real-time implementation of adaptive fuzzy hysteresis-band current control technique for shunt active power filter,” *IET Power Electron.*, vol. 5, no. 7, pp. 1188–1195, Aug. 2012.

[144] S. K. Chauhan and P. N. Tekwani, “Current error space phasor based hysteresis controller for two-level and three-level converters used in Shunt Active Power Filters,” in *IECON 2013 - 39th Annual Conference of the IEEE Industrial Electronics Society*, 2013, pp. 8522–8527.

[145] S. Swain, P. C. Panda, and B. D. Subudhi, “Three phase shunt Active Power Filter using a new Weighted Adaptive Hysteresis Band Current Controller,” in *2014 International Conference on Circuits, Power and Computing Technologies [ICCPCT-2014]*, 2014, pp. 781–786.

[146] H. Komurcugil, “Double-band hysteresis current-controlled single-phase shunt active filter for switching frequency mitigation,” *Int. J. Electr. Power Energy Syst.*, vol. 69, pp. 131–140, Jul. 2015.

[147] S. Gautam and R. Gupta, “Three-level inverter based shunt active power filter using generalized hysteresis current control method,” in *2010 International Conference on Power, Control and Embedded Systems*, 2010, pp. 1–6.

[148] R. L. de A. Ribeiro, T. de O. A. Rocha, R. M. de Sousa, E. C. dos Santos, and A. M. N. Lima, “A Robust DC-Link Voltage Control Strategy to Enhance the Performance of Shunt Active Power Filters Without Harmonic Detection Schemes,” *IEEE Trans. Ind. Electron.*, vol. 62, no. 2, pp. 803–813, Feb. 2015.

[149] S. Rahmani, N. Mendalek, and K. Al-Haddad, “Experimental Design of a Nonlinear Control Technique for Three-Phase Shunt Active Power Filter,” *IEEE Trans. Ind. Electron.*, vol. 57, no. 10, pp. 3364–3375, Oct. 2010.

[150] Chen Weiji, Chen Wenhong, Ma Xiaojun, Chen Jianye, Wang Zhonghong, and Han Yingduo, “An adaptive noise canceling theory based single-phase shunt active

power filter," in *Proceedings of Power Conversion Conference - PCC '97*, 1997, vol. 1, pp. 191–196.

[151] F. R. Zaro., "Efficient Techniques for Detection and Mitigation of Power Quality Events," King Fahd University of Petroleum and Minerals University, Dhahran, Saudi Arabi, 2013.

[152] R. Kuffel, J. Giesbrecht, T. Maguire, R. P. Wierckx, and P. McLaren, "RTDS-a fully digital power system simulator operating in real time," in *IEEE WESCANEX 95. Communications, Power, and Computing. Conference Proceedings*, 1995, vol. 2, pp. 300–305.

[153] W. Ren, M. Steurer, and T. L. Baldwin, "An effective method for evaluating the accuracy of Power Hardware-in-the-Loop simulations," in *2008 IEEE/IAS Industrial and Commercial Power Systems Technical Conference*, 2008, pp. 1–6.

[154] X. Yang, X. Zha, and S. Li, "Study on Hardware-in-the-Loop of Active Power Filer Based on RTDS," in *2010 International Conference on Electrical and Control Engineering*, 2010, pp. 4295–4298.

[155] M. Dargahi, A. Ghosh, G. Ledwich, and F. Zare, "Studies in power hardware in the loop (PHIL) simulation using real-time digital simulator (RTDS)," in *2012 IEEE International Conference on Power Electronics, Drives and Energy Systems (PEDES)*, 2012, pp. 1–6.

APPENDIX A

EXPERIMENTAL SETUP COMPONENTS FOR POWER QUALITY MONITORING

This appendix briefly explains the components used in this work for building the experimental setup. The appendix describes the software and hardware components used for building the real time power quality monitoring and mitigation system.

A.1 Software Used in the Experimental Setup

The NI LabVIEW (Laboratory Virtual Instrument Engineering Workbench) software is used to design and develop different engineering applications using visual programming. LabVIEW provides a graphical user interface to design, run, operate and troubleshoot the power system design.

LabVIEW mainly consist of two parts namely *Block Diagram* and *Front Panel*. The block diagram is used to design the system by copying and pasting the individual components called virtual instruments (VI) from the user library as shown in Figure A.1. A number of VIs are readily available in the library that are designed and refined over the time. After the successful design and compilation of the designed program the code can be sent to the real time controller using FPGA block set or it can be run using standalone workstation. The LabVIEW Front panel can be used to observe record and control the real time simulation using controls and graph indicators as shown in Figure A.2.

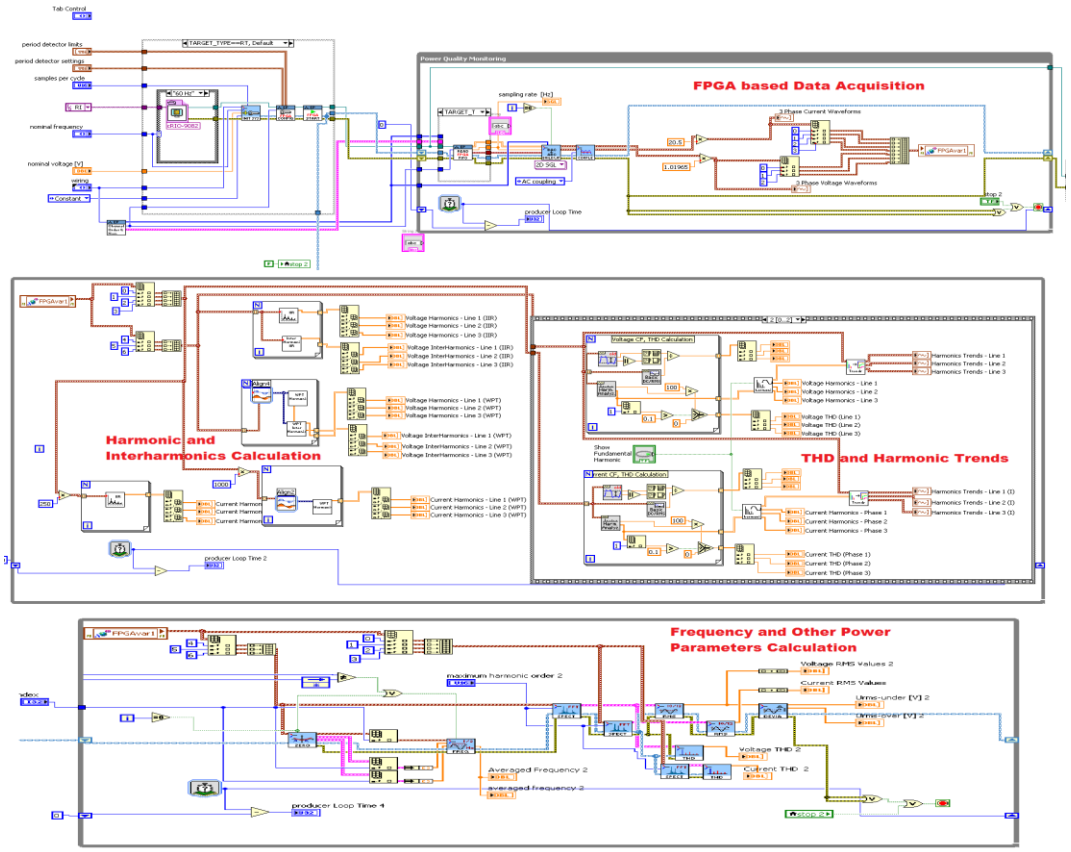

Figure A.1 Block Diagram of Real Time LabVIEW Program

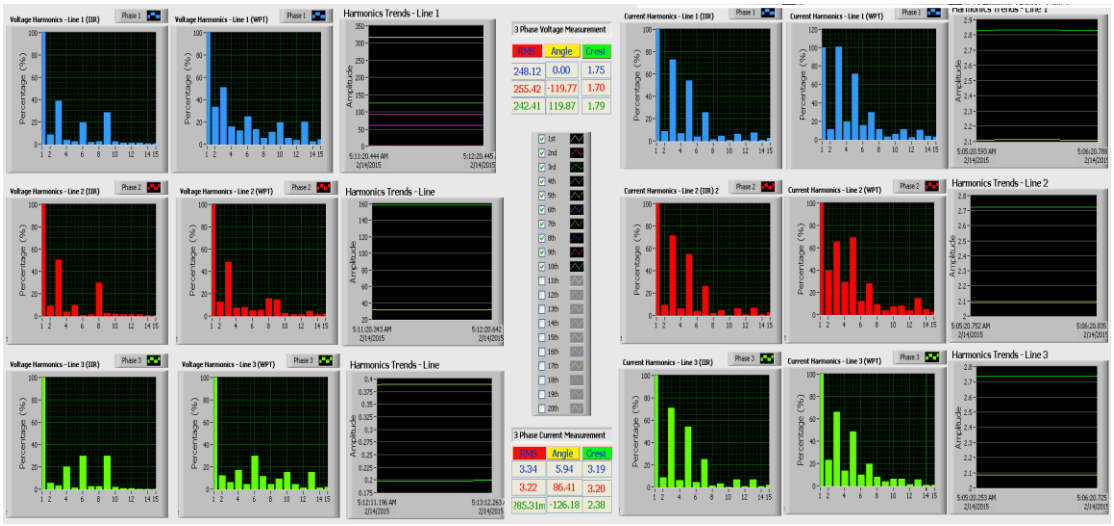

Figure A.2 Real Time Harmonics and Interharmonics Measurement Using FPGA-LabVIEW

A.2 Hardware Components used in the Prototype

The monitoring, control and mitigation hardware setup is developed using National Instrument (NI) hardware, programmable sources and loads, real time inverter and dSPACE controller. The real time setup developed in this thesis is responsible for collecting current and voltage waveforms, process them using digital processors, implement controls and take necessary actions to mitigate the potential threats to the power system.

A.2.1 National Instrument Hardware

National Instrument offers a wide range of real time controllers, digital processors and data acquisition cards for real time measurement and control. The NI hardware used in this thesis consists of NI Compact RIO and real time data acquisition cards. The details of the hardware components used to build the prototype are explained in the subsequent sections.

A.2.1.1 NI Compact RIO

NI cRIO is National Instrument Compact Reconfigurable Input/Output. cRIO mainly consists of three parts, namely an embedded controller, a reconfigurable chassis and I/O modules. The controller part is responsible for communication and processing, a reconfigurable chassis contains the user-programmable field programmable gate array FPGA and the hot-swappable I/O modules are used for data acquisition applications. The data acquisition on I/O modules can be performed using high-speed FPGA clock.

There are a number of different cRIO modules available depending on their capabilities and features. I this work, cRIO-9082 is used for real time controller implementation and data acquisition as shown in Figure A.3. The main feature of cRIO-9082 are listed below:

Processor:	1.33 GHz dual-core Intel Core i7
Memory:	32 GB nonvolatile storage, 2 GB DDR3 800 MHz RAM
Operating System:	Windows Embedded Standard 7
Connectivity:	4 USB Slots, 2 Gigabit Ethernet Slots, and 2 serial ports
Reconfigurable FPGA:	Spartan-6
I/O Slots:	8 slots for hot swappable I/O modules

Figure A.3 NI Compact RIO and Data Acquisition Cards

A.2.1.2 Voltage and Current Acquisition Cards

NI offers a wide range of analog and digital data acquisition cards for real time data fetching. These hot swappable input/output modules can be used in real time monitoring and control of different applications. The voltage and current modules used for real time monitoring and measurement of harmonics in this work are listed below:

(a) Analog Current input module NI-9227

The NI-9227 data acquisition card has been selected to measure the real time current in distribution system as shown in Figure A.4. It has four input channel for three phase and neutral current monitoring. It can measure 5 Arms (14A peak current) current directly from the distribution feeder and can be used along with a current transformer to measure the current greater than 5A rms. In this work, 100/5A current transformer is used along with

the NI-9227 current module for real time current monitoring. The sampling rate of NI-9227 is 50 KS/s/ch and offers 250 Vrms isolation between adjacent channels.

Figure A.4 The NI-9227 Analog Current Input Module

(b) Analog Voltage Input Module NI-9225

The NI-9225 data acquisition card has been selected to measure the real time grid voltage in distribution system as shown in Figure A.5. It has three input channel for three phase voltage monitoring. It can measure voltage upto 300 Vrms directly from the distribution feeder. The sampling rate of NI-9225 is 50 KS/s/ch and offers 600 Vrms isolation between adjacent channels.

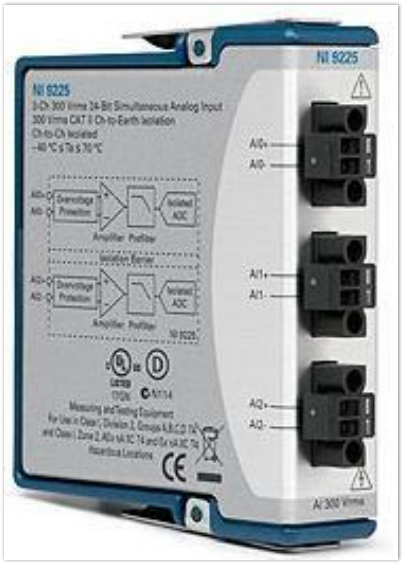

Figure A.5 The NI-9225 Analog Voltage Input Module

APPENDIX B

EXPERIMENTAL SETUP COMPONENTS FOR HARMONIC MITIGATION

B.1 Programmable AC Source

Programmable AC source provides powerful functions to simulate the standard power quality disturbances. In this work, Chroma 61511 is used as a grid source for the distribution system as shown in Figure B.1. It can provides upto 300 Vac output voltage and 12 KVA power ratings. It is capable to generate the first forty harmonics and interharmonics ranging from 0.01 Hz to 2400 Hz.

Figure B.1 Programmable AC Source Chroma 61511

B.2 Programmable Electronic Load

Programmable electronic loads are designed to to simulate the AC/DC loads. The programmable AC/DC load chroma 63800 is selected to simulate the non-linear rectified loads and load conditions under high crest factor as shown in Figure B.2. It is capable of working under distorted mains voltage. The chroma-63800 can be configured as a constant power source up to 1800W, while as a constant current load up to 45 Arms at the voltage range is 50V – 350 Vrms. Three identical units of chroma-63800 are used separately to simulate the three-phase load.

Figure B.2 Programmable Electronic Load

B.3 dSPACE Controller

dSPACE is an industrial controller mainly used for the application development and prototyping. In this study, DS-1103 is used for the real time controller implementation of SAPF as shown in Figure B.3. It has two major parts expansion box and connection panel.

The connection panel consists of 50 bit analog and digital I/O channels including 20 analog to digital input channel (ADCH) and 8 digital to analog output channels (DACH). dSPACE can be easily programmed with the Matlab/Simulink with the aid of real time interface (RTI) blocksets. All I/O's can be configured for real time applications using RTI. dSPACE uses controlDesk as a software for the real time monitoring, measurement and control actions. DS-814 interface card is used in the expansion box while DS-817 card in the workstation for real time monitoring and control of the system.

Figure B.3 dSPACE DS-1103 Controller

B.4 Inverter/Rectifier Module

SEMITEACH – IGBT inverter and rectifier are used for real time SAPF implementation. It has three major functions including single and three phase inverter, buck or boost converter and brake chopper as shown in Figure B.4. An isolated uncontrolled rectifier is

also a part of this embedded system. A pair of 2200μF dc capacitor is also installed for energy storage purpose. The rectifier input is 230/ 400V while the output of may vary up to 600V DC. The input output range of inverter can also varied up to 400V AC and 600V DC with 30A as a maximum current.

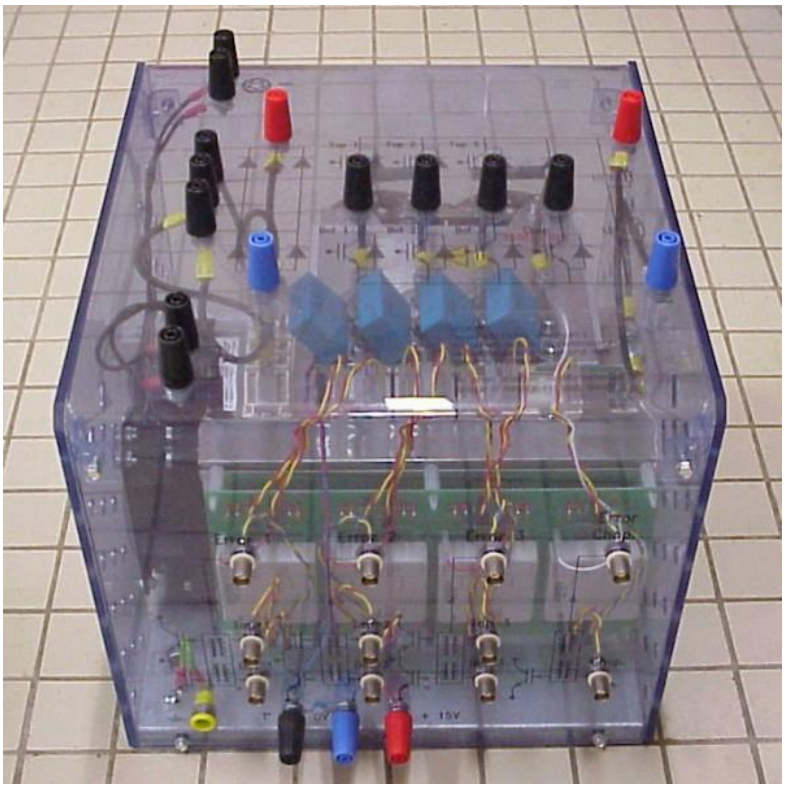

Figure B.4 Real Time Inverter and Rectifier Module

B.5 Mixed Domain Oscilloscope

Tektronix 4104B-3 mixed domain oscilloscope is used to record the experimental results as shown in Figure B.5. It is capable of analyzing signals in both frequency and time domain. It can be used a spectrum analyzer. It has four channels that can be used for the measurement of voltage and current signals.

The voltage probe Tektronix TPP-1000 is a 1GHz bandwidth probe used for the measurement of voltage signals up to 300 volts. It offers 10X and 2X attenuation factors. Tektronix TCP0030A probe is utilized for the measurement of source, load and SAPF current signals. This probe provides the selectable measurement of 5A and 30A with the bandwidth greater than 120 MHz.

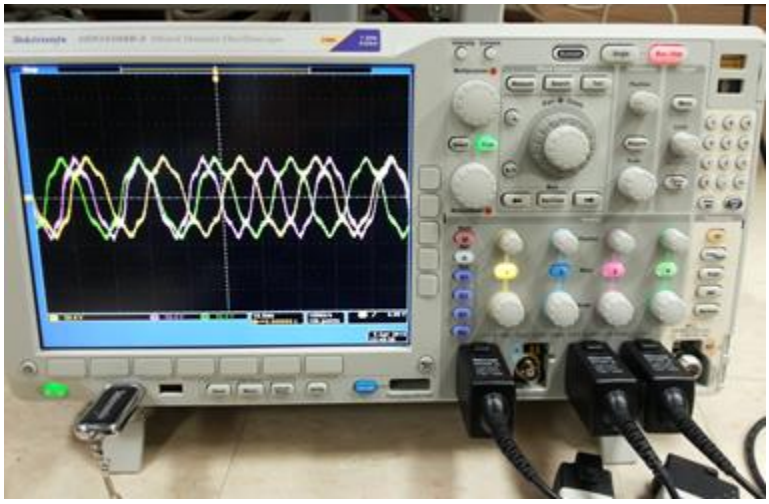

Figure B.5 Mixed Domain Tektronix Oscilloscope

B.6 Voltage and Current Transducers

Voltage and current transducers are utilized to reduce the voltage and current signals of distribution system, which can be fed to the controller for a possible control action. The dSPACE controller, used in this work has input output range up to ±10V while the actual voltage and current ratings are much higher. So, voltage and current transducers are used to make the input voltage and current signals compatible with the controller I/O range.

(a) Voltage Transducer

LEM LV 25P/SP5 sensor is used as a voltage transducer for the real time measurement of voltage signal. It is a closed loop sensor, which can measure DC, AC and pulsed voltage

signals from 10 to 1500 V using the Hall effect as shown in Figure B.6. A user specified input resistor is used to induce a current in the secondary side of the transducer, where a measurement resistor can be used to obtain the output voltage from the induced current. In this work, input resistor of 47 kΩ is used for the three-phase voltage measurement while 94 kΩ is used for the DC bus side with a 500Ω as a measurement resistor.

Figure B.6 Voltage Transducers LEM LV 25P/SP5

(b) Current Transducer

HAS 50-s sensor is used as a current transducer for the real time measurement of source load and active power filter current. It is a closed loop sensor, which can measure DC, AC and pulsed current signals up to 50A using the Hall effect as shown in Figure B.7. The output of this sensor is an AC voltage signal which can be easily used in any industrial controller like dSPACE.

Figure B.7 Current Transducers HAS 50-s

APPENDIX C

REAL TIME DIGITAL SIMULATOR (RTDS)

C.1 Real Time Digital Simulator (RTDS)

In power systems, a power hardware in loop (PHIL) systems represents the power systems interfaced with a piece of hardware. PHIL simulations plays a vital role in the design and testing of power system problems [152]–[154].

RTDS is one the most advance simulator that solves the complex power systems in near real time. RTDS consists of the specialized dedicated hardware and software that specifically designed to efficiently solve the electromagnetic transients as shown in Figure C.1. RTDS is capable of solving a wide range of power system application with the aid of wide variety of built in power system components and friendly graphical user interface [152], [155].

Figure C.1 Real Time Digital Simulator (RTDS)

C.1.1 RSCAD Software

RSCAD is the graphical user interface used to design, run, operate and troubleshoot the power system. RSCAD mainly consist of two parts namely DRAFT and RUNTIME. The Draft file is used to create the power system circuit by copying and pasting the individual power system components from the user library as shown in Figure C.2. A number of power system components are available in the library that are designed and refined over the time. After the power system network has been constructed, the draft file is compiled to create the simulation code required by the simulator.

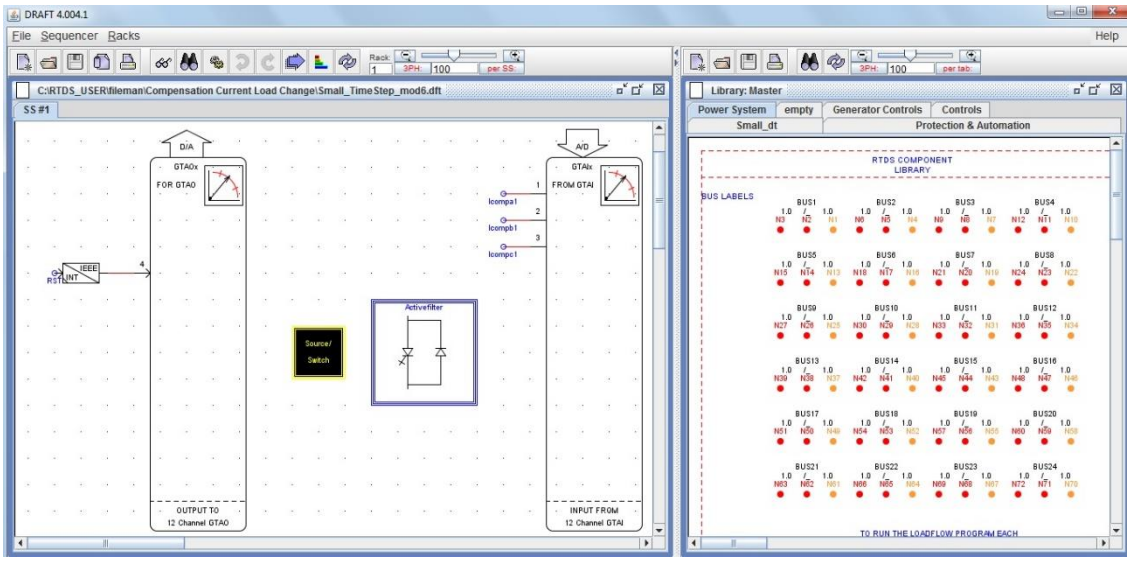

Figure C.2 RSCAD Draft File

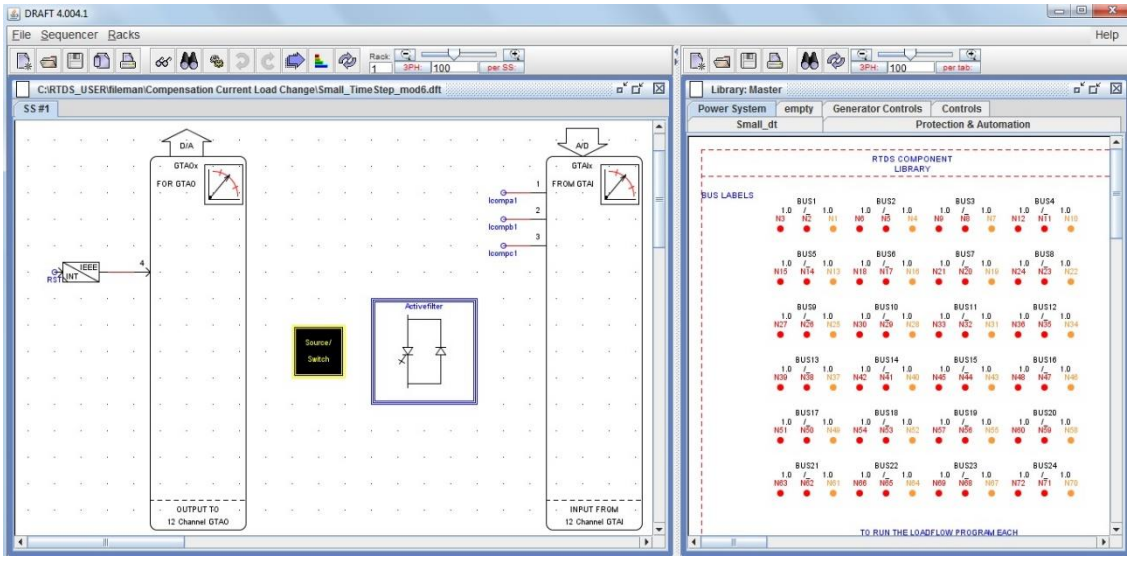

Figure C.3 RSCAD Run Time File

After the successful compilation of the draft file, the simulation code can be downloaded to the simulator using the run time file. Run time files can be used to observe, record and control the real time simulation using controls and graph indicators as shown in Figure C.3. Power system parameters like voltage, current frequency, power etc. can be examined

using plots and other indicators. The transient behavior of the system can be easily observed and recorded.

C.1.2 Hardware Components

The RTDS simulator hardware is based on the modular architecture. It can be easily extendable by adding modules or racks to accommodate the larger models power system. Each rack contains three different cards for communication and processing such as:

- Inter-Rack Communication card (IRC)
- Giga Transceiver Workstation Interface Card (GTWIF)
- Giga Processor Card (GPC)

The GTWIF card is responsible for the synchronization between the racks. It also communicate with the RSCAD to start and stop the simulation. GPC is used to solve the power/control systems components equations. Every GPC card contains two IBM 1GHz processor each can solve 66 power system nodes. GPC card also govern the connection to the gigabit transceiver analog input/output card (GTIO). The GTAI/O input/output cards are used to interface the RTDS with external devices as shown in Figure C.4. Each GTAI/O contains 12 input/output channel available for the external connection, while the gigabit transceiver digital input/output (GTDI/O) cards contains 64 digital input/output channels.

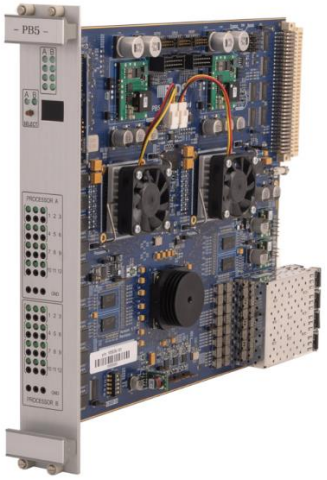

a) PB5

b) GTWIF

c) GTAO

d) GTAI

e) GTDI

Figure C.4 RTDS Processors and I/O Cards

LIST OF PUBLICATIONS

1. M. Ijaz, M.A.Abido "*Monitoring of Power Quality Disturbances using Wavelet Packet Transform*" Saudi Arabia Smart Grid Conference (SASG), 15-16 December 2014

2. M. Ijaz, M.A.Abido "*Characterization of Power Quality Disturbances using Wavelet Packet Transform*" International Conference on Applied Energy (ICAE2015), 28-31 March, 2015 (Accepted)

3. M. Ijaz, Md. Shafiullah, M.A.Abido *"Classification of Power Quality Disturbances using Wavelet Transform and Optimized ANN"* 12th Intelligent Systems Applications to Power Systems Conference (ISAP) 2015. (Submitted)

4. M. Ijaz, M. A. Abido, M. Deriche "*Efficient Technique for Harmonic Measurement in Power Systems Using IIR Filters"* (Submitted for Review)

5. M. Ijaz, M. A. Abido *"Real-Time RTDS Based Performance Analysis of Three-Phase Shunt Active Power Filters"* (Under Prepration)

6. M. Ijaz, M.Usman, M. A. Abido *"Real time implementation of shunt active power filter for mitigation of harmonics with different control strategy"* (Under Prepration)

VITAE

Name	:Muhammad Ijaz
Nationality	:Pakistani
Date of Birth	:5/10/1989
Email	:hmijaz@gmail.com
Address	:A-108, DHA-EME Sector Multan Road Lahore, Pakistan
Academic Background	:**MS Electrical Engineering** May, 2015 King Fahd University of Petroleum and Minerals Dhahran, Saudi Arabia **BS Electrical Engineering** March, 2011 COMSATS Institute of Information Technology Lahore, Pakistan